THE EFFECT OF SCREEN GEOMETRY ON THE PERFORMANCE OF A TUNED LIQUID DAMPER

THE EFFECT OF SCREEN GEOMETRY ON THE PERFORMANCE OF A TUNED LIQUID DAMPER

By

JAMIE HAMELIN, B.A.Sc.

A Thesis

Submitted to the School of Graduate Studies

In Partial Fulfillment of the Requirements

For the Degree

Master of Applied Science

McMaster University

MASTER OF APPLIED SCIENCE (2007) McMaster University
(Civil Engineering) Hamilton, Ontario

TITLE: The Effect of Screen Geometry on the Performance of a Tuned Liquid Damper

AUTHOR: Jamie Hamelin, B.A.Sc. (University of Waterloo)

SUPERVISORS: Dr. Michael Tait and Dr. John Wilson

NUMBER OF PAGES: 185, xxii

Abstract

In recent years, the use of tuned liquid dampers (TLD) as dynamic vibration absorbers has increased in popularity due to their low cost and ease of installation. A TLD is a partially fluid filled tank (commonly water) that has a fundamental sloshing frequency close to the natural frequency of the structure in the vibration mode to be suppressed. Typically, water alone is insufficient to achieve the required level of optimal damping. One approach that is used to increase the damping of the TLD is to install flow damping devices (screens) into the tank. In this study horizontal slat screens are selected for investigation. For a given target response acceleration an optimal level of damping can be achieved. However, as the structural response deviates from this target value the efficiency of the structure-TLD system is significantly reduced. To increase the efficiency, an investigation into the applicability of slat screens with a varying loss coefficient is undertaken in this study.

A TLD equipped with slat screens of different slat heights, edge geometries, and solidities is experimentally investigated. The TLD is subjected to shake-table tests under sinusoidal excitation for a range of amplitudes that correspond to a practical range of peak hourly horizontal structural accelerations. The variation in screen losses (C_L) is correlated with the Keulegan-Carpenter (KC) number.

An equivalent mechanical model is utilized by analyzing the TLD as an equivalent tuned mass damper (TMD). In addition, a nonlinear numerical model

based on shallow water theory is investigated. The influence of slat height on the free surface response, base shear forces, and energy dissipation is assessed.

A TLD equipped with various screen geometries is mathematically modelled in a hypothetical structure-TLD system. This system demonstrates the ability of slat screens with a varying loss coefficient to maintain a near optimum level of damping over a wide range of structural accelerations.

Acknowledgements

I would like to extend my thanks and gratitude to my research supervisors, Dr. Mike Tait and Dr. John Wilson. Dr. Tait's guidance, patience, and encouragement made this journey possible. Dr. Wilson's engineering experience and advice is rarely found in a supervisor and I am grateful for his assistance.

I would like to thank all the technical staff at the Advanced Dynamics Laboratory and Engineering Machine Shop. In particular, Peter Koudys, Geotechnical Lab Technician for his time, knowledge, and craftmanship. I would also like to thank the faculty and staff of the department, especially Carol Robinson, for her time and resourcefulness throughout my time at McMaster.

I would like to express my sincere thanks to my friends and colleagues who I met while attending McMaster. Specifically Marcus, for sharing his work and thoughts on this topic both in the lab and in the writing of this thesis. Eric, for his help in our endless food and coffee runs and his encouragement on the links, just trust it. Lastly, to my friends from 76 Gary, I thank you for your support and encouragement throughout this process. I think our lack of air conditioning allowed me to finish on time.

I would like to thank my family for their endless support and encouragement. This thesis is dedicated to Sarah for her continuous support, understanding, and patience throughout this study. Your influence on this work and my life is unsurpassed.

Table of Contents

List of Tables

List of Figures

Nomenclature

A	excitation amplitude
A/L	normalized excitation amplitude
b	tank width
c	damping coefficient (structural damping, C)
c_{cr}	critical damping coefficient
C_c	contraction coefficient
C_D	drag coefficient
C_L	velocity loss coefficient
C_L^{steady}	velocity loss coefficient at steady state
C_m	inertia component
D	slat height
D_{eff}	effective slat height
E_d	energy dissipation
E_s	strain energy
f	excitation frequency
f_{EXP}	experimentally measured natural frequency
f_n	natural frequency of sloshing fluid
F_D	damper force
F_s	sloshing base shear force
F_T	total base shear force
g	gravitational constant
$\lvert H_s(f)\rvert$	frequency-response function of structure
$\lvert H_\eta(f)\rvert$	frequency-response of free surface

h	still water fluid depth
h_{trib}	tributary height of fluid
k	stiffness (structural stiffness, K)
KC	Keuelegean-Carpenter number
L	tank length
m	mass (structural mass, M)
m_{eff}	effective mass (portion contributing to fluid sloshing)
m_o	non-participating mass of fluid
m_w	total mass of water
n	mode number
Δp	pressure loss at screen location
P_o	amplitude of applied force
q	generalized coordinate
R	relative motion between absorber and structure under random excitation
R_d	dynamic amplification factor
S	screen solidity
t	time
T	period of oscillation, kinetic energy
T_o	averaging time
u	horizontal components of fluid velocity
U_{max}	maximum fluid velocity at screen
V	potential energy
x	horizontal displacement
X	horizontal motion of tank
x_r	relative displacement between the structure and absorber
β	forcing frequency ratio

β_{eff}	effective damping
γ	modal participation factor
Γ	normalized fluid velocity
ζ	damping ratio
ζ_{eff}	effective damping
ζ_w	linearized damping term due to sloshing fluid
η	free surface response (wave height)
θ	phase angle
κ	wave number
μ	mass ratio
ρ	density of fluid
σ_F	amplitude of random force
σ_s	structural response
$\sigma_{s\text{-}target}$	target response of structure
υ	cycling frequency
υ_w	kinematic viscosity of water
Φ	velocity potential
ϕ	mode shape
ψ	efficiency of structure-TLD system
ω_n	natural circular frequency
Ω	tuning ratio

Common Superscripts

a'	normalized value of a
$\dot{a}$	time derivative of a
$\overline{a}$	average value of a
a^*	generalized property of a

Common Subscripts

a	dynamic vibration absorber property
eff	effective parameter
eq	equivalent mechanical parameter
opt	optimized parameter
s	structure property
w	property of water

Common Acronyms

DVA	dynamic vibration absorber
MDOF	multi degree of freedom
PF	peak factor
SDOF	single degree of freedom
RMS	root mean square
TLD	tuned liquid damper
TMD	tuned mass damper

Chapter 1 : Introduction

1.1 *Introduction*

Tall, flexible structures are often susceptible to wind-induced vibrations due to low levels of inherent damping. A common approach to mitigate this response is to attach a dynamic vibration absorber to the main structure. The two most popular types of vibration absorbers are the tuned mass damper (TMD) and the tuned liquid damper (TLD).

A tuned liquid damper consists of a tank that is partially filled with a fluid (usually water) and is located in a structure at or near the location of maximum modal displacement. A TLD operates analogous to a TMD with the main difference being that the TLD relies upon the inertial force of the sloshing fluid in order to suppress the vibratory motion. Flow-damping devices (screens) have been utilized in the design of TLD's in order to increase the TLD damping since the inherent damping associated with the fluid alone is often less than optimal. In design, the screens are selected so that the TLD provides an optimal level of effective damping to the structure for a given response acceleration. However, as the structural acceleration deviates from this target value, the efficiency of the TLD is reduced.

To date, no published research work has been aimed at determining the influence that the geometry of the screens has on the TLD response. In this

investigation, the primary focus is to determine the influence that slat height has on the performance of a TLD. In particular, can the efficiency range of a structure-TLD system be extended by simply modifying the slat height?

1.2 *Research Scope and Objective*

The primary objective of this research program is to investigate the influence that screen geometry, in particular slat height, has on the performance of a tuned liquid damper. An extensive experimental program is conducted in order to measure the free surface response and base shear forces of a TLD with various screen geometries subjected to sinusoidal shake-table tests. Two numerical models are utilized in this study to compare the numerical and experimental results: one is based on linearized potential flow theory while the other utilizes nonlinear shallow water wave theory. These models are subsequently utilized to determine the influence that screen slat height has on the efficiency of a structure-TLD system subjected to random excitation.

1.3 *Organization of Thesis*

Chapter 2 contains the literature review and background information that corresponds to the topic of dynamic vibration absorbers. The theory of tuned mass and tuned liquid dampers is presented. A review of experimental work and real-world application is given.

Chapter 3 describes the experimental set-up and testing program that was undertaken in order to measure the response of a TLD subjected to sinusoidal shake-table tests.

Chapter 4 examines the experimental results of a TLD equipped with slat screens of different heights, corner geometries, and solidities. The influence of these parameters on the hysteretic response, free surface response, and base shear forces is discussed.

Chapter 5 presents two numerical models to investigate slat screens with a varying loss coefficient. Both a nonlinear model based on shallow water wave theory and a linearized potential flow model are used. A comparison between the numerical model predictions and the experimental results from Chapter 4 is presented.

Chapter 6 looks at the influence that slat screens with a varying loss coefficient have on the efficiency of a structure-TLD system. The ability of the system to maintain an optimal damping ratio over an increased range of structural accelerations is the primary focus.

Chapter 7 reviews the major findings from each chapter and presents some recommendations for future research work.

Chapter 2 : Literature Review and Background Information

This chapter begins by presenting the role of damping in the dynamic response of structural systems. The concept of equivalent viscous damping is presented and techniques used to calculate the damping ratio from experimental tests is discussed. Various forms of damping are outlined with the focus being on dynamic vibration absorbers, specifically, tuned mass dampers and tuned liquid dampers. The theoretical behaviour of a TMD is presented and used as an analogy for the development of TLD theory. Experimental work on the performance of TLD and their application is discussed and the impetus of this current study is presented.

2.1 *Damping*

Damping is a measure of a structure's ability to dissipate vibratory energy. In order to illustrate the importance of damping consider the single degree of freedom model shown in Figure 2.1 subjected to a force $P_o(t)$.

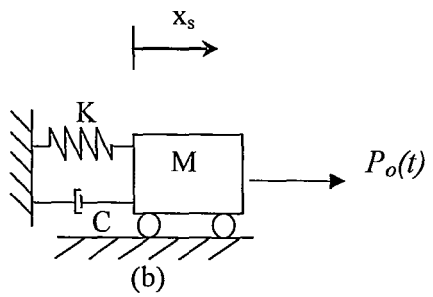

Figure 2.1 - Single Degree of Freedom Model

The equation of motion governing this system is a second order non-homogenous differential equation described in equation (2.1).

$$M\ddot{x}_S + C\dot{x}_S + Kx_S = P_o(t) \tag{2.1}$$

where M is the mass of the structure, C is the damping coefficient, K is the structural stiffness, and $P_o(t)$ is the applied force. The natural circular frequency, ω_n, is given in radians/sec as (Chopra, 2000)

$$\omega_n = \sqrt{\frac{K}{M}} \tag{2.2}$$

The critical damping coefficient of the structural system, C_{cr}, is given by (Chopra, 2000)

$$C_{cr} = 2M\omega_n \tag{2.3}$$

and the damping ratio, ζ, is expressed as (Chopra, 2000)

$$\zeta = \frac{C}{C_{cr}} \tag{2.4}$$

where the damping coefficient, C, is a measure of the energy dissipated in one cycle of free or forced vibration. If equation (2.1) is divided through by M, and equations (2.2) - (2.4) are substituted, the equation of motion describing the SDOF system in Figure 2.1 is given as

$$\ddot{x}_s + 2\zeta\omega_n\dot{x}_s + \omega_n^2 x = \frac{P_o(t)}{M} \tag{2.5}$$

The solution to equation (2.5) can be solved by standard differential equation techniques based on the initial conditions and loading. The steady-state deformation of the SDOF system due to the harmonic force, $P_o(t)$, can be express by a dynamic amplification factor R_d as (Chopra, 2000)

$$R_d = \frac{x_s}{x_{s-st}} = \frac{1}{\sqrt{\left[1-(\beta)^2\right]^2 + \left[2\zeta(\beta)\right]^2}} \tag{2.6}$$

where x_{s-st} is the maximum static displacement of the system and is calculated as $\frac{P_o}{K}$ where P_o is the amplitude of the applied force. The forcing frequency ratio, β, is the ratio of the applied frequency to the natural frequency of the system given as ω / ω_n. The phase angle between the applied force and the displacement of the system is given as (Chopra, 2000)

$$\theta = \tan^{-1}\left(\frac{2\zeta\beta}{1-\beta^2}\right) \tag{2.7}$$

If the special case of resonance ($\beta = 1$) is considered, (2.6) reduces to

$$R = 1/2\zeta \tag{2.8}$$

Equation (2.8) shows that the resonant response of the structure is controlled entirely by damping. In the analysis of wind-induced vibrations typical damping ratios for steel and concrete structures are 1.0% and 2.0%, respectively. In general, civil engineering structures have a damping ratio ranging from 1% to

10% (Chopra, 2000). Figure 2.2 is used to illustrate the relationship between the dynamic amplification factor, frequency ratio, and damping level.

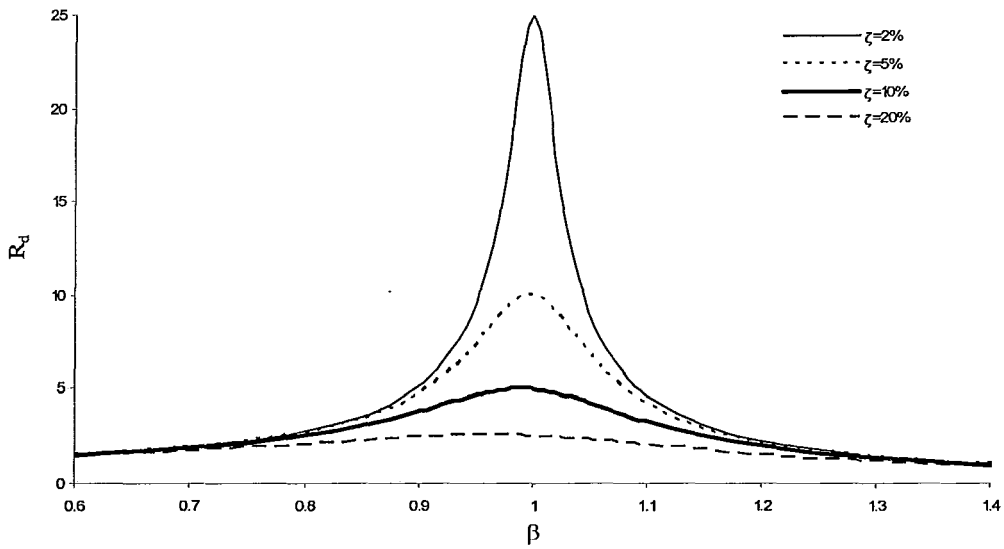

Figure 2.2 - Effect of Damping (ζ) on the Dynamic Amplification Factor (R_d)

Figure 2.2 shows the influence that damping has on the dynamic amplification of the system. For a lightly damped structure (ζ=2%) the amplification of the dynamic response is extremely high (*R*=25). This occurs because the structure dissipates only a small amount of energy in each cycle of excitation. This response can be mitigated by increasing the amount of damping until a desired response is achieved.

2.2 *Mathematical Representation of Damping*

Damping in structures is usually represented in a highly idealized manner. The aim is to match the damping raio, ζ, to the amount of energy dissipated by all

damping mechanisms. The most common model is the linear viscous damper where the damping force, F_D, is directly proportional to the velocity. However, in many applications the energy dissipated per cycle does not follow the viscous damper model. It is possible to define an equivalent viscous damper coefficient, ζ_{eq}, to use in analysis. The idea is to equate the energy dissipated per cycle in the real structure to that of an equivalent viscous system (Chopra, 2000). For a SDOF system subject to harmonic loading the equivalent damping ratio is given as (Chopra, 2000)

$$\zeta_{eq} = \frac{1}{4\pi\beta}\frac{E_D}{E_S} \tag{2.9}$$

where E_D is the energy dissipated in one cycle of vibratory motion and E_S is the elastic strain energy given as $kx_s^2/2$. Equation (2.9) can be used if the force-displacement relationship of the structure or system is known.

2.3 *Evaluating Structural Damping*

The damping ratio of a structure is a property that cannot be theoretically calculated in design. As such, experimental testing in a laboratory or in as-built conditions is required. The response of a structure can be considered a function of amplitude and damping. If a structure is excited by a known force then the experimental response can be compared to the theoretical response, and the corresponding level of damping can be computed. A brief overview of the

common techniques used to evaluate damping is provided in the following sections.

2.3.1 Free Decay

A structure is excited under an external force and then allowed to decay. The ratio of the amplitude of any two successive peaks separated by n periods for a lightly damped structure is related to the damping coefficient as

$$\zeta = \frac{1}{2\pi n} \ln\left(A_i / A_{n+1} \right) \tag{2.10}$$

The advantage of this technique is its simplicity. Its drawbacks are that this technique is generally limited to damping in the fundamental mode with weak nonlinearities and well separated natural frequencies (Blevins, 1977).

2.3.2 Half Power Bandwidth Model

The half power bandwidth method is a convenient approach used to determine the level of damping in a structure. The structural damping is related to the half power frequencies, ω_1 and ω_2, as

$$\zeta = \frac{\omega_2 - \omega_1}{2\omega_n} \tag{2.11}$$

The half power frequencies are the frequencies where the displacement response is equal to $1/\sqrt{2}$ times the maximum displacement (Chopra, 2000). The advantage of this technique is that is can be applied with only the knowledge of

the frequency-response of the structure. The disadvantages are that a complex measurement system is needed. If the amplitude of the exciting force is not held constant then an error in the order of ζ^2 is introduced. Finally, the bandwidth technique neglects any amplitude dependence.

Other techniques are available to estimate structural damping. These include Magnification Factor, Response Method, and the Energy Loss per Cycle Method. Discussion of these techniques can be found in Clough and Penzien (1975) and Blevins (1977).

2.4 *Forms of Damping*

Generally speaking, damping is generated by four mechanisms in a structural system: fluid damping, material damping, structural damping, and secondary vibration absorbers.

Fluid damping is the result of energy dissipated through viscous and pressure drag as the structure moves relative to the fluid (Blevins, 1977). The viscous drag is a result of shear layers, turbulent transition, and boundary layer separation. The pressure drag is caused by flow (wind) separating as it passes around corners of the building and forms a turbulent wake.

Material damping is caused by deformation of a member or structure. Blevins (1977) explains that as a block of material is loaded, the groups of atoms break down into smaller groups and crystal grains are rearranged. When the material is unloaded, not all of the energy can be released since some is lost due to

heat and molecular reorganization. After many loading, and unloading cycles, a load path is traced as shown in Figure 2.3 (Blevins, 1977) which forms the hysteresis loop for the material or structure. The area enclosed by the hysteresis loop is the amount of energy dissipated per cycle and is related to the level of damping.

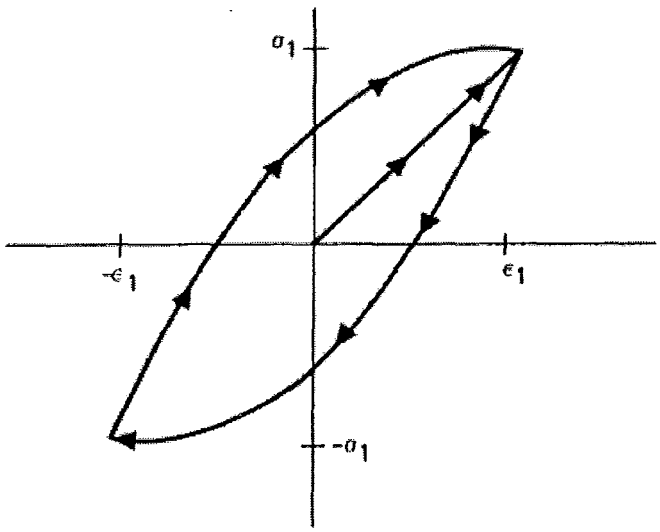

Figure 2.3 - Hysteresis Loop (Blevins, 1977)

Structural damping is a result of energy dissipated through friction at steel connections, opening and closing of micro cracks in concrete or masonry, and friction between non-structural members such as partitions and secondary framing (Chopra, 2000).

If the fluid, material, and structural damping do not provide enough damping to the system then the need may arise to install secondary vibration absorbers. These devices are designed specifically to increase the amount of energy dissipated under wind and seismic excitation. Examples include metallic dampers, friction dampers, viscoelastic dampers, viscous fluid dampers, tuned

mass dampers, tuned liquid column dampers, and tuned liquid dampers. Theory and application of these devices can be found in Soong and Dargush (1997) and a discussion of tuned liquid dampers and tuned mass dampers is presented in a later section.

2.5 *Structural Response*

This section begins by introducing the concept of root mean square (RMS) and peak structural response. A discussion on human perception of wind-induced vibrations follows. The section concludes with a comparison of perception limits based upon different building codes.

2.5.1 Root Mean Square Response vs Peak Response

The RMS response of a structure is measured as the standard deviation of the buildings displacement or acceleration over a desired time period (commonly one hour). Conversely, the peak response is taken as the average of the maximum hourly response for a set period of time (i.e. eight hours). The peak response can be obtained from the RMS response through a peak factor given by Davenport (1964) as

$$PF = \sqrt{2\ln(\nu T_o)} + \frac{0.5772}{\sqrt{2\ln(\nu T_o)}} \tag{2.12}$$

where ν is the cycling frequency and T_o is the averaging time.

2.5.2 Human Perception to Wind-Induced Vibration

With the trend towards taller, lighter, and more flexible structures the wind-induced vibrations at a serviceability limit state must be carefully examined. While the design strength of the structure may be sufficient, the structure may still undergo large displacements or accelerations causing discomfort to its occupants. The wind-induced motions trigger responses that may include; concern, anxiety, fear, vertigo, dizziness, headaches, and nausea (McNamara et. al, 2002). Perception limits have traditionally been determined by subjecting humans to motion simulators in a moving room. However, these tests were conducted under sinusoidal excitation and in the absence of video or audio cues. An investigation by Hansen et al. (1973) determined that there is also a frequency dependence on perception levels since with a decreasing frequency of oscillations there is an increase in perception levels. This led to work by Irwin (1983), which has become the ISO 6897 standard, accounting for the period of oscillations in the perception limits. In North America it is common practice to use peak hourly structural accelerations, limiting accelerations to 10-15 milli-g at the top floor of a residential building and to 20-25 milli-g in office buildings (Isyumov, 1993). This is based on a 10 year return period. A comparison between annual occurrence and peak hourly horizontal accelerations is shown in Figure 2.4.

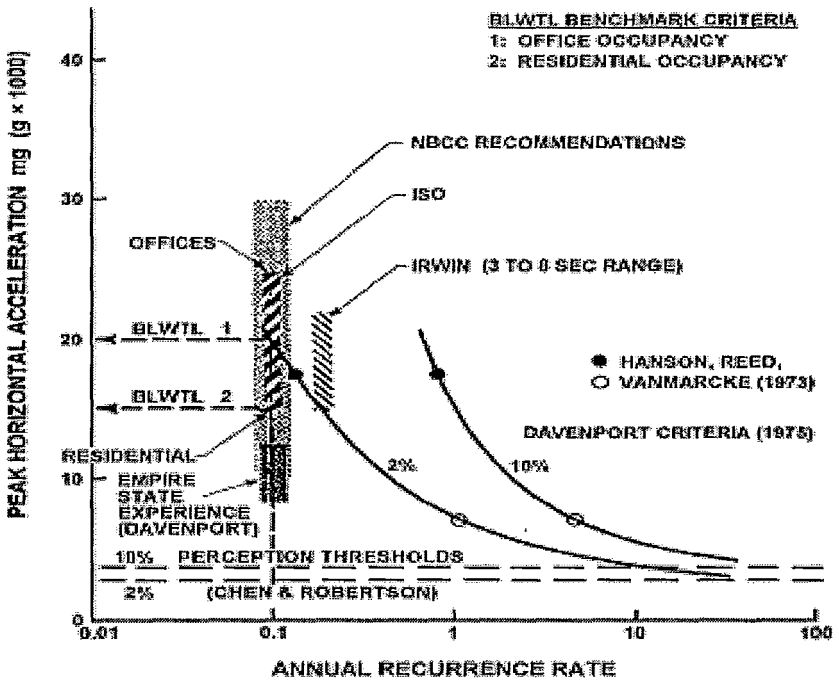

Figure 2.4 - Wind-Induced Acceleration Criteria (Boggs, 1995)

Figure 2.4 compares the target peak hourly structural acceleration for various building occupancies. The National Building Code of Canada (NBCC) provides guidelines on allowable structural accelerations of up to 15 milli-g for residential buildings and up to 25 milli-g for office buildings corresponding to a 1 in 10 year return period. The Boundary Layer Wind Tunnel Lab (BLWTL) at the University of Western Ontario uses its own benchmark criteria which limits the peak acceleration of an office building and residential building to 20milli-g and 15milli-g, respectively.

2.6 *Dynamic Vibration Absorbers*

Commonly, dynamic vibration absorbers (DVA) are installed in a structure in order to reduce its susceptibility to wind-induced vibrations and to meet peak acceleration limits. The concept of the DVA can be traced to work accredited to H. Frahm in 1909 (Den Hartog, 1956). The theory was developed to solve problems associated with the rolling of large tankers in rough seas. Large tankers have their own natural frequencies but were commonly exposed to large disturbing couples caused by the rolling motion of the sea. Large displacements occurred when the waves were close to the natural frequency of the ship. In 1902, Frahm installed two tanks half filled with water that communicated through a water pipe below, and an air valve above (Figure 2.5). The anti-rolling tanks were installed on large German liners and although the technology has been improved with time, they formed the basis for the dynamic vibration absorber that is used today.

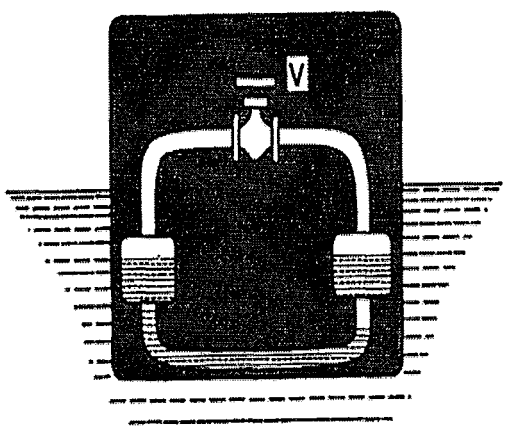

Figure 2.5 - Frahm's Anti-rolling Tanks (Den Hartog, 1956)

Today, the most common type of vibration absorber used in structural engineering is the tuned mass damper. The concept for the TMD stems from work done by Frahm in 1909 and theoretical work published by Ormondroyd and Den Hartog in 1928.

2.6.1 Mathematical Derivation of DVA Behaviour

Consider the following system (Figure 2.6) where M^*, K^*, and C^* are the generalized mass, stiffness, and damping of the main structure. A DVA with mass M_A, stiffness K_A, and damping C_A is attached to the main structure. The system is excited by an external harmonic force of amplitude P_o.

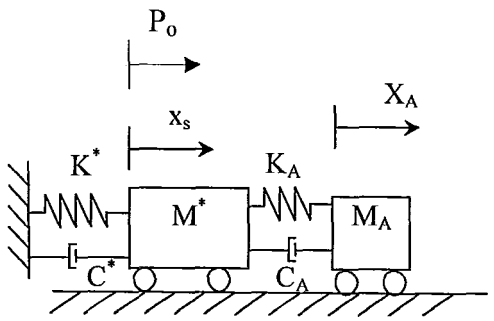

Figure 2.6 - Mechanical Representation of Secondary Auxiliary Mass

The equations of motion governing the main mass (2.13) and the secondary mass (2.14) are given as

$$M^*\ddot{x}_s + C^*\dot{x}_s + K^*x_s = P_o + C_A(\dot{x}_s - \dot{x}_A) + K_A(x_s - x_A) \tag{2.13}$$

$$M_A(\ddot{x}_A - \ddot{x}_s) + C_A(\dot{x}_A - \dot{x}_s) + K_A(x_A - x_s) = -M_A\ddot{x}_S \tag{2.14}$$

Summation of (2.13) and (2.14) leads to the equation of motion of a structure with a secondary mass attached and is given as

$$(M^* + M_A)\ddot{x}_s + C^*\dot{x}_s + K^*x_s = P_o - M_A(\ddot{x}_A - \ddot{x}_s) \tag{2.15}$$

Thus, it is evident from equation (2.15) that the effect of adding a secondary mass to the main system, aside from slightly increasing the natural frequency due to M_A, is the addition of an inertial force term $M_A(\ddot{x}_A - \ddot{x}_s)$. This inertial force term is dependent on the absorber mass and the relative acceleration between the absorber and structure. If the special case of $C_A = C^* = 0$ is considered it can be shown that the main mass remains completely stationary if the natural frequency of the attached absorber is set equal to the frequency of the exciting force. This occurs because the absorber mass vibrates 180° out of phase to the applied force (Den Hartog, 1956) resulting in no net force being applied to the structure.

2.6.2 Dynamic Vibration Absorbers and Structural Response

The first published work on the topic of DVA-structure interaction was made by Den Hartog in 1928. He examined the efficiency of a TMD by comparing the dynamic response of an undamped structure to the static response. This solution is

commonly known as the Den Hartog solution and is adapted by Soong and Dargush (1997) as

$$R = \frac{x_s}{(x_s)_{st}} = \sqrt{\frac{\left(\Omega^2 - \beta^2\right)^2 + \left(2\zeta_a \Omega\beta\right)^2}{\left[\left(\Omega^2 - \beta^2\right)\left(1 - \beta^2\right) - \Omega^2\beta^2\mu\right]^2 + (2\zeta_a\Omega\beta)^2\left(1 - \beta^2 - \beta^2\mu\right)^2}} \quad (2.16)$$

where R is the dynamic amplification factor, Ω is the tuning ratio given as

$$\Omega = \frac{f_a}{f_s} \quad (2.17)$$

where f_a is the natural frequency of the absorber and f_s is the natural frequency of the structure. The mass ratio, μ, is defined as

$$\mu = \frac{m_a}{M} \quad (2.18)$$

where m_a is the absorber mass. ζ_a is the damping ratio of the absorber and is found through equation (2.3) and equation (2.4). To illustrate the influence that a DVA has on the response of a structure, a perfectly tuned (Ω=1) TMD with a mass ratio of 5% is attached to a SDOF system and the frequency response is compared to the same structure without a damper in Figure 2.7.

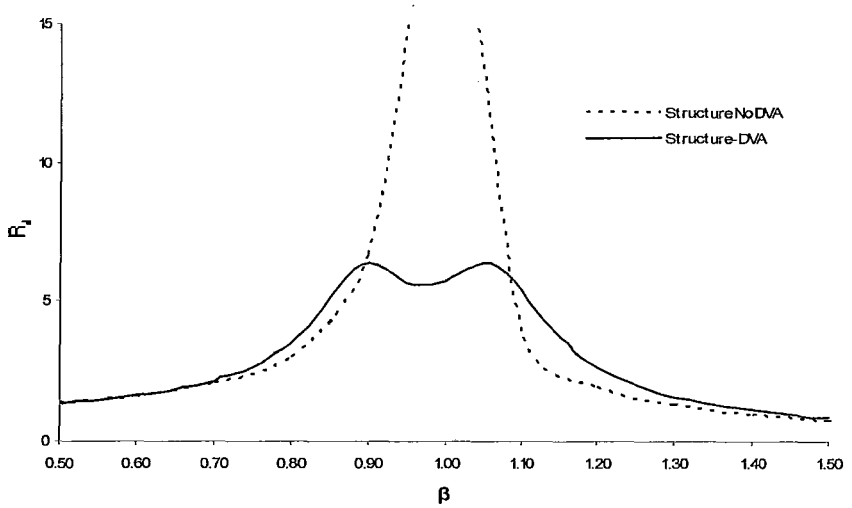

Figure 2.7 - Frequency Response of Structure with and without a DVA

This figure illustrates that the dynamic vibration absorber modifies the frequency response of the system and reduces the peak response of the structure. Conceptually, the DVA functions by adding effective damping (ζ_{EFF}) to the structure. For a structure subjected to random excitation the amount of additional effective damping can be quantified by comparing the area under the dynamic amplification curve for a SDOF structure to that of a structure-damper system.

2.7 *Overview of Research on Tuned Mass Dampers*

Considerable work has been done on TMD's. Den Hartog (1956) was the first to publish a theory that accounted for a damped vibration absorber attached to an undamped system. Damping in the main system was included in the analysis of dynamic vibration absorbers by Bishop and Welbourn (1952). Further research in the area is reviewed in detail by Soong and Dargush (1997) and includes optimum absorber parameters (Warburton, 1982), dampers aimed at reducing

bending and torsion effects, and dampers utilized to broaden the operational frequency range over which they are most efficient.

In practice a TMD consists of a secondary auxiliary mass that is attached to a structure through a spring and a dashpot. It is typically located at the level of the building where the maximum response occurs. The TMD works by imposing an inertial force on the structure that is in the opposite direction of the applied loads and its effectiveness is dependent on their dynamic characteristics, stroke, and mass (Kareem, 1983).

2.7.1 Application of Tuned Mass Dampers

Tuned mass dampers and their variations constitute the majority of secondary damping systems currently used in modern structures (Kareem et al., 1999). William LeMessurier, the structural engineer responsible for the design of the Citicorp building in New York is credited with developing the first TMD for installation in the United States. The 410 tonne damper, shown in Figure 2.8, was installed in the 915ft. (279m) tall Citicorp building in New York in 1977 (Figure 2.9).

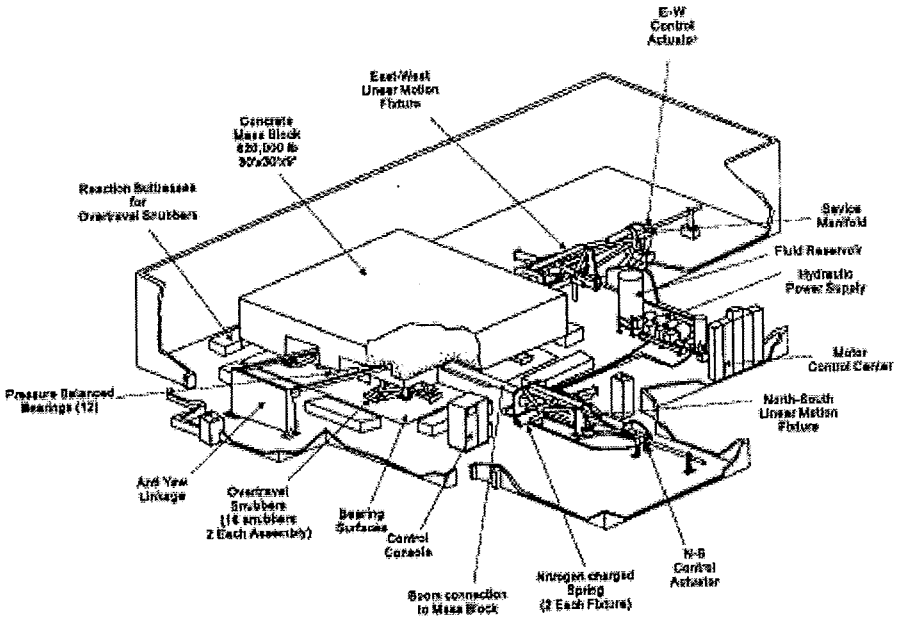

Figure 2.8 - Tuned Mass Damper Used for Citicorp Building (Soong and Dargush, 1997)

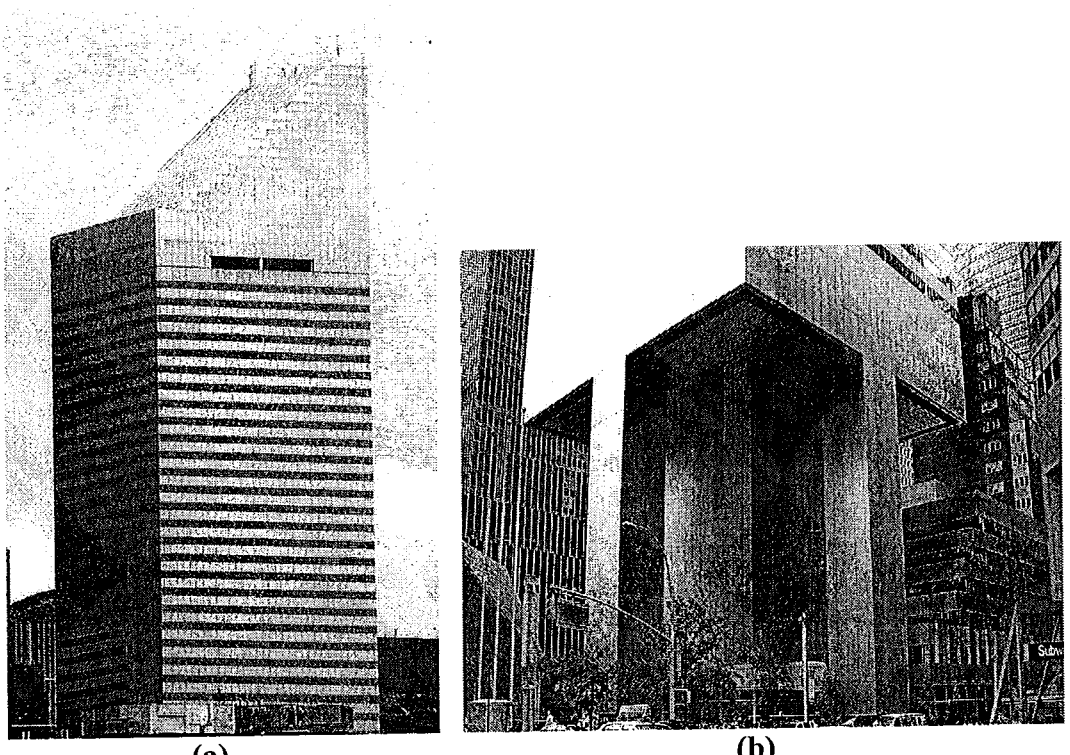

(a) **(b)**

Figure 2.9 - Citicorp Building, New York, NY. (a) Structure (b) Base (www.skyscrapers.com)

This unit measures 9.14m x 9.14m x 3.05m and consists of 340 tonnes of concrete connected to the structure through a two-spring damping mechanism. One system was installed to mitigate north-south motion while the other was in place for east-west motion. The system was designed to become active at 3 milli-g's of acceleration and is monitored by computer controlled actuators to ensure that it behaves as a bi-directional TMD (Soong and Dargush, 1997). It was found that the system reduced the structural motion by 40% in both the east-west and north-south directions (Soong and Dargush, 1997).

Shortly after LeMessurier had completed his work on the Citicorp TMD he was hired by the owner of the John Hancock Building in Boston, Figure 2.10, to help reduce the wind-induced accelerations of the building. Many upper-floor occupants had suffered from motion sickness when the structure swayed in the wind.

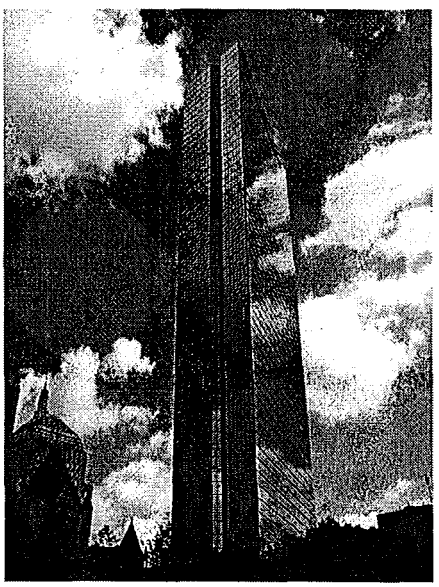

Figure 2.10 - John Hancock Building in Boston, MA (www.skyscrapers.com)

Two TMD's were installed in June 1977 at opposite ends of the 58th floor in order to counteract torsional moments. Each unit was 5.2m x 5.2m x 1m and was a steel filled box weighing approximately 270 tonnes. The system was designed to be active at 3 milli-g's of excitation (Campbell 1995) and was able to reduce the structural motion by 50% (Wiesner 1979).

Tuned mass dampers have been used extensively since they were first installed in New York and Boston. Currently, the world's tallest structure, Taipei 101 , has the world's largest TMD in operation and is shown in Figure 2.11.

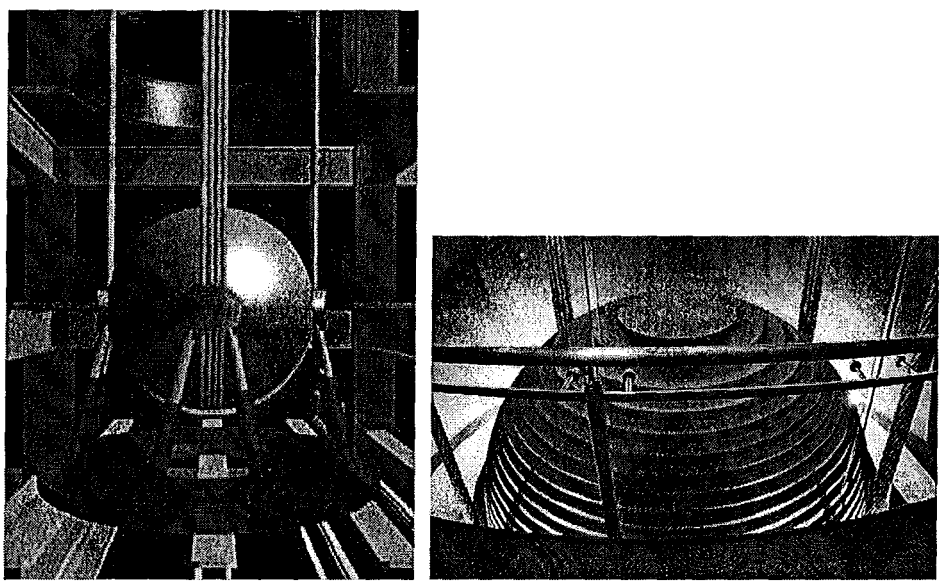

(a) (b)

Figure 2.11 - Tuned Mass Damper in Taipei 101 (a) Schematic (b) View from Restaurant (www.taipei-101.com)

The 660 tonne tuned mass damper (Figure 2.11 (a)) is installed between the 88th and 92nd floors of the structure. Too heavy to be lifted by a crane the damper was assembled on-site and is comprised of 41 steel plates. The damper hangs from

eight 3.5"(89mm) thick cables and is supported by eight viscous dampers that act like shock absorbers when the ball sways. The damper is able to move 5 ft. (1.5m) in any direction and is viewable from restaurants, bars, and observation decks near the 88^{th}-92^{nd} floors (Figure 2.11 (b)).

TMDs have also been widely used in bridge engineering. Most notably in the construction of cable-stayed bridges where the cable stays are sensitive to vortex shedding. In addition, the TMD can also be used to reduce the wind-induced vibration of the bridge pylons during the construction process. These installations appear to be most common in Japan with applications to Aratsu Bridge, Yokohama Bay Bridge, and the Bannaguru Bridge (Holmes, 1995).

Other notable installations of TMD's include the Trump Towers in New York, Bally's-Bellagio in Las Vegas, London Millenium Bridge, and the Burj Al Arab in Dubai. For a comprehensive listing of auxiliary damping system installations see Kareem et al. (1999) and Holmes (1995).

2.8 *Tuned Liquid Damper*

A tuned liquid damper is a vibration absorber that is comprised of a tank which is partially filled with a fluid, commonly water, and utilizes the inertial force of the sloshing fluid to suppress the dynamic response of the structure. Typically, it is installed at the rooftop level of the structure. It can be used to mitigate the dynamic resonant response of a structure and it is often designed to reduce the structure's acceleration at a serviceability limit state. A 1:10 scale model of a 1-D TLD is shown Figure 2.12.

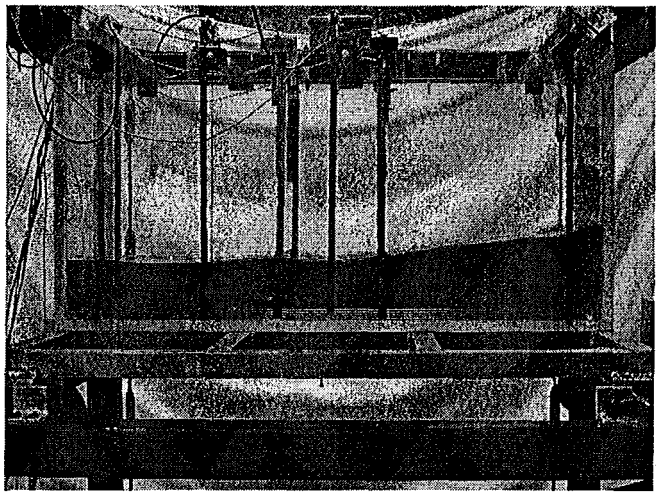

Figure 2.12 - Tuned Liquid Damper Photograph

A TLD operates analogous to that of a tuned mass damper and most of the theory developed for the TMD can be applied directly to a TLD. The effectiveness of the TLD is obtained by tuning the natural frequency of the device to the natural frequency of the structure so that when excited, the damper will resonate out of phase with the structure's motion.

Historically, the TLD has been categorized as a form of nutation damper. The geometry of this class of dampers includes toroidal, circular, U-shaped, and rectangular devices (Modi and Munshi, 1998). They have been in use for many decades and were initially used to control the librational motion of satellites (Figure 2.13) which had periods ranging from 1.5h to 24h (Modi and Munshi, 1998). Modi recognized that most bluff geometries operated under a frequency of 1Hz and decided to apply the nutation damper theory to this class of problems. Modi, along with other researchers have carried out parametric studies on various

aspects of sloshing dampers (Modi and Welt, 1985; Welt and Modi,1992; Modi and Seto, 1995)

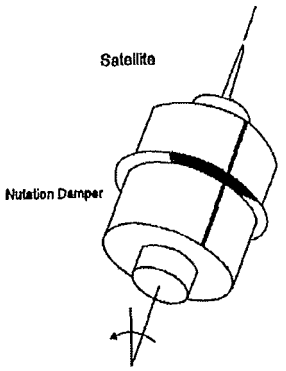

Figure 2.13 - Nutation Damper Used for Satellites (Fujino et al., 1988)

Tuned Liquid Dampers are being incorporated into new or existing buildings by modifying the existing water storage tanks often used for fire protection. Popularity in their use has grown since little additional mass is added to the structure and the device requires minimal maintenance. Furthermore, the device is easy to operate and modifications in its design can be made by simply adjusting the water depth or tank length.

2.8.1 Mathematical Representation of a Structure-TLD System

The mechanical model representing a structure-TLD system is similar to the DVA-structure model presented in Section 2.6.1. The main difference between the previously presented model and the TLD model is that not all of the fluid mass participates in the sloshing motion. Figure 2.14 illustrates how the multi-degree of

freedom structure-TLD system is represented as an equivalent two degree of freedom system.

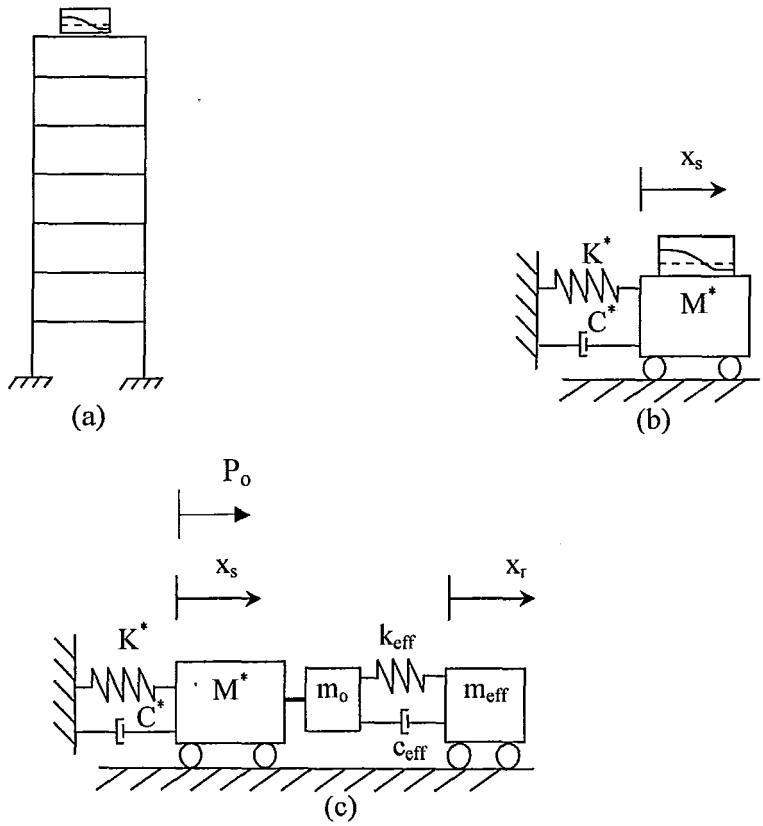

Figure 2.14 - Mechanical Model of a Structure-TLD System

Figure 2.14(a) represents a MDOF structure with a TLD attached at the rooftop level. This system is represented in Figure 2.14(b) as an equivalent SDOF structure with an attached TLD. The values of M^*, K^*, and C^* correspond to the generalized mass, stiffness, and damping of the structure in the mode of vibration that is being investigated. Figure 2.14(c) presents the equivalent two degree of freedom system where m_o is the mass of the fluid that does not participate in the sloshing motion of the fluid. The effective mass, m_{eff}, is the portion of the fluid

that contributes to the fundamental sloshing of the contained fluid. It can be estimated based on potential flow theory as (Graham and Rodriguez, 1952)

$$m_{eff} = \frac{8\tanh\left(\pi\frac{h}{L}\right)}{\pi^3\left(\frac{h}{L}\right)} m_w \tag{2.19}$$

where h is the quiescent fluid depth, L is the tank length, and m_w is the total mass of the fluid. The equations of motion describing Figure 2.14(c) can be derived similar to Section 2.6.1 and are given as

$$\begin{bmatrix} M^* + m_o & m_{eff} \\ m_{eff} & m_{eff} \end{bmatrix} \begin{bmatrix} \ddot{x}_s \\ \ddot{x}_r \end{bmatrix} + \begin{bmatrix} C^* & 0 \\ 0 & c_{eff} \end{bmatrix} \begin{bmatrix} \dot{x}_s \\ \dot{x}_r \end{bmatrix} + \begin{bmatrix} K^* & 0 \\ 0 & k_{eff} \end{bmatrix} \begin{bmatrix} x_s \\ x_r \end{bmatrix} = \begin{bmatrix} P_o \\ 0 \end{bmatrix} \tag{2.20}$$

2.8.2 Application of Tuned Liquid Dampers

Nagasaki Airport Tower (NAT)

The Nagasaki Airport Tower was constructed in 1974 on an artificial island surrounded by the Omura Bay in Nagasaki Prefecture. The air traffic control tower is a steel framed tower, placed on a low-rise reinforced concrete building at its base. Full scale measurements of the tower equipped with liquid dampers was investigated in 1987. An assemblage of 25 cylindrical vessels containing only water, were installed on the floor of the air traffic control room and stair landings for two weeks. Full-scale measurements were taken over a one month period. Results showed that without a TLD the structure had a damping

ratio of 0.93%. As the number of TLD vessels increased from 7,14,19, to 25 the amount of damping was 2.2%, 3.1%, 4.1%, to 4.7% (Tamura et al., 1995)

Yokohama Marine Tower (YMT)

The Yokohama Marine Tower is a steel trussed structure with a height of 101.3m and has the highest lighthouse in the world atop. TLDs were installed in June 1987 and are similar to the one installed at the Nagasaki Airport Tower. In total 39 cylindrical multilayered vessels containing water were installed at the top of the tower. Free oscillation tests were conducted on the tower and it was found that the damping ratio was 4.5% with the TLD installed, which is seven times larger than the damping ratio without a TLD (Tamura et al, 1995).

Shin-Yokohama Prince Hotel (SYPH)

The Shin-Yokohama Prince Hotel was constructed in 1992 and is a cylindrical structure with a height of 149m and a diameter of 38.2m (Tamura et al., 1995). The TLD was installed on the roof floor in March 1992 and is an assembly of 30 cylindrical multilayered vessels that contain only water. A variation in this design included 12 protrusions within the vessel to stop the swirling motion of the liquid and to increase energy dissipation. In this structure-TLD system, a 50% reduction in the RMS acceleration was obtained (Tamura et al., 1995).

Tokyo International Airport Tower (TIAT)

The Tokyo International Airport Tower was constructed in 1993 alongside a new air traffic control tower situated in the Tokyo Bay area. The tower is 77.6m high

and has the control room located near the top on two vertical shafts. A total of 1400 tanks containing water and floating particles, which increase the energy dissipation of the fluid, were installed in the tower. Full scale measurements of wind-induced responses were observed for a period of 13 months. The average damping value for the structure without a TLD was 1.2%. A significant improvement in the damping values was observed as the damping ratio increased to 7.6% with the addition of the TLD with floating particles. It is estimated that 6% of the additional damping is attributed to the presence of the floating particles. A summary of the full-scale measurements is presented in Table 2-1.

Table 2-1: Summary of Full Scale Measurements on the Effectiveness of TLDs

Structure	Height (m)	Mass Ratio	ζ_s	$\zeta_s + \zeta_{TLD}$
NAT	42	0.56	0.9	2.2
YMT	101.3	0.29	0.6	4.5
SYPH	149.4	0.39	1.0	N/A
TIAT	77.6	0.70	1.2	7.6

The two most recent applications of TLD's in Canada are in One Wall Centre in Vancouver, BC, and One King West in Toronto, ON.

Figure 2.15 – One Wall Centre (Left) and One King West (right)

One Wall Centre

One Wall Centre is the tallest structure in Vancouver measuring 150m (491ft.). It is a slender glass structure with an elliptical footprint having a 7:1 aspect ratio. Two tuned liquid column dampers (TLCD) were designed to control expected wind-induced vibrations that would have caused discomfort to the occupants. Each TLCD consists of a 4 storey high, 50,000 gallon (230 ton) water tank and is oriented across the narrow aspect of the building. This solution was the first of its kind in the world and saved an estimated $2,000,000 in construction costs compared to other damping systems. Additional cost savings were realized by using the TLCD as a water storage tank for fire suppression (Motioneering, 2004).

One King West

One King West in Toronto is a newly constructed residential-commercial structure built upon the historic 1912 Dominion Bank Head Office in downtown Toronto. The 51-storey structure is the most slender structure in the world (11:1 aspect ratio) and is considered the tallest residential building in Canada (Cement, 2006). Two insulated concrete TLDs are equipped with damping screens and are located on the 51st floor. The units are 12x9x2m in size and are divided into 5 sub chambers to ensure the water flows in the East-West direction, which is the critical direction for this building. This application of TLD's is the first of its kind in Canada.

2.8.3 Review of Experimental Work

The major source of inherent damping generated by the fluid contained inside a TLD is due to viscous dissipation between the fluid at the tank side and end walls. Fediw (1995) discussed contributions from capillary hysteresis (surface tension) in and near the surface but found that for the tanks used in this application the contribution was minimal. Furthermore, it is known that wave-breaking of the free surface provides a significant increase in the inherent damping but tends to alter the natural frequency of the TLD (Sun and Fujino, 1994). This will lead to mistuning which causes an overall reduction in the efficiency of the TLD (Tait et al. 2005).

In general, TLDs that do not incorporate additional damping mechanisms provide inherent damping values in the order of 0.5% while the target damping

value is the order of 3-10% (Tait et al., 2005). Modi and Welt (1992) have carried out studies aimed at improving the energy dissipation characteristics of a TLD by placing objects (wedges) at the base of the tank, adding small particles to the liquid to increase collision rates of particles, and experimented with different liquids.

In 1998, Modi and Munshi conducted a parametric free vibration study aimed at optimizing the size and location of a flow obstructing object. They found that a 60% increase in the energy dissipated was achieved by placing semi-circle cylinders along the base of the tank. It was found that the presence of an obstacle led to a higher damping value over an extended range of liquid frequencies. Furthermore, the authors conducted an extensive wind tunnel test program to substantiate the effectiveness of the new damper on suppressing building motions. They demonstrated that the damper reduced the vibration amplitude during galloping by 55% and that the introduction of an optimum obstacle substantially reduced the mass ratio required for vibration control of full-scale structures.

Recently, Modi et al. (2003) conducted a parametric study aimed at increasing the energy dissipation characteristics of a TLD by utilizing two-dimensional objects along with floating particles. The object that provided the largest increase in energy dissipation was a wedge with an angle at 4° relative to the bottom of the tank. This lead to a 20% increase in the damping. Using particles that have a 30% seeding density (fraction of surface area covered with particles), and a wedge at 4°, the damping increased by 40%. Furthermore, by

roughening the surface of the wedge, and drilling small diameter holes, an increase in the damping of roughly 88% was obtained.

Fediw (1992), Tait (2004), and Cassolato (2007), have investigated the use of damping screens to help increase the damping of the TLD. Fediw conducted work at the University of Western Ontario in the early 1990's. His work centered on understanding and improving the performance of a one dimensional sloshing damper (TLD). The main objective in his work was to improve the inherent damping of a TLD. His work required a TLD with an inherent damping value in the range of 5 – 10% while the water-only tank in use had an estimated damping of 0.5%. Several different approaches were considered but it was decided to install sharp-edged lattice screens (Figure 2.16) in the high velocity region of the tank .

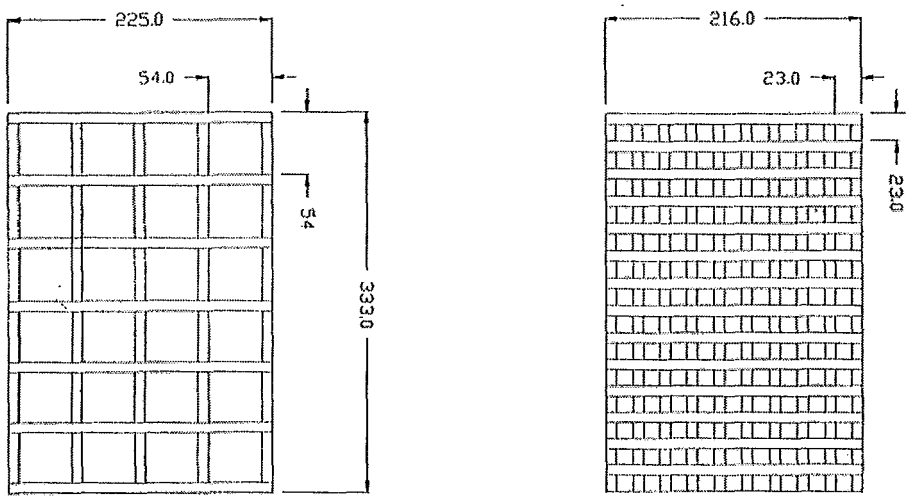

(a) (b)

Figure 2.16 - Lattice Screens Used in Fediw Study (a) S=0.30 (b) S=0.60 (Fediw, 1992)

Fediw conducted his study using one screen, two screens, and four screens and their locations are outlined in Table 2-2.

Table 2-2 : Location of Damping Screens in Fediw's Study

Number of Screens	Locations
1	0.5L
2	0.4L and 0.6L
4	0.3L, 0.4L, 0.6L and 0.7L

Theoretically, the pressure losses across the screen would increase the energy dissipated and hence the effective damping (Fediw et. al 1995). Linear wave theory was used to describe the motion of the fluid within the tank while a nonlinear velocity loss coefficient was used to account for the increase in damping that occurs near resonance.

Experimental work was conducted to determine the loss coefficient of the screens and the performance of the TLD as a unit. It was found that lattice screens were effective in increasing the damping of the TLD and that increasing the number and/or solidity of screens resulted in a more linear TLD response. Furthermore, a study aimed at determining the effect of adding a TLD to a structure was completed. It was found that the response of the structure was significantly reduced by the presence of the TLD and that the nonlinearities observed for the TLD alone did not have a negative impact on the performance of the TLD-Structure system (Fediw et al., 1995).

Tait et al. (2005) carried out a rigorous parametric study on both a 1-D and 2-D TLDs and examined the effect of screen location and number of screens. He compared the experimental results to both linear and nonlinear models. The two models were studied for a range of excitation amplitudes and the resulting base shear forces, wave heights, and amount of energy dissipated were compared to the predicted values using both models. It was found that the overall performance of the TLD was improved by adding damping screens.

The efficiency (ψ) of a TLD is often denoted as a function of the amount of effective damping (ζ_{eff}) that it provides to the primary structure given as

$$\psi = \frac{\zeta_{eff}}{\zeta_{eff-opt}} \tag{2.21}$$

The effective damping is the amount of additional linear viscous damping that must be added to the primary structure in order to reduce its response to the same level as that of the structure-TLD system (Vickery and Davenport, 1970). The optimal amount of effective damping, $\zeta_{eff-opt}$, has been derived by Warbuton (1982) for a linear DVA (TMD) attached to an undamped structure subjected to white noise excitation and is given as

$$\zeta_{eff-opt} = \frac{1}{4}\sqrt{\frac{\mu+\mu^2}{1+\frac{3\mu}{4}}} \tag{2.22}$$

Tait et al. (2005) found that the efficiency of the system increased 300% from the water only case to the case with screens installed. This result illustrated that a

TLD must possess a level of inherent damping near the optimal value, otherwise a significant reduction in efficiency will be observed. Further, it was found that three screens located at 0.25L, 0.50L, and 0.75L provided the largest reduction in the amount of energy dissipated and were less impacted by nonlinearities when compared to 1 and 2 screen tests.

A major part of Tait's work was aimed at ascertaining the applicability of the linear and nonlinear models. It was found that the linear model adequately predicts the energy dissipating characteristics of the TLD. However, it is does not provide realistic estimates of the free surface response or base shear forces. Conversely, the nonlinear model accurately describes the free surface response, base shear forces, and energy dissipation characteristics over the range of amplitudes that were tested (Tait, 2004).

2.9 *Tuned Liquid Damper Efficiency*

As mentioned previously, the major disadvantage of a TLD in comparison to other Dynamic Vibration Absorbers is its nonlinear dynamic response which creates a more complex analysis and design process. This results in a damping device that does not function with optimal efficiency if the excitation varies from the design target response (Figure 2.17).

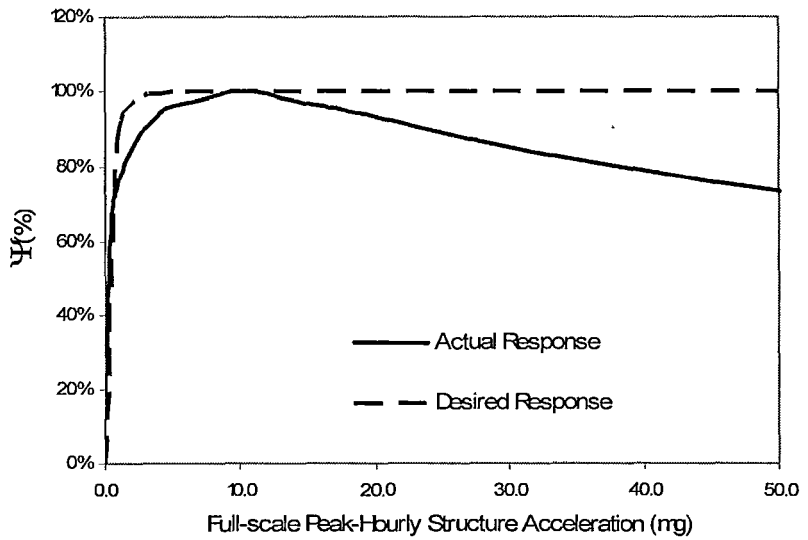

Figure 2.17 - TLD Efficiency vs Peak Hourly Acceleration

It can be seen that for a target response level of 10 milli-g, the TLD is operating at approximately 100% efficiency. As the excitation deviates from the target level there is a drastic reduction in the overall efficiency. Due to the stochastic nature of wind and seismic loading, it is preferred to have a damper system that has a broader range of efficiency shown by the dashed line. This has been the aim of recent work completed by Cassolato (2007). It has been shown that a major reason for this lack of efficiency in TLD performance is the nonlinear losses that occur through the screens (Cassolato and Tait, 2005). Therefore, it is desirable to utilize a screen geometry that generates a linearized response.

Cassolato (2007) investigated the effect of screen angle on the performance and efficiency of a TLD. Previously, Fediw (1992) and Tait (2004) had conducted research based on vertical screens that have a constant drag coefficient. Yeh and Shrestha (1989) showed that screen losses are a function of

orientation angle. Cassolato (2007) proposed a 'smart screen' that rotated as the fluid response increased. Theoretically, this produces a loss coefficient that is a function of fluid response and resulted in a structure-TLD system that operated at 100% efficiency over a broad range of amplitudes. The difficulty that Cassolato had was ensuring that the screens rotated to the target angle without the use of an external control. Therefore, while his work showed positive theoretical results, it may be most applicable in a semi-active TLD application.

2.9.1 Increasing TLD Efficiency Through Damping Screens

Work by Fediw et al. (1995) and Tait et al. (2005) was based on sharp-edged screens that had a constant drag coefficient. Some initial analytical work was completed using a linear mathematical model in MATLAB. The objective of this work was to determine the effect that the drag coefficient had on the energy dissipation characteristics of a TLD (Figure 2.18). The analysis was completed on a TLD equipped with two damping screens located at 0.4L and 0.6L, with a drag coefficient of 5.16 and a solidity ratio of 42%.

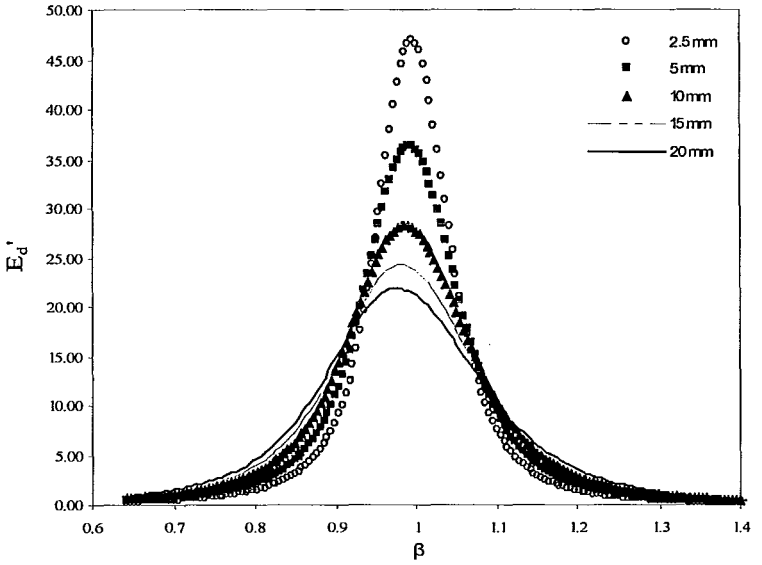

Figure 2.18 - Energy Dissipation vs Amplitude (Constant Drag Coefficient)

Figure 2.18 demonstrates the amplitude dependence of the TLD response. For a linear DVA the response of the system, in this case the amount of normalized energy dissipated per cycle, would remain constant as the excitation amplitude changed. However, for a TLD equipped with damping screens having a constant loss coefficient the normalized energy dissipated per cycle is amplitude dependent. Further analysis was conducted in order to determine the required loss coefficient that would generate a linear response over the full range of amplitudes. This was quantified by varying the drag coefficient until the peak value from the energy dissipation plots was equal for two different amplitudes. The resulting relationship between drag coefficient and amplitude is shown in Figure 2.19.

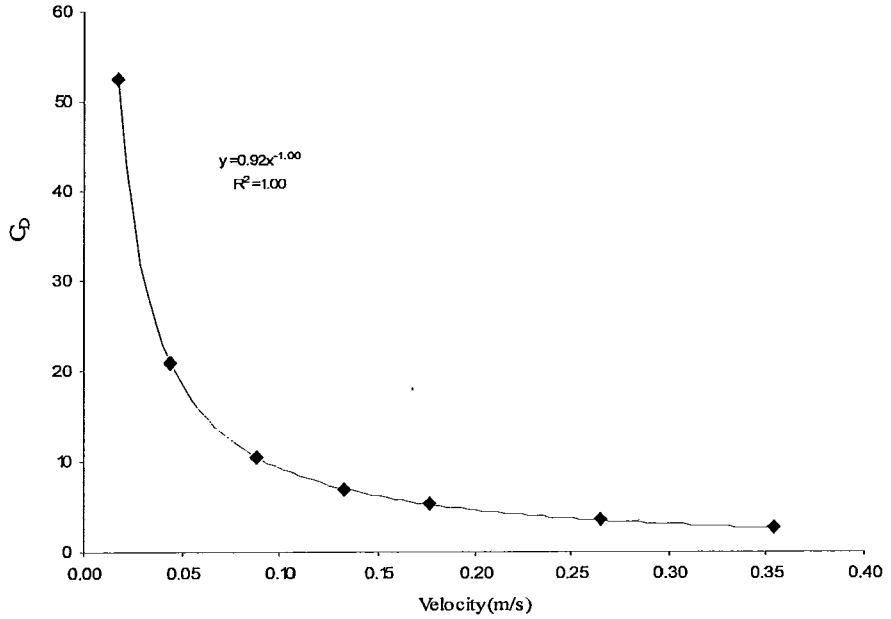

Figure 2.19 – Drag Coefficient vs Velocity at Screen

It is evident from Figure 2.19 that in order to have a TLD that is amplitude independent the energy losses from the screens must be inversely proportional to the velocity. It is the objective of this current work to investigate slat screens of different geometry in order to determine their effect on both the drag coefficient and efficiency of the TLD.

2.9.2 Keulegan-Carpenter Work

Research on flow past submerged bluff bodies has been covered in great detail. Factors such as Reynolds number, object geometry, and drag have all been correlated for the case of laminar and turbulent flow in a non-oscillating fluid. In the late 1950's, Keulegan and Carpenter published work on the forces acting upon plates and cylinders in oscillating flow (Keulegan and Carpenter, 1958). Their

work involved calculating the inertial and drag coefficients of cylinders and plates in simple sinusoidal flow. They were unable to find a relationship between the Reynolds number and the drag force, results that have been verified more recently (Sarpkaya, 1975). However, Keulegan and Carpenter were able to show a correlation between the drag coefficient of a plate or cylinder and a period parameter known commonly as the Keulegan-Carpenter (*KC*) number. The *KC* number is defined as:

$$KC = \frac{U_m T}{D} \tag{2.23}$$

where U_m is the maximum amplitude of velocity at the object (screen) after one half cycle of oscillation, T is the excitation period, and D is the width of the object perpendicular to the flow. The relationship between drag and the *KC* number for a thin plate as determined by Keulegan and Carpenter is shown in Figure 2.20.

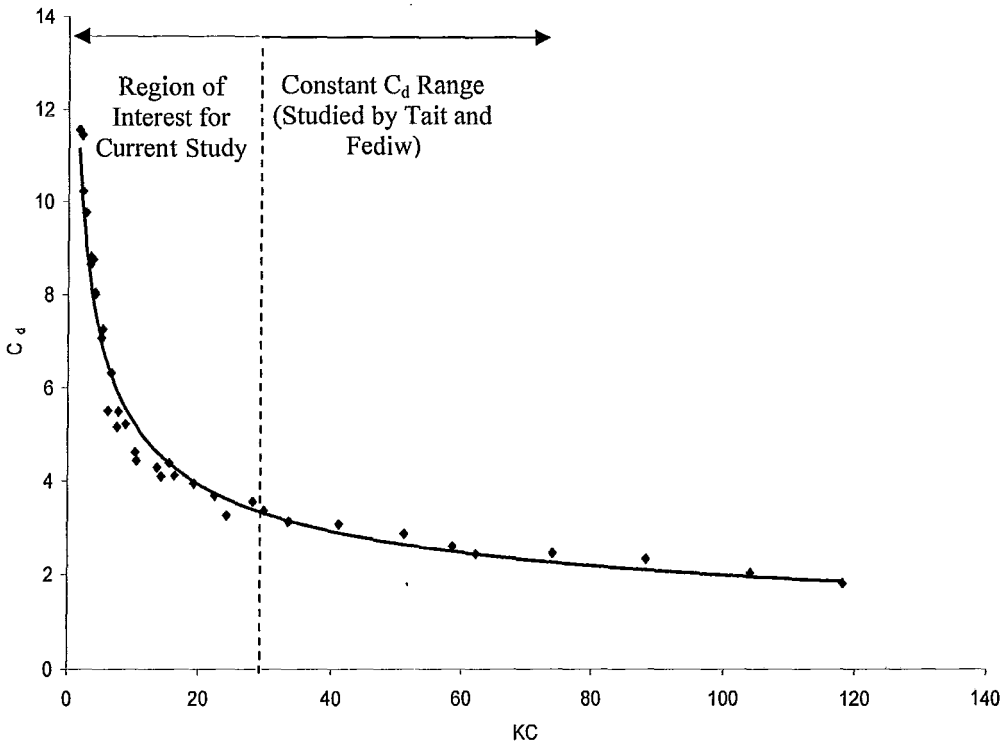

Figure 2.20 - Drag Coefficient vs Keulegan Carpenter Number for a Plate

There are two regions of interest in the above figure. Region 1, which is for a *KC* number less than 30, shows a rapid change in the drag coefficient as the *KC* number approaches zero. Conversely, as the *KC* number increases past 30 the drag coefficient approaches a near constant value. It was found in work by both Fediw et al. (1995) and Tait et al. (2005) that once the *KC* number increases past a value of 30 the drag coefficient for their screens could be considered constant.

2.9.3 Focus of Current Study

It has been shown in the previous sections that a TLD with damping screens having a constant loss coefficient is inefficient when operating outside of the

target design range. The objective of this current work is to investigate the effects that screen geometry has on the performance of the TLD. Keulegan-Carpenter showed that at low *KC* numbers the loss coefficient becomes dependent on the *KC* number. This results in a variation of the loss coefficient with the response of the TLD. A simple approach to ensure that the TLD operates at low *KC* numbers is to utilize larger slat heights in the construction of the slat screens. Therefore, slat screens with various slat heights will be investigated in this study. The primary focus of the study is to determine if the efficiency of a structure-TLD system can be improved by utilizing larger slats in the construction of the screens.

2.9.4 Full-Scale Properties of Prototype Structure and TLD

In this investigation the performance of a TLD is investigated at a 1:10 scale model. At full scale, this TLD matches the TLD installed at Highcliff in Hong Kong. Highcliff is a 73 storey residential building having a height of 253m. The TLD is installed in order to reduce the peak hourly structural accelerations due to wind excitation.

Chapter 3 : Experimental Set-Up

This chapter describes the experimental set-up that was used in this study. Shake-table experiments were completed on a 1-D scale model TLD with damping screens. The chapter begins by presenting details of the testing frame and water-tank that was used. It is followed by a discussion of the instrumentation that was used to capture the free surface response, base shear forces, and table motion. It concludes by presenting the experimental testing program that includes frequency sweeps over a range of amplitudes for various screen configurations.

3.1 *Testing Frame*

The test set-up used in this study is derived from work completed by Tait (2004) and follows work completed by Cassolato (2007). A schematic illustrating the general set-up of the shake-table tests is shown in Figure 3.1.

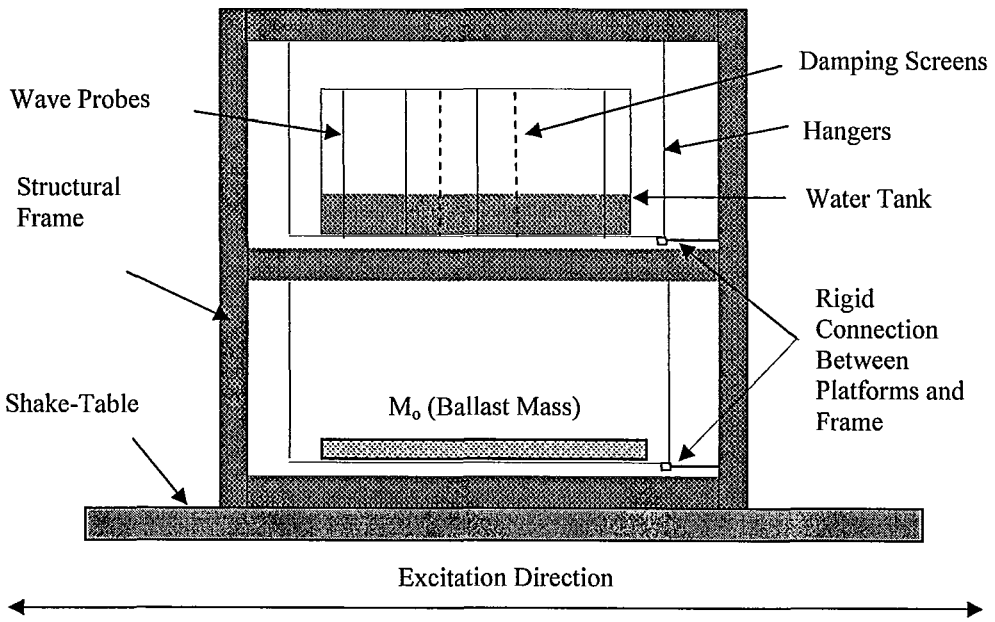

Figure 3.1 - Schematic of Test Set-Up

The main structural support frame used in this study is constructed of welded hollow structural steel sections measuring 76mm x 76mm x 4.8mm. The frame was designed to be 1.5m tall and is bolted rigidly to the shake table. Two hanging platforms are connected to the testing frame using a rod and turnbuckle system. Both platforms are constructed from aluminum rectangular hollow sections welded together to form two $1m^2$ surface areas (Figure 3.2). The top platform is used to hold the water-tank and is connected rigidly to the test frame. This connection is made with a brass link that connects the platform to a load cell attached to the frame (Figure 3.3). This ensures that no relative motion between the platforms and the frame can occur, and the link is designed to yield or buckle before the capacity of the load cell is reached. Similarly, the bottom platform is hung from the mid-height of the frame and carries a ballast mass that is connected to the frame in the same manner. The ballast mass is used so that the dynamic sloshing force can easily be measured. The concept is that the mass of the bottom platform and ballast mass is equal to the mass of the top platform, tank, fluid, and attached instrumentation (screens, wave probes etc...). Theoretically, if the fluid was replaced with a solid that had the same mass, the forces measured from the top and bottom platforms would be equal. However, since the tank contains a fluid, the difference in forces is a direct measure of the dynamic sloshing forces.

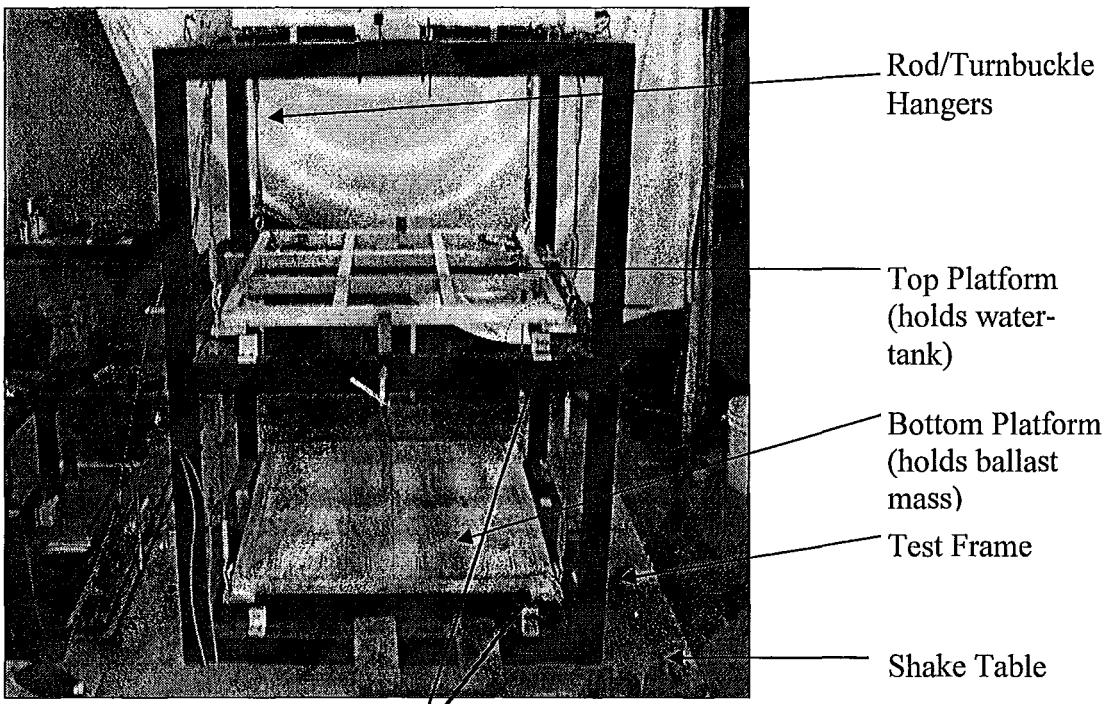

Figure 3.2 - Testing Rig

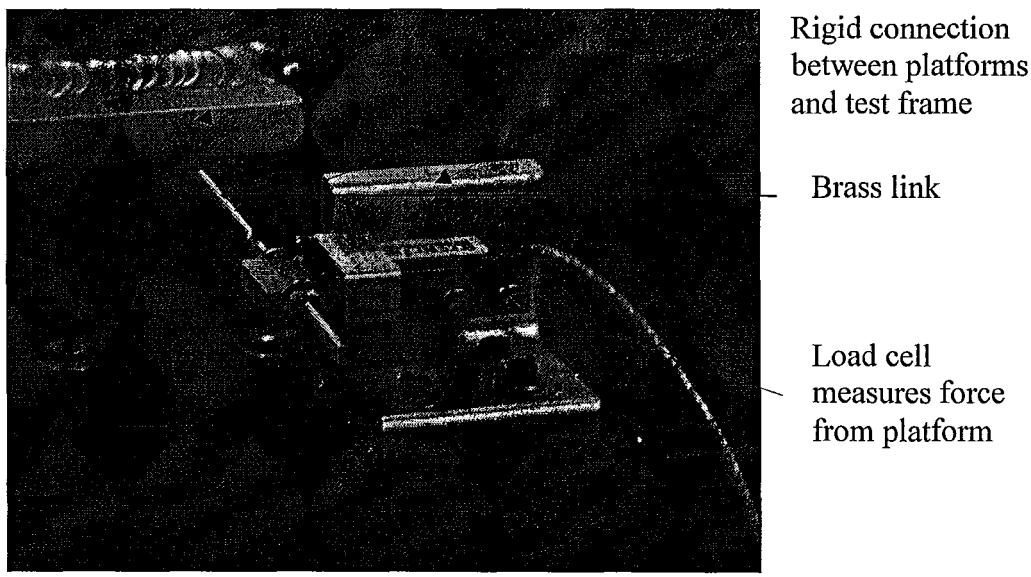

Figure 3.3 - Typical Platform-Frame Connection

Due to the dynamic nature of the shake-table tests it was important to determine if the natural frequency of the testing frame would have an impact on the response of the TLD. A model created by Cassolato (2007) in SAP2000 predicted the

fundamental natural frequency of the testing frame to be approximately 28 Hz. The natural frequency of the sloshing fluid is approximately 0.55Hz. Therefore, the dynamic response of the testing frame is expected to have a negligible influence on the fluid response over the range of frequencies tested.

3.2 *Tuned Liquid Damper Description*

This section introduces the water-tank and damping screens that were used in this study.

3.2.1 Water-Tank Description

A 1:10 scale model of a 1-D tuned liquid damper was used in this study. This tank is a scaled model of a tank that was considered for installation in Highcliff. The tank was fabricated from a 19 mm thick acrylic sheet with inner dimensions of 360x480x966 mm (Figure 3.4).

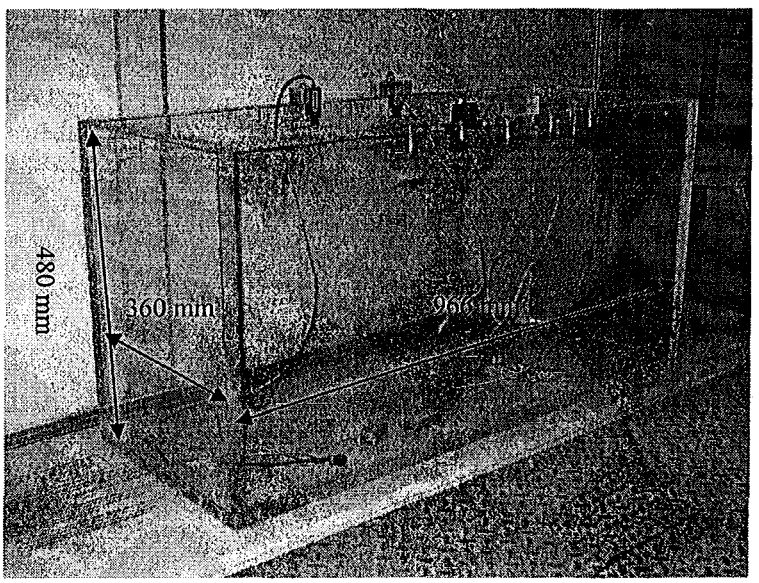

Figure 3.4 - 1:10 Scale Model of TLD

This tank is similar to the tank used by Tait (2004) and the same as Cassolato (2007). The quiescent water depth, h, was 119mm for all tests and was selected so that comparisons between this work and previous researcher's work could be made.

3.2.2 Damping Screens

Horizontal slat screens were used in this investigation to increase the damping of the TLD. The pressure losses that occur at the screen location are dependent on the fluid velocity squared (V^2). The velocity of the fluid in its fundamental mode $(n=1)$ is maximum at the centre of the tank $(0.5L)$. Therefore, the most efficient location for one screen to be placed is at the centre of the tank. However, it has been shown by Tait (2004) that one screen does not sufficiently reduce the nonlinear response of the TLD rendering the device less efficient than a TLD with multiple screens. Tait (2004) also conducted experiments on a TLD with three screens and found that the response became more linear as the number of screens increased. However, the efficiency of each individual screen was reduced because it must be placed further away from the centre of tank. As a result, two damping screens are placed at 0.4L and 0.6L for this study. This is considered an efficient and cost-effective selection. The aluminum slats were connected to vertical stiffeners to reduce relative motion between the bottom of the screen and the load cells and to minimize deflections. The screens were hung from load cells that were rigidly connected to the tank walls as shown in Figure 3.5.

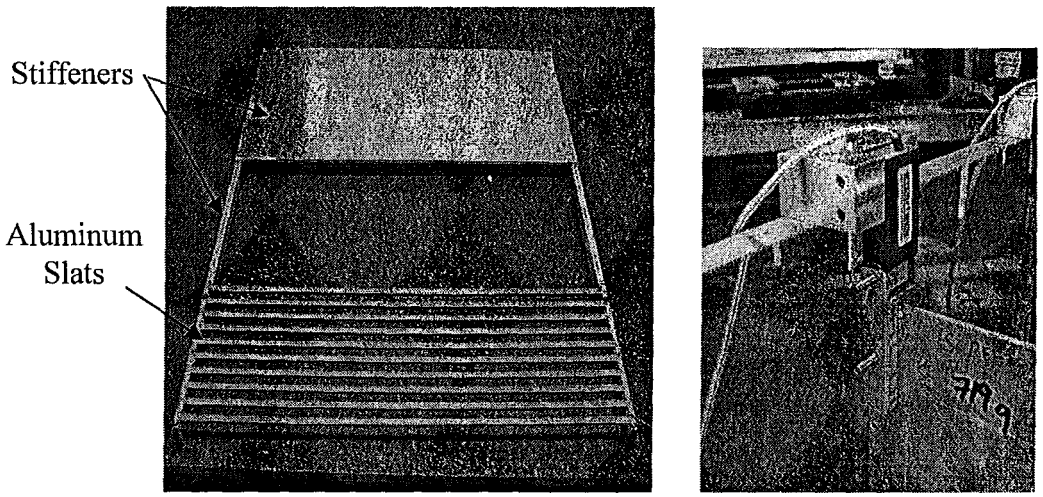

Figure 3.5 - (a) Typical Slat Screen (b) Screen Connection to Tank

The main focus of this investigation is to determine the influence that slat height has on the performance of a TLD. Three different slat sizes were selected for testing in this program. The slat heights were 5mm, 19mm, and 25mm (Figure 3.6). These heights are chosen in order to ensure a wide range of *KC* numbers are investigated.

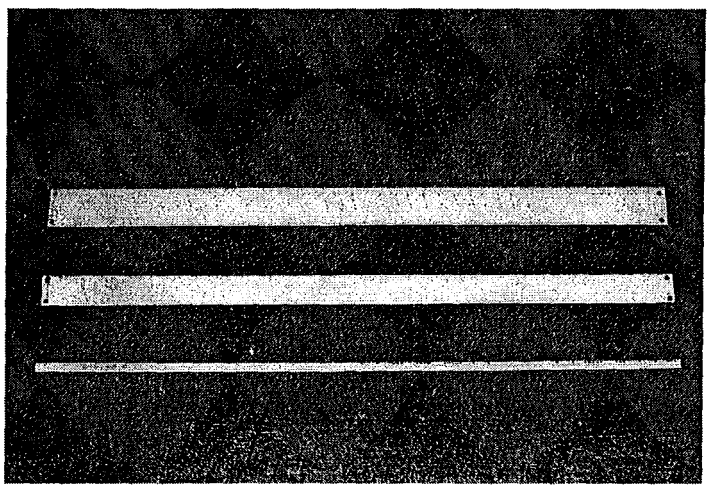

Figure 3.6 - Comparison of Slat Heights

Two different screen solidities were selected in order to ensure that the relationship between KC and C_L is well defined. In this investigation the screen solidity is defined the ratio between the screen area and fluid area given as

$$S = \frac{nb_s D}{bh} \tag{3.1}$$

Where S is the screen solidity, n is the number of slats, b_s is the width of the slat and D is the slat height. In addition to the two screen solidities, two different screen configurations were investigated. One screen configuration is considered a 'partial height' screen shown on the left of Figure 3.7. This arrangement has no slats above the still water while the 'continuous' screen shown on the right of Figure 3.7 have continuous slats for the full height of the screen.

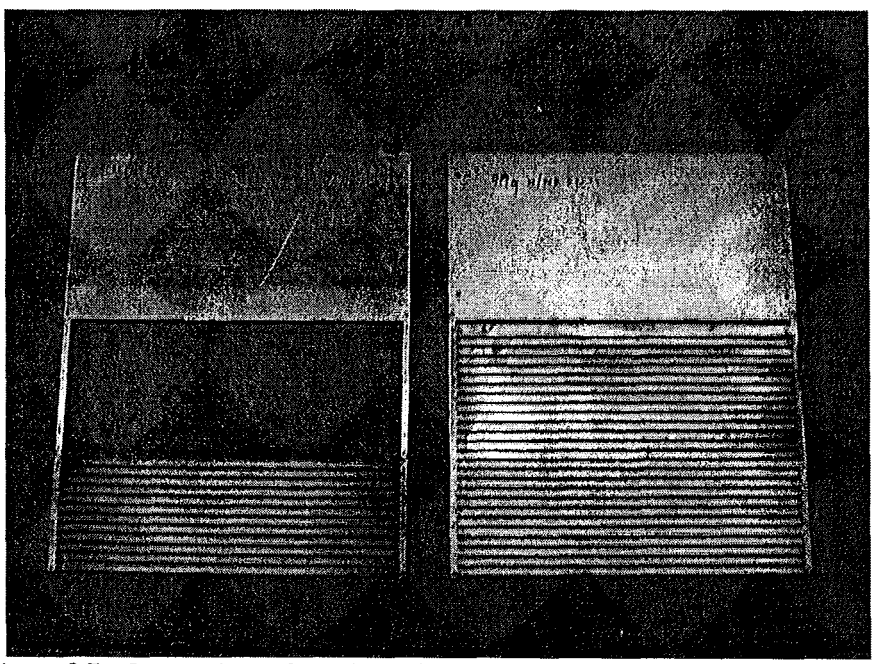

Figure 3.7 - Comparison of Partial Height (left) and Continuous (right) Screens

The use of partial height screens was investigated to ensure that the solidity of the screens remains constant through the range of slat heights tested. A more detailed discussion will be presented in Chapter 4. When constructing the partial height screens it was necessary, in some instances, to use a combination of slat heights. For example, the 42% solid 19mm screens required the use of 2-19mm slats along with 1-12mm slat. Similarly, the 50% solid 25mm screens used 2-25mm slats along with 1-3mm slat.

In addition, a small number of tests were completed on slat screens with rounded edges. A schematic comparing the edge geometry of the rounded and sharp-edged slats is shown in Figure 3.8.

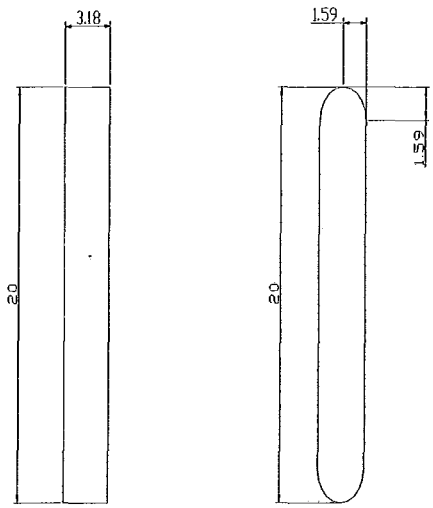

Dimensions are in mm

Figure 3.8 – Cross-Sectional Schematic of Edge Geometry of Slats

The aim of this series of tests was to determine the influence that corner edge geometry had on the response of the TLD.

3.3 *Instrumentation*

This section begins by introducing a mechanical model that represents the shake-table test of a TLD. A description of the equipment that was used to measure base shear forces, free surface response, and table motion follows.

3.3.1 Mechanical Model of Shake-Table Experiments

The TLD that is used in this experimental program is easily represented by the SODF model shown in Figure 3.9. The effective mass m_{eff} represents the portion of the fluid that generates the dynamic sloshing force F_S. The summation of m_{eff} and m_o is the amount of fluid mass that contributes to the total base shear force F_T. The stiffness of the TLD is generated by the gravitational restoring force that acts on the displaced fluid. Finally, the damping of the TLD c_{TLD} is generated mainly through pressures losses at the screen locations while a small contribution is made by viscous losses at the tank walls.

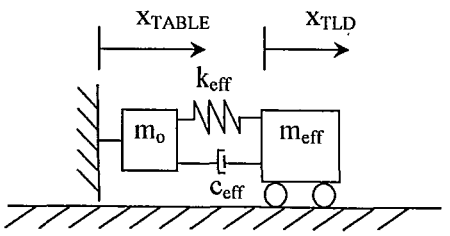

Figure 3.9 - SDOF Representation of Shake-Table Set-Up

3.3.2 Base Shear Forces

As discussed earlier, the top and bottom platforms are rigidly connected to the test frame through a link to a load cell. In total, four load cells, each with a capacity of 111N (25 lbf.) were used to measure the top and bottom platform shear forces. The base shear force measured by the top platform load cells, F_{Top}, is comprised of three components. The force due to the inertia of the empty tank F_A, the force due to the inertia of the contained fluid F_M and the dynamic force due to the sloshing of the liquid F_S (Figure 3.10).

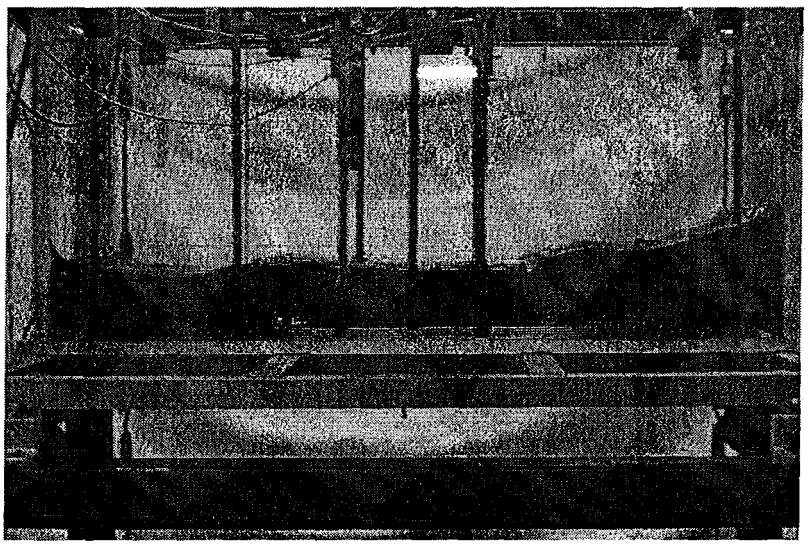

Figure 3.10 - Force Captured by Top Platform Load Cells

The base shear force, F_{Bot}, measured by the bottom platform load cells measures the inertial force due to the mass of the empty tank F_A and the fluid F_M (Figure 3.11).

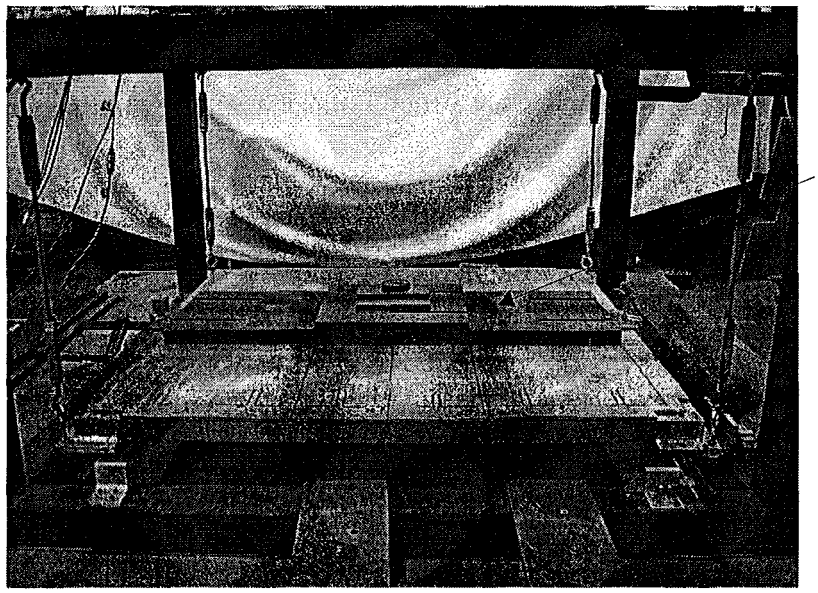

Figure 3.11 - Load Captured by Bottom Platform Load Cells

As a result, the dynamic sloshing force F_S can easily be obtained by subtracting the bottom platform force from the top platform force

$$F_S = F_{Top}(t) - F_{Bot}(t) \tag{3.2}$$

Similarly, the total base shear force, F_T, can be obtained as

$$F_T = F_{Top}(t) - F_A(t) \tag{3.3}$$

This set-up was verified with an empty tank test. Since there is no contained fluid the total base shear force given from equation (3.3) should be zero. This result was confirmed for five different frequencies and three amplitudes.

3.3.3 Table Motion

The table motion was measured with a cable-extension transducer (CET). The table was excited at 45 discrete frequencies ranging from 0.35Hz to 0.80Hz to ensure proper resolution of the frequency-response curve. The table excitation

ranged from 2.5mm to 30mm. These amplitudes were selected because they corresponded to the target range of full scale structural accelerations (3milli-g to 37milli-g) of the prototype building.

Accelerometers were used in this study to measure the table acceleration, top platform acceleration, and bottom platform acceleration. The platform accelerometers were used to validate the measured base shear forces while a comparison of the three accelerometers ensured that no relative motion existed between the frame and table.

3.3.4 Free Surface Measurements

Capacitance type wave probes were used to measure the free surface profile, $\eta(x,t)$, in four locations. The wire was supported by an aluminum bow and connected to an aluminum channel that was hung from the tank walls (Figure 3.12).

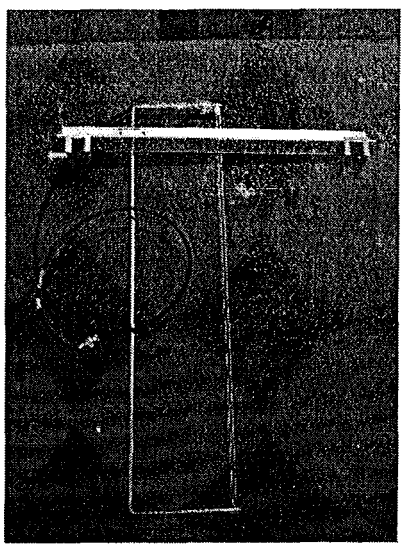

Figure 3.12 - Typical Wave Probe

Figure 3.13 shows the location of the screens and wave probes. The probes were located at 0.05L and 0.95L to measure the free surface at the end walls and to capture the response of the fundamental mode. A wave probe was located at 0.5L to measure the response at the centerline of the tank and the contributions from the second sloshing mode. The fourth probe was located at 0.25L to capture the contribution of the first and third sloshing mode.

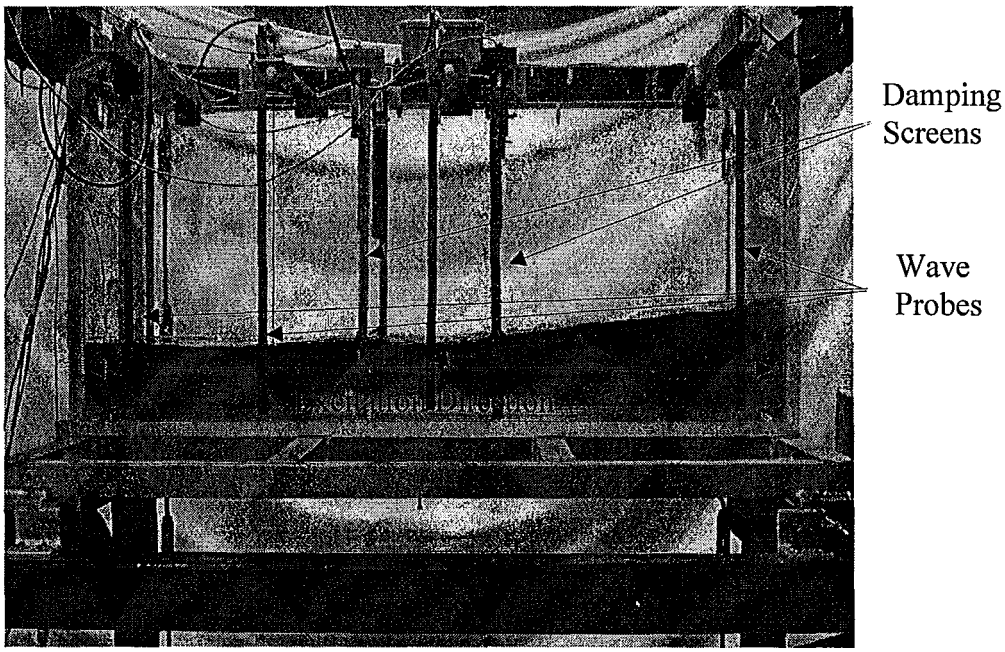

Figure 3.13 - Wave Probe and Screen Locations

3.4 *Description of Experiments*

All of the shake-table tests were completed as forward frequency sweeps. The sweep was completed by subjecting the TLD to a constant frequency and amplitude for 120 seconds. Once the time-history measurements were obtained the excitation frequency was increased to the next value, while maintaining the same amplitude. This procedure was repeated for the 45 discrete frequencies. Earlier work completed by Fediw (1992) showed that the fluid response was

independent of the sweep direction if damping screens are utilized. The table excitation was sinusoidal in nature and a constant frequency range was maintained for all tests. In this investigation a test is considered a full frequency sweep at a constant amplitude. In order for comparisons to be made between these test results and others, a normalized amplitude ratio is given as A/L where A is the amplitude of excitation and L is the tank length.

Table 3-1 : Test Matrix

Screen Geometry	Solidity	Normalized Amplitudes (A/L)	Slat Heights
Continuous	42%	0.0026 – 0.031	5mm, 19mm, 25mm
Partial Height	42%	0.0026 – 0.021	5mm, 19mm, 25mm
Partial Height	50%	0.0026 – 0.021	5mm, 20mm, 25mm
Rounded Edge – Partial Height	50%	0.0026 – 0.021	20mm
Single Screen – Partial Height	42%	0.0052	5mm, 25mm
Single Screen- Partial Height	50%	0.0052	5mm

For each frequency a 120 second time history was captured at a sampling rate of 50Hz. No data was captured until the fluid had reached steady-state response. The experimental data was low-pass filtered at 10Hz to eliminate high-frequency noise. A 16-channel data acquisition system was used to capture data from load cells (8 channels), table displacement, accelerometers (3 channels), and wave probes (4 channels).

Chapter 4 : Experimental Study of a TLD with Various Slat Heights

This chapter presents the results obtained from a series of shake-table experiments that were conducted on a 1-D TLD in order to assess the influence of screen geometry on TLD performance. Frequency-response curves, time history responses, and force-displacement loops are all presented for three different slat sizes. In addition, two screens solidities are investigated. The following sections will present the influence that slat height, amplitude, solidity, edge geometry, and the *KC* number have on the fluid response of the TLD.

4.1 Discussion on the use of Partial Height and Continuous Slat Screens

As mentioned in Chapter 3 two different screen configurations (Figure 3.7) were experimentally investigated. One configuration is comprised of slats that are distributed over the full tank height ('continuous' screens) as shown in Figure 4.1. Conversely, the second configuration was made using slats that continued to the quiescent fluid height ('partial height' screens). As a result, at higher free surface response amplitudes the fluid is free to flow over the screens unobstructed as shown in Figure 4.2.

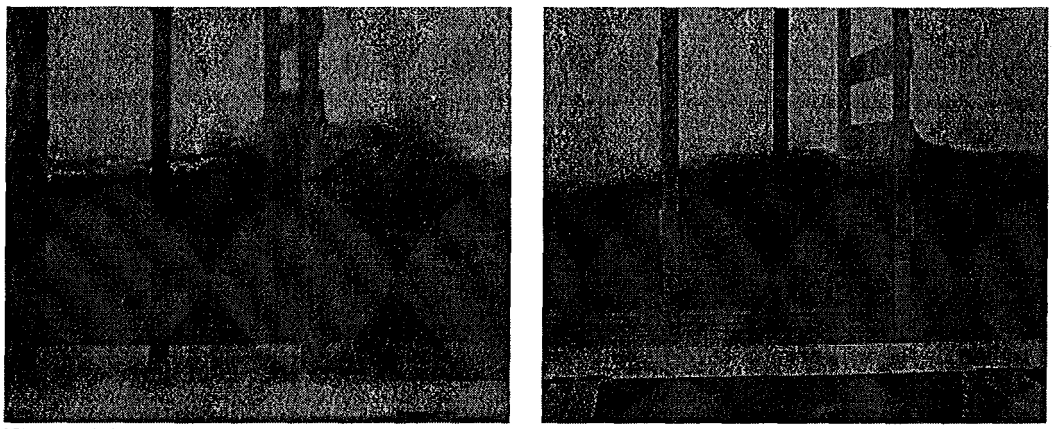

Figure 4.1 - Free Surface Response at the Screen for Continuous Slat Screens (a) 19mm Slats (b) 25mm Slats

A comparison between continuous screens with slat sizes of 19mm and 25mm is shown in Figure 4.1 at A/L=0.0207. It is observed in the photo on the left that the fluid is flowing around three full slats of 19mm and is in contact with a fourth slat. The photo on the right shows the fluid flowing over two 25mm slats and in contact with a third slat. As a result, the screens with 19mm slats have an effective solidity (S') different than the 25mm slats. Where S' is defined as

$$S' = \frac{A_E}{A_{Sloshing}} \tag{4.1}$$

and A_E is the total effective screen area engaged in the flow, i.e. number of slats multiplied by the slat height and $A_{Sloshing}$ is the effective area of the sloshing fluid, i.e. average water depth (across the width of the tank) at the screen multiplied by the tank width. In order to accurately compare the results it is necessary that all screen configurations have the same effective solidity. The most efficient approach in this case is to use slat screens that have a mixture of slat heights and are continuous through the quiescent water depth only. The 'partial height'

screens have the same amount of slat material in the fluid when the TLD is at rest for all three slat heights. This results in an effective solidity that is equal for all the slat heights that were tested as shown in Figure 4.2.

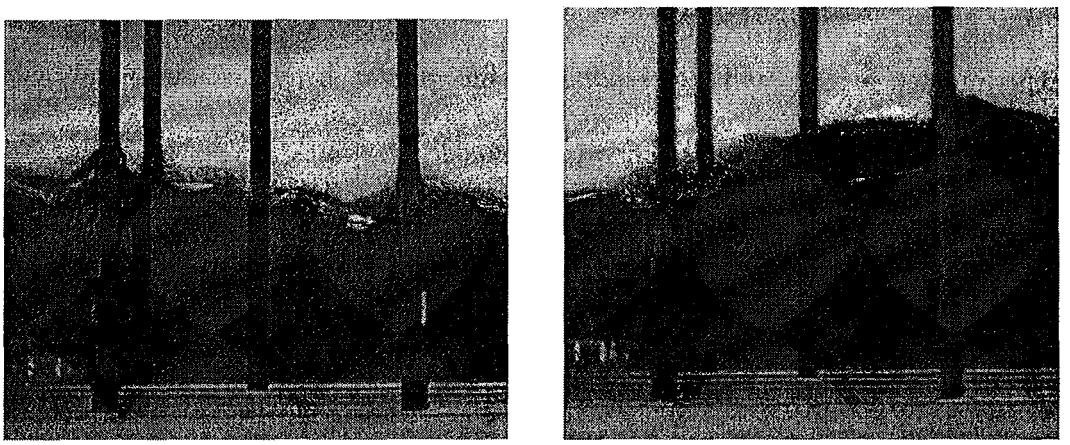

Figure 4.2 - Free Surface Response at the Screen Location for Partial Height Slat Screens (a) 19mm Slats (b) 25mm Slats

The free surface response of the partial height screens with 19mm and 25mm slats is shown for A/L = 0.0207. It is observed in the photo on the left that the fluid is flowing over two 19mm slats and one 12mm slat resulting in a total slat height of 50mm. Similarly, the photo on the right shows the fluid flowing over two 25mm slats resulting in a total height of 50mm. Since some of the screens tested utilize a mixture of slat heights it is necessary to use an effective slat height D_{eff} when investigating the KC number influence. The effective slat height is given as

$$D_{EFF} = \frac{\sum_{i=1}^{n} Dh_{TRIB}}{\sum h} \tag{4.2}$$

where n is the number of slats, D is the slat height, h_{TRIB} is the tributary height of fluid taken as half of the height between adjacent slats, and h is the still water fluid depth. The partial height screens were used for the majority of the experimental work. Therefore, the analysis, discussion, and presentation of experimental results will correspond to the partial height screens and any reference to the continuous screens will be noted.

4.2 Influence of Slat Height on TLD Response for a Screen Solidity of 42%

This section presents the experimental results from the series of shake-table tests completed on a TLD equipped with 42% solid screens. The influence of slat height on the response of the TLD will be compared for A/L values of 0.0052, 0.0104, and 0.0207. These amplitudes were chosen because they cover the range of amplitudes tested and they correspond to both the RMS and peak response of the structure being investigated in Chapter 6. The experimental results presented in this section correspond to tests completed with two sharp edge slat screens located at 0.4L and 0.6L. Three different slat heights are compared; 5mm, 19mm, and 25mm and will be referred to as TS5, TS19, and TS25. The letter abbreviation indicates tests completed with two screens (TS) and the number is the slat height in mm.

4.2.1 Influence of Slat Height on Free Surface Response

The free surface motion of the sloshing fluid is an important measure of TLD response. In practice, it is important to be able to predict the maximum wave amplitude within the TLD in order to properly determine the required freeboard and overall tank height. In experimental work, measurements of wave amplitude permit the level of damping and fluid velocity to be estimated and the presence of higher harmonic modes observed.

The nonlinear response of fluid sloshing is a well documented phenomenon in TLD studies (Shimizu and Hayama 1987, Fediw 1992, Tait 2004). The effect of this nonlinear response is that higher modes, or superharmonics are excited (Tait, 2004). Shimizu and Hayama (1987) outline a method to approximate the frequency at which these higher modes will be excited. The natural frequency in the n^{th} sloshing mode is given from shallow water wave theory (Lamb, 1932) as

$$f_n = \frac{1}{2\pi}\sqrt{\frac{n\pi g}{L}\tanh\left(\frac{n\pi h}{L}\right)} \tag{4.3}$$

where h is the quiescent fluid depth, L is the tank length, and g is the acceleration due to gravity. Substitution of the appropriate values provide the natural frequencies for the first three sloshing modes as shown in Table 4-1 along with the frequency ratio, β, at which the superharmonics are excited.

Table 4-1 : Natural Frequency of First Three Sloshing Modes

Mode (n)	Frequency (Hz)	β
1st Mode (1)	0.545	1.00
2nd Mode (2)	1.023	0.938
3rd Mode (3)	1.374	0.840

The superharmonics are excited at frequencies that are integer multiples less than their natural frequency (Shimizu and Hayama, 1987). The second sloshing mode is excited at a frequency of one half its natural frequency while the third sloshing mode is excited at a frequency of one-third its natural frequency (Shimizu and Hayama, 1987).

Four wave probes are installed within the TLD in order to capture the free surface response at 0.05L, 0.25L, 0.50L, and 0.95L. These locations are chosen so that the relative contributions of different sloshing modes can be assessed. Figure 4.3 compares the estimated normalized fluid velocity (Γ) and the screen locations, mode shapes, and wave probe locations (Adapted from Tait, 2004).

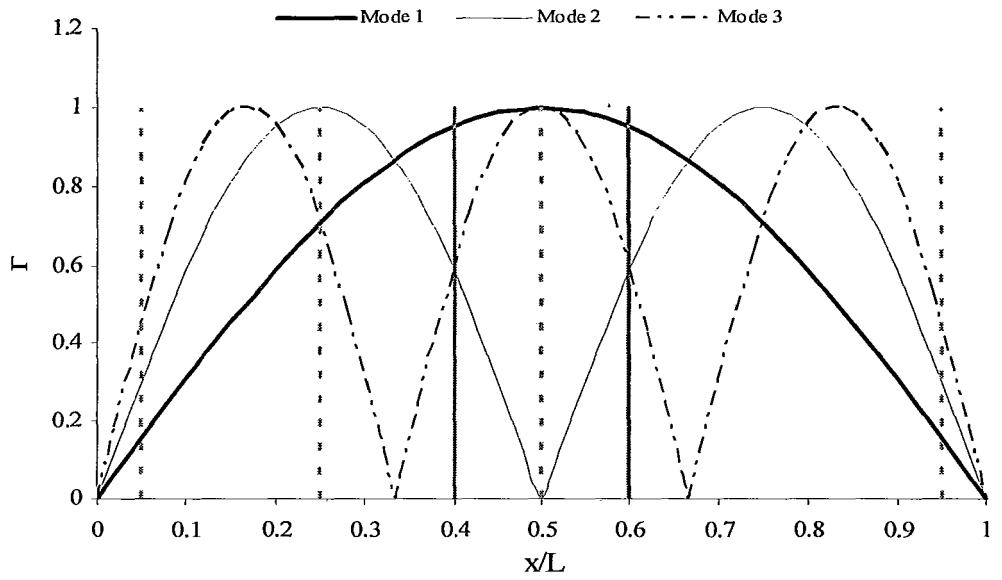

Figure 4.3 - Estimated Normalized Fluid Velocity for the First Three Sloshing Modes, Wave Probes, and Screen Locations inside the Tank

The screen locations are shown at x=0.4L and 0.6L. These locations were selected because they correspond to the high velocity region of fluid sloshing in its fundamental mode. Figure 4.4 to Figure 4.6 show the time history response of the free surface motion captured by the four wave probes for test TS5 excited at A/L=0.0078.

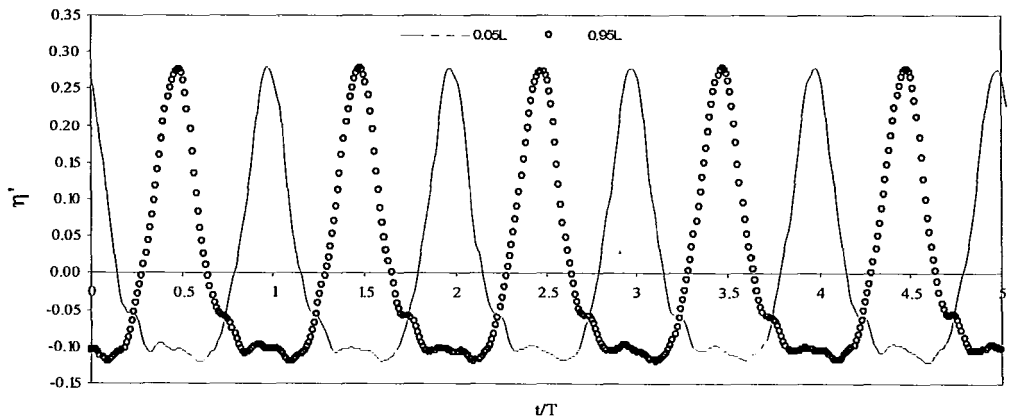

Figure 4.4 - Time History of the Free Surface Response at x=0.05L and x=0.95L β=1.00, S=42%

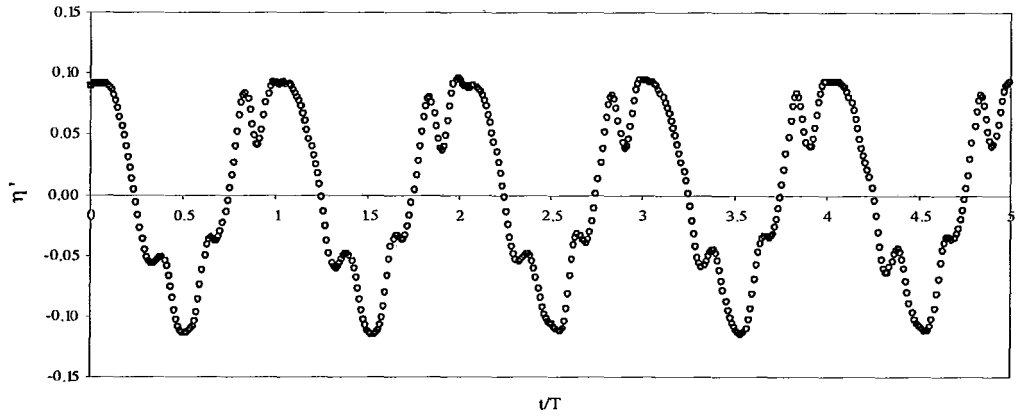

Figure 4.5 - Time History of the Free Surface Response at x=0.25L, β =1.00, S=42%

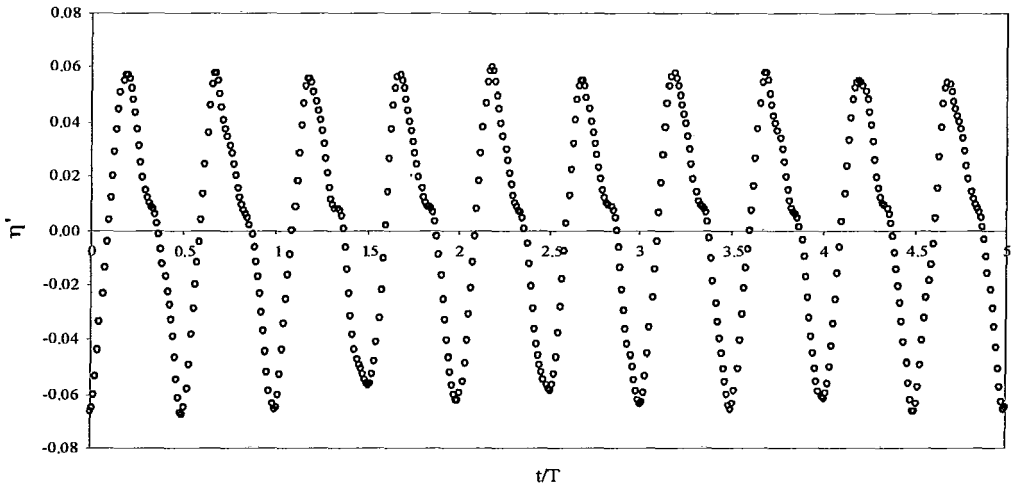

Figure 4.6 - Time History of the Free Surface Response at x=0.5L, β =1.00, S=42%

Figure 4.4 shows the response at the two tank end walls corresponding to x=0.05L and 0.95L. It is observed that both probes reach the same peak wave amplitude but at different times. It is seen that when one probe reaches it peak response the other probe is near its minimum. Furthermore, it is observed that each maximum and minimum peak occurs once per excitation cycle or that their frequency is equal to the excitation frequency. This indicates that the wave probes at the tank end walls sufficiently capture the response of the fundamental sloshing mode.

Figure 4.6 shows the time history response of the free surface motion at x=0.5L which corresponds to the centerline of the tank. It is observed that the maximum and minimum peaks occur twice per excitation cycle indicating that the fluid is responding at a frequency of $2f$. This indicates that the wave probe at the centerline of the tank is capturing the contribution of a second harmonic. Finally, it is seen that the maximum wave height at this location, and x=0.25L, is significantly lower than that at the tank end walls. This shows that the behaviour of the TLD is dominated by the response of the fluid sloshing in its fundamental mode.

The normalized free surface response, $\eta' = \eta / h$, where η is the wave height, is low-pass filtered to obtain the response of the fundamental mode exclusively. Figure 4.7 to Figure 4.9 show the frequency response of η' for test TS5, TS19, and TS25 at three different excitation amplitudes.

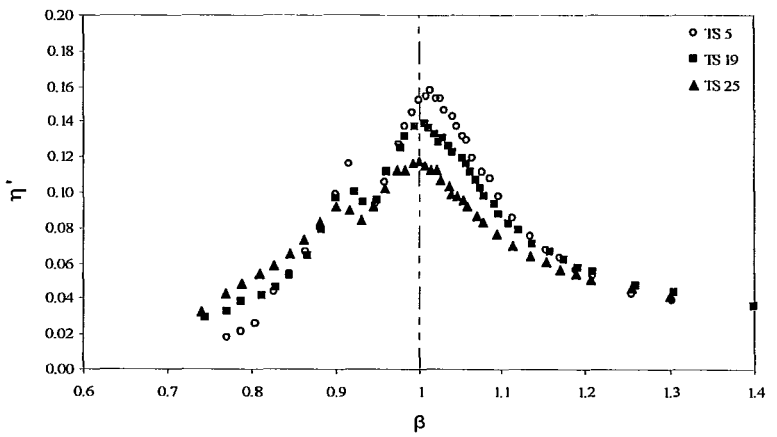

Figure 4.7 - Frequency-Response of η', S=42%, for A/L = 0.0052

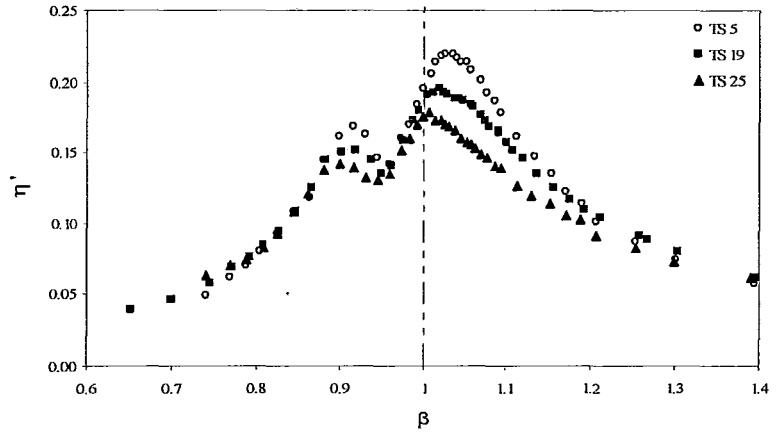

Figure 4.8 - Frequency-Response of η', S=42%, for A/L = 0.0104

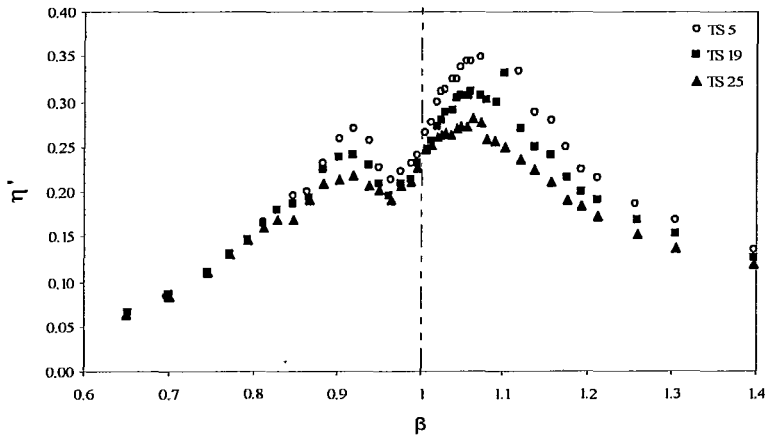

Figure 4.9 - Frequency-Response of η', S=42%, for A/L = 0.0207

Figure 4.7 to Figure 4.9 show a similar frequency response trend. At low amplitudes of excitation, A/L=0.0052, the peak response of the fluid has been reduced by 27% by increasing the slat height from 5mm to 25mm. A similar response is found at A/L=0.0104 and A/L=0.0207 with a 19% and an 18% reduction in the peak response of the fluid, respectively. This reduction in fluid response indicates that the fluid velocity has been decreased. Thus, an increase in slat height is found to increase ζ_{TLD} for the slat heights tested. Figure 4.10

compares the free surface response amplitude of the sloshing fluid in its fundamental mode. The comparison is made between the 5mm slats at A/L=0.0104 and the 19mm slats at A/L=0.0129.

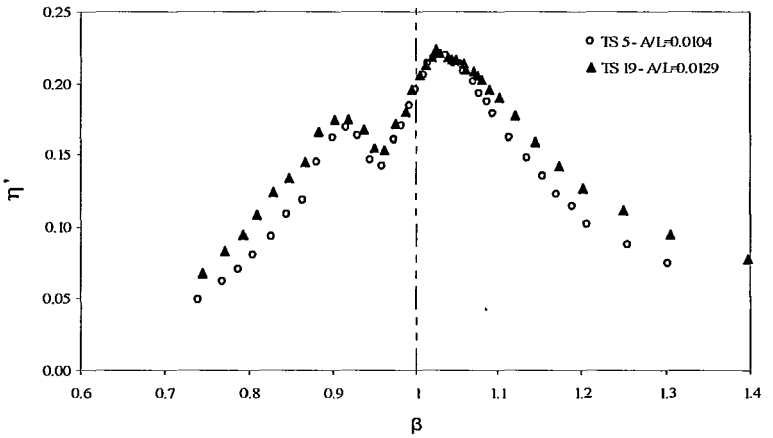

Figure 4.10 - Comparions of the Free Surface Response for TS5 - A/L= 0.0104 and TS19 - A/L=0.0129

This plot shows that there is negligible difference in the peak response of η' and negligible difference in the frequency at which the peak value occurs. Furthermore, the value of η' at $\beta = 0.90$ is the same for both slat heights. This comparison shows that an increase in slat height does not reduce the nonlinearities in the sloshing fluid. In addition, it shows that an increase in slat height reduces the peak value η' due to increased damping caused by an increase in the loss coefficient.

4.2.2 Hysteretic Loops

An estimate of the amount of mass that participates in the fluid sloshing motion for a horizontal rectangular tank can be obtained from equation (2.19).

Substituting the values for water depth, and tank length provides m_{eff} =0.77 m_w. The total base shear force, F_T, is the force due to the sloshing motion plus the inertial force of the non-participating fluid ($\doteq 0.23\, m_w$). For comparative purposes we are interested in the normalized base shear forces, $F_S^{'}$ and $F_T^{'}$, given by

$$F_S^{'} = \frac{F_S}{m_w (2\pi f)^2 A} \tag{4.4}$$

where A is the excitation amplitude and $F_T^{'}$ is found by substituting F_T for F_S. The denominator represents the inertial force of the fluid if it was treated as a solid mass. Figure 4.11 to Figure 4.13 represent the relationship between the normalized base shear forces and table displacements. The figures show distinct loops for $F_S^{'}$ and $F_T^{'}$. Each loop corresponds to one full cycle of table motion and is the hysteric loop for the TLD excited at β.

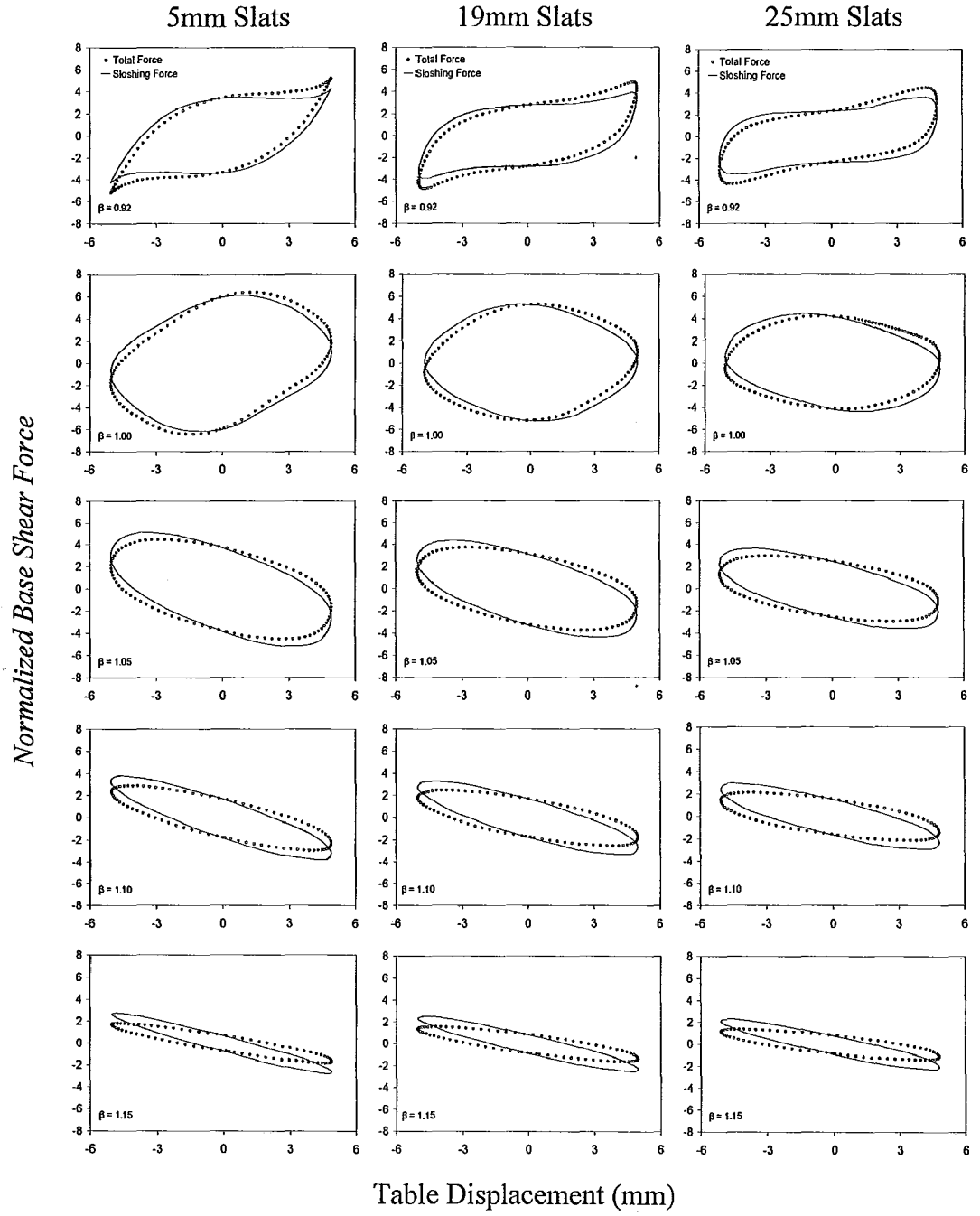

Figure 4.11 - S=42%, *A/L*=0.0052mm, Hysteretic Loops for TS5, TS19, and TS25

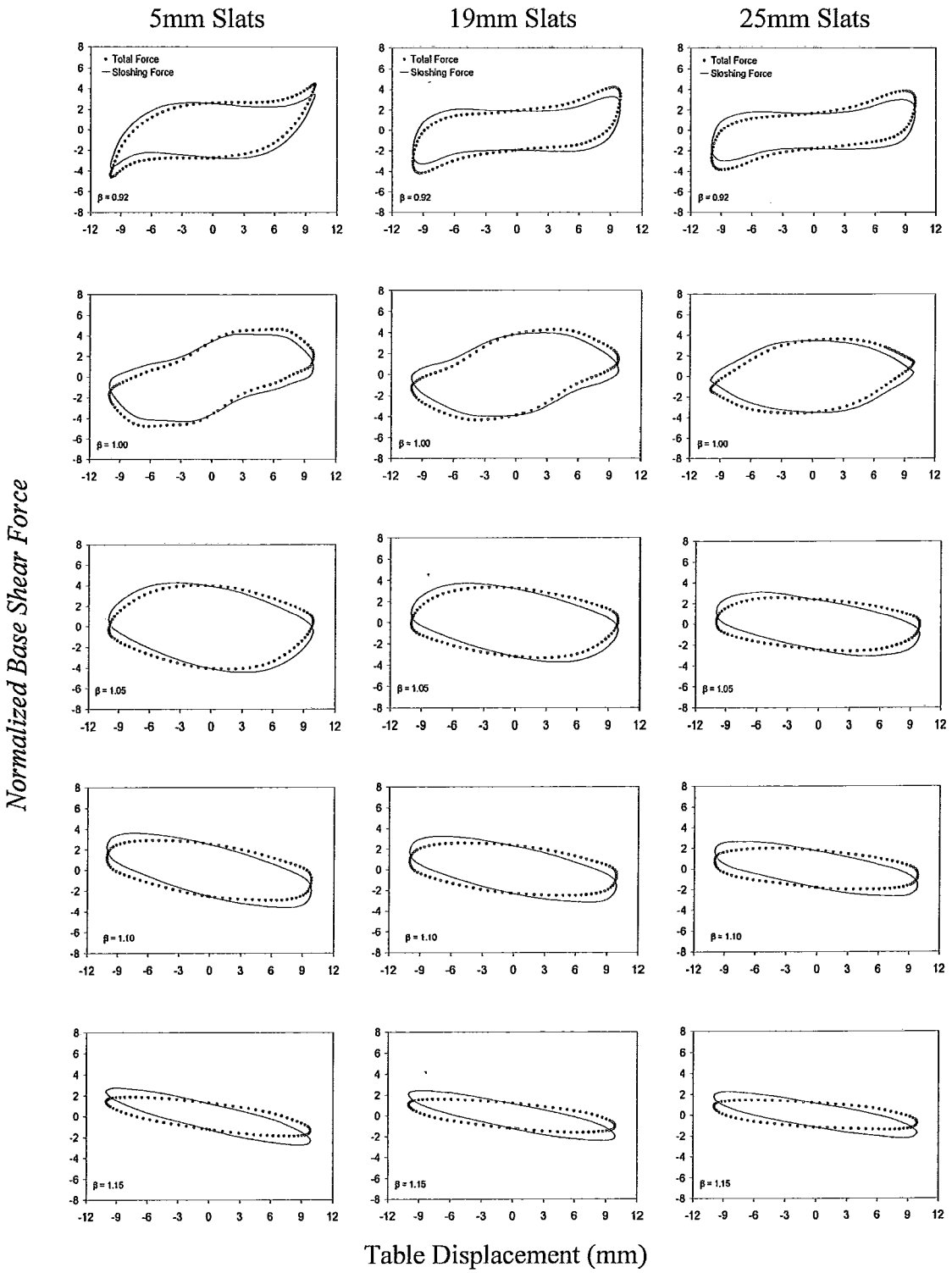

Figure 4.12 - S=42%, *A/L*=0.0104, Hysteretic Loops for TS5, TS19, and TS25

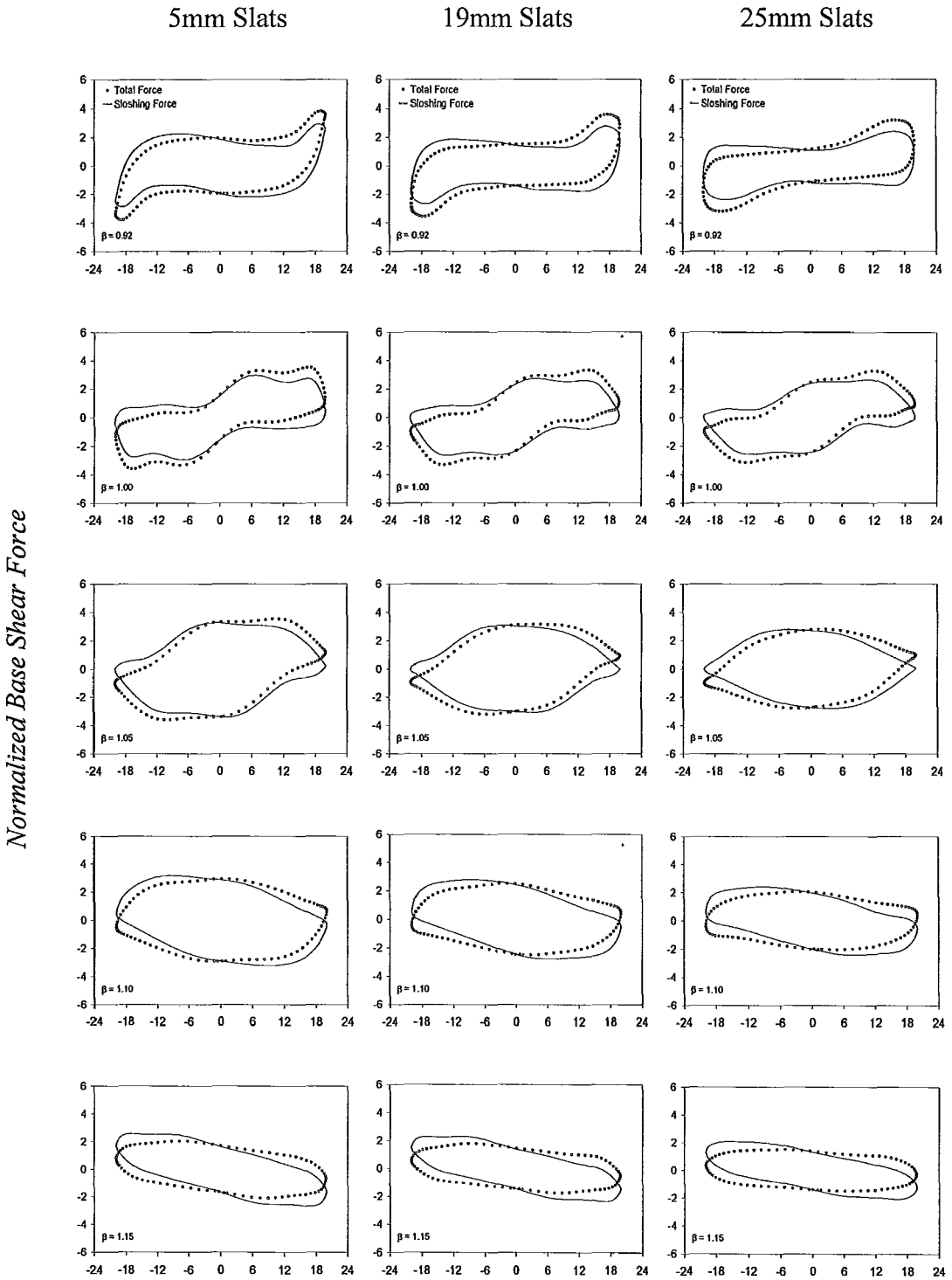

Figure 4.13 - S=42%, *A/L*=0.0207, Hysteretic Loops for TS5, TS19, and TS25

Comparing the effects that slat height and amplitude have on the force-displacement loops leads to the following observations;

- The presence of superharmonics alter the shape of the hysteretic loops indicating a nonlinear response. As A/L increases the presence of superharmonics is more pronounced due to fluid nonlinearities. Conversely, the superharmonics are suppressed as the slat height is increased due to an increase in the damping.
- The hysteretic loops based on $F_S^{'}$ and $F_T^{'}$ enclose the same amount of area. However, the orientation of the loops is different. $F_T^{'}$ includes the effect of the non-participating fluid which is a conservative force that does not increase the energy dissipated. However, it does result in $F_T^{'}$ having a different phase angle than $F_S^{'}$ when compared to the shake-table displacement.
- The largest loops occur when the excitation frequency is near the natural frequency of the TLD ($\beta = 1.00$) indicating that the TLD dissipates the most energy when the excitation frequency is equal to the natural frequency of the sloshing fluid.

4.2.3 Influence of Slat Height on the Energy Dissipation

The amount of energy dissipated in one cycle of vibration, E_d, can be found from the hysteresis loops and is given as

$$E_d = \int_T F dx \tag{4.5}$$

where F is the base shear force, T is the period of shake table motion, and x is the shake table displacement. For comparative purposes the normalized energy dissipated per cycle E_d' is given by

$$E_d' = \frac{E_d}{\frac{1}{2} m_w (2\pi f A)^2} \tag{4.6}$$

The denominator represents the amount of kinetic energy in the fluid if it was treated as a solid mass. For each frequency the amount of normalized energy dissipated, E_d', is plotted versus the frequency ratio, β. Figure 4.14 to Figure 4.16 illustrate the effect that excitation amplitude has on the hysteretic response of the TLD.

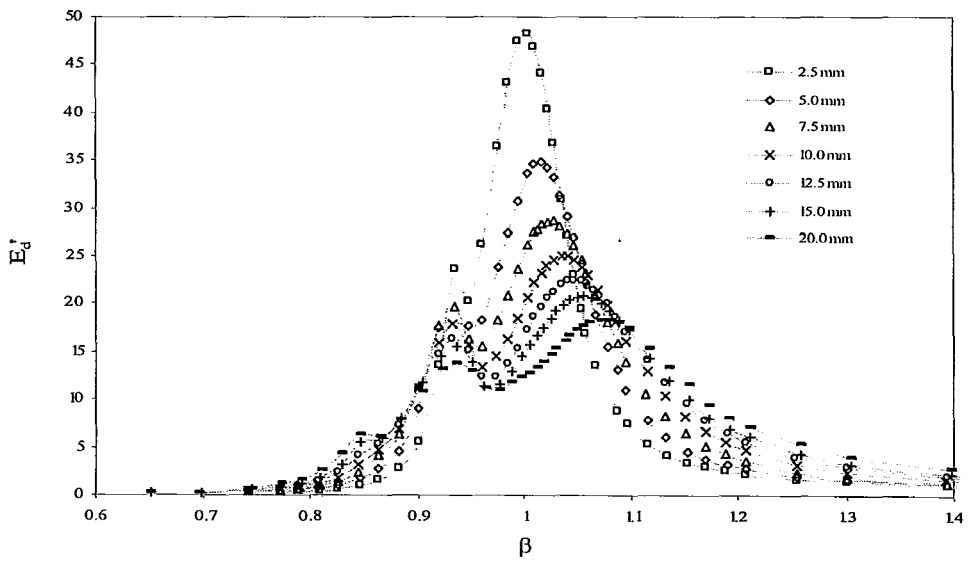

Figure 4.14 - E_d' Comparison, S=42%, TS5

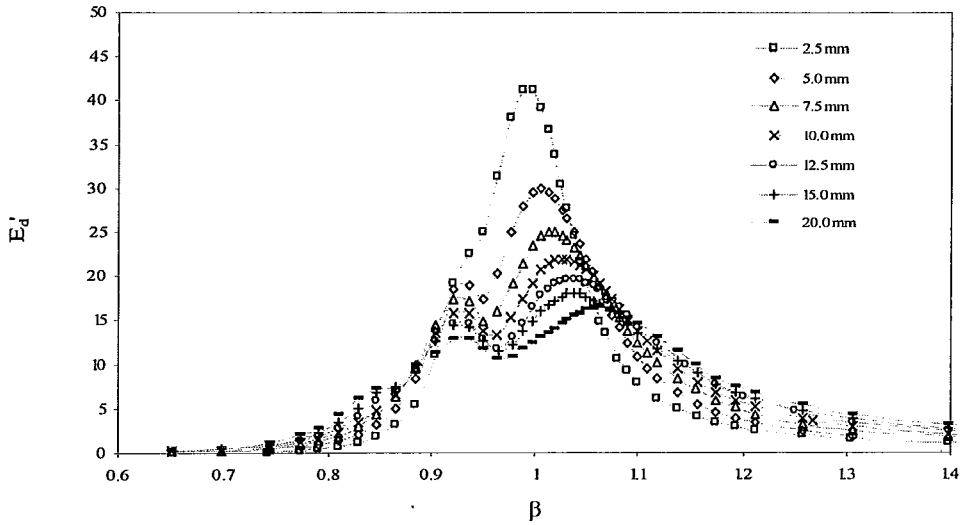

Figure 4.15 - $E_d^{'}$ Comparison, S=42%, TS19

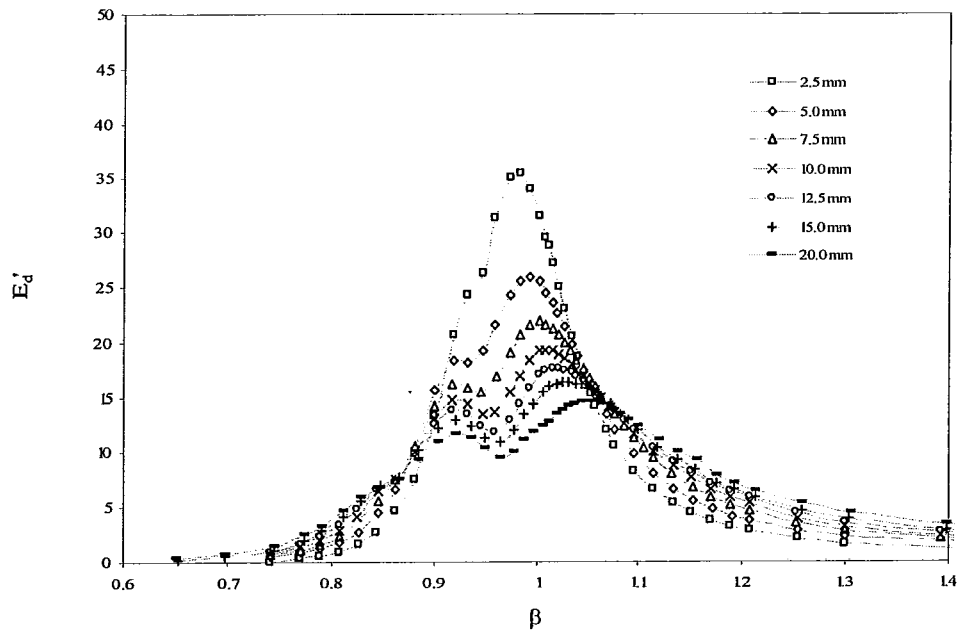

Figure 4.16 - $E_d^{'}$ Comparison, S=42%, TS25

Figure 4.14 to Figure 4.16 show a similar type of frequency-response curve. In particular it is observed that in all cases this TLD operates in a hardening type

manner. This is evident by observing the increase in natural frequency with amplitude. The value of $E_d^{'}$ decreases with amplitude which may seem counterintuitive, but recall that the amount of energy dissipated per cycle is normalized by a factor dependent on A^2. This illustrates that the response of the fluid is increasing at a slower rate than the excitation and indicates that ζ_{TLD} is amplitude dependent.

It is observed that the peak values in the $E_d^{'}$ plots become closer together as the slat heights are increased. This means that the range of $E_d^{'}$ is smaller for the larger slats indicating that the variation in ζ_{TLD} is being reduced. Finally, the natural frequency of the TLD, indicated by the peak response in the $E_d^{'}$ plots changes with slat height and differs slightly from the theoretical value predicted according to equation (4.3). It is postulated that this is a result of the larger slats influencing the flow of the fluid and further discussion on this topic is found in Section 4.2.4.

In order to assess the effect that slat height has on the hysteretic behaviour of the TLD comparisons are made between the $E_d^{'}$ plots for *A/L* values of 0.0052, 0.0104, and 0.0207 and shown in Figure 4.17 to Figure 4.19.

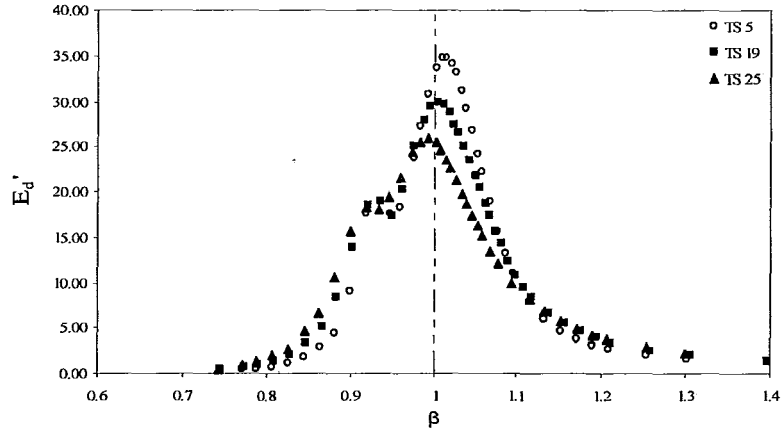

Figure 4.17 - $E_d^{'}$ Comparison, S=42%, *A/L*=0.0052

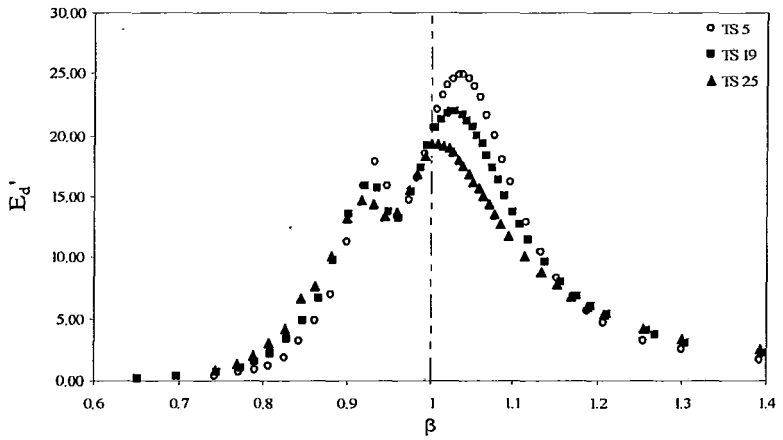

Figure 4.18 - $E_d^{'}$ Comparison, S=42%, *A/L*=0.0104

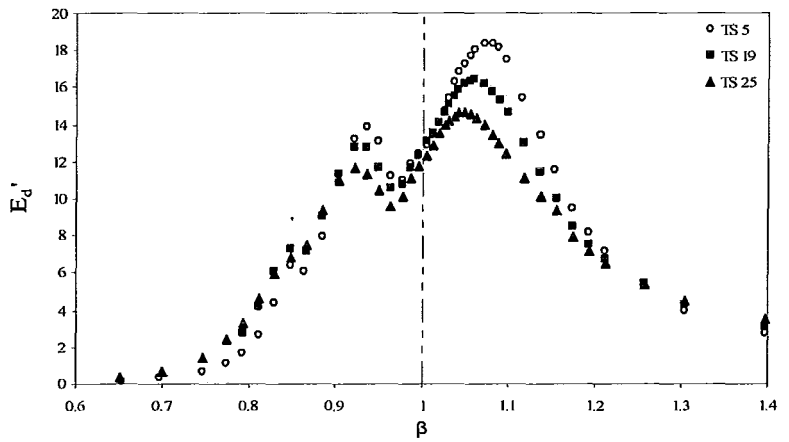

Figure 4.19 - $E_d^{'}$ Comparison, S=42%, *A/L*=0.0207

In the plots an increase in the slat size from 5mm to 25mm reduces the value of E_d' by 25%, 23%, and 20% for A/L values of 0.0052, 0.0104 and 0.0207 respectively. This indicates that ζ_{TLD} is increasing and is caused by an increase in the loss coefficient C_L.

4.2.4 Influence of Slat Height on TLD Natural Frequency

The theoretical fundamental sloshing frequency of the fluid, f_{TLD}, can be estimated using equation (4.3). Substitution for the tank length and water depth used in this study (Chapter 3) provides a theoretical value of $f_{TLD} = 0.546$. The time history response for test TS5 at A/L = 0.0052 is shown in Figure 4.20 to Figure 4.22 for three different excitation frequencies.

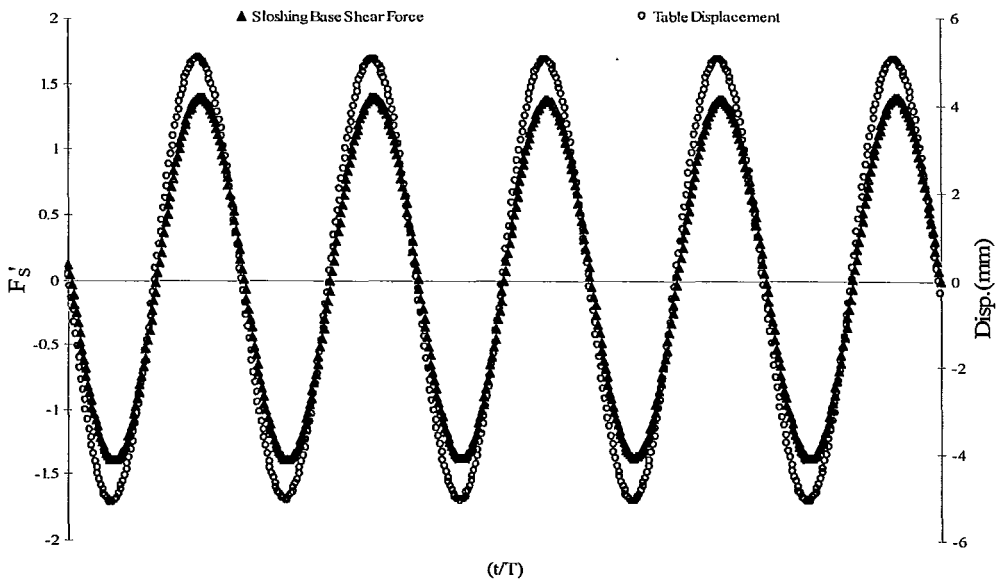

Figure 4.20 - Time History Response, TS5, S=42%, A/L=0.0052, β =0.78

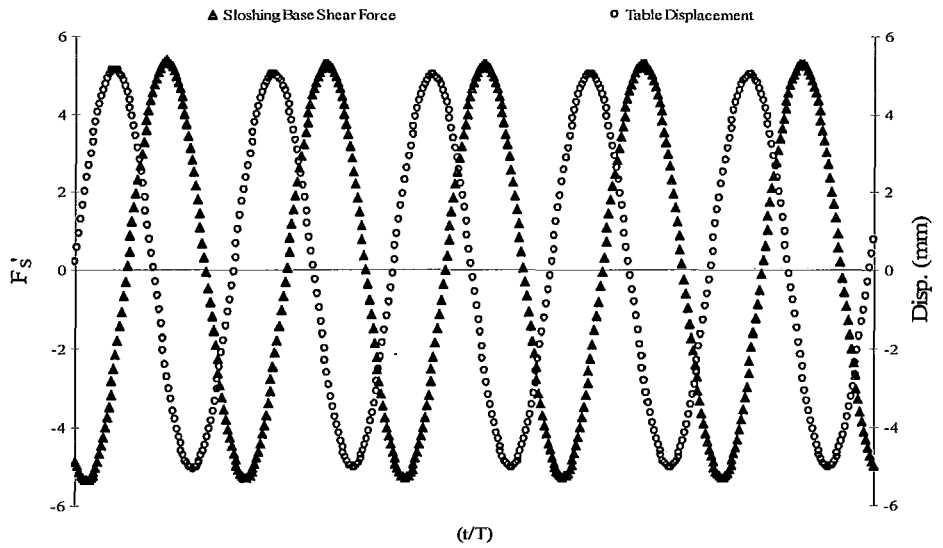

Figure 4.21 - Time History Response, TS5, S=42%, A/L=0.0052, β = 1.00

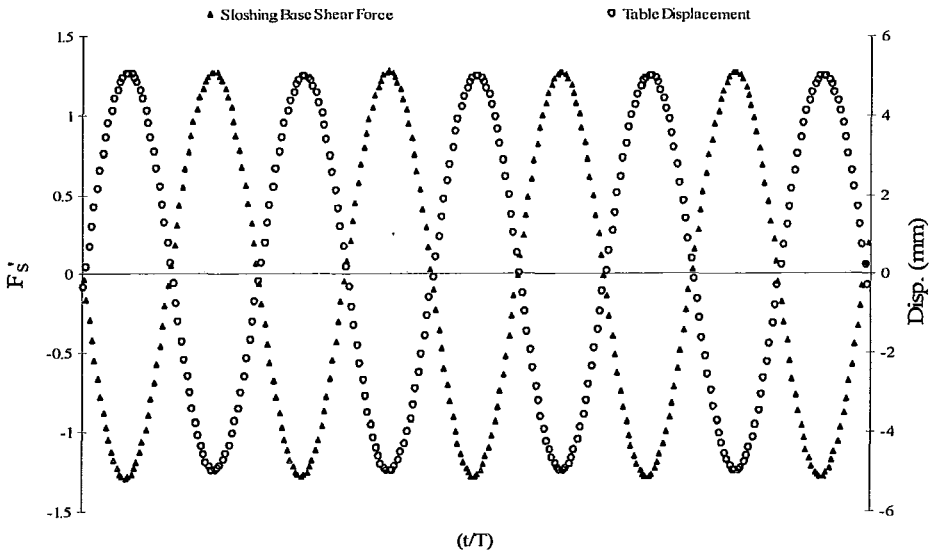

Figure 4.22 - Time History Response, TS5, S=42%, A/L=0.0052, β = 1.49

These figures show the response in the time domain of the table displacement and sloshing base shear force. It can be seen that a phase angle

exists between the peaks of the two curves. Furthermore, it is observed that the phase angle changes as β is increased. This phase angle, θ, is given by

$$\theta = 360^{\circ} f \Delta t \tag{4.7}$$

where Δt is denoted here as the time difference between the peak response of the two signals. The natural frequency of the sloshing fluid determined experimentally, f_{EXP}, occurs when the phase angle θ between the table displacement and sloshing base shear force is 90°. The frequency-response curve for the phase angle corresponding to tests TS5, TS19, and TS25 are shown for three different amplitudes in Figure 4.23 to Figure 4.25.

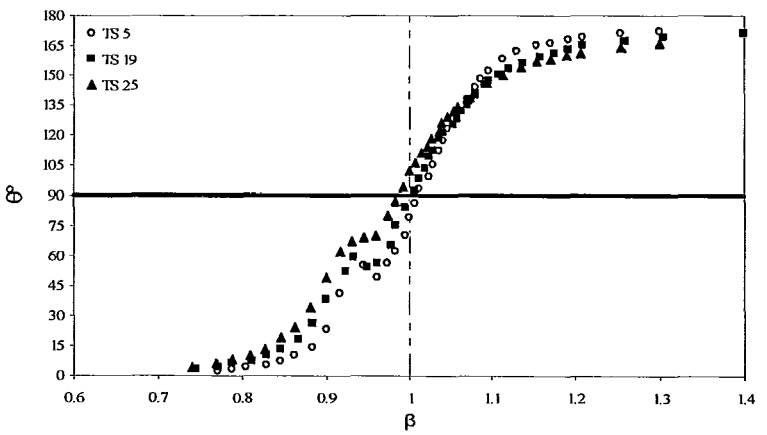

Figure 4.23 - Influence of slat height on θ, S=42%, A/L=0.0052

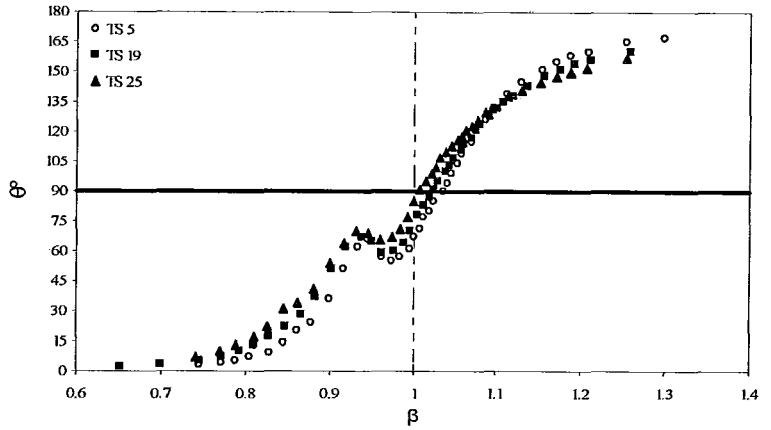

Figure 4.24- Influence of slat height on θ, S=42%, A/L=0.0104

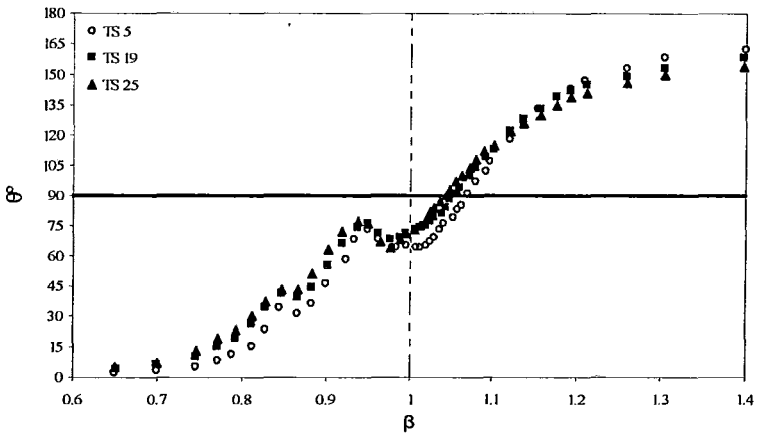

Figure 4.25 - Influence of slat height on θ, S=42%, A/L=0.0207

It is found that at low excitation amplitudes, i.e. A/L=0.0052, the experimentally determined natural sloshing frequency, f_{EXP}, is in good agreement with the theoretical value calculated in equation (4.3). However, as the amplitude of excitation increases the value of f_{EXP} also increases. This is representative of a hardening device and is a result of the nonlinearities associated with the sloshing fluid (Sun et al.,1995). In addition, the phase angle plots rotate in a clockwise direction as both the slat height and amplitude increase. This trend is indicative of

a system that has an increasing damping ratio (Chopra, 2000) and illustrates that the damping ratio, ζ_{TLD}, increases with slat height and amplitude.

Figure 4.26 compares the experimentally determined natural frequency to the theoretical natural frequency for the full range of A/L values tested.

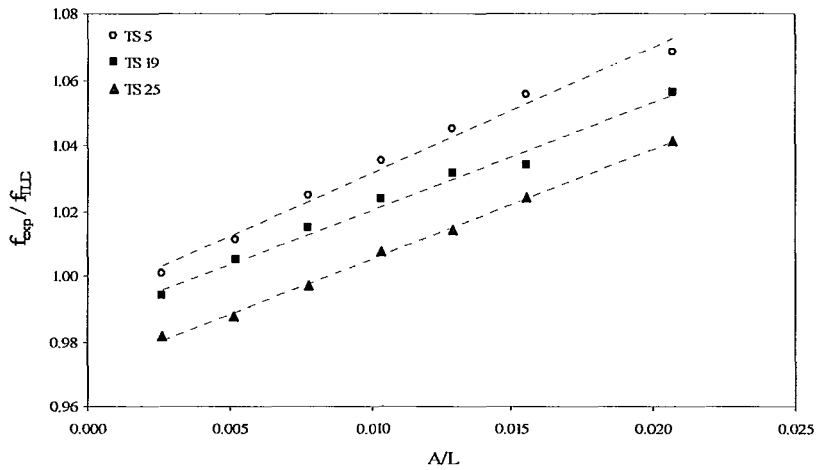

Figure 4.26 - Influence of Slat Height on f_{EXP} for $0.00259 \leq A/L \leq 0.0207$

A linear relationship is observed between experimentally determined natural frequency and the excitation amplitude. An increase in slat height reduces the value of f_{EXP} for each amplitude tested. It is postulated that this is a result of the larger slat heights influencing the flow of the fluid. If the slat height was increased to a large enough value, i.e. 200mm, then the TLD would essentially be divided into three sub-tanks and the natural frequency would be significantly different. Although the slat heights in this study are not increased that drastically it does appear that they alter the flow in a way that is similar to having a longer tank length. This can occur if the slat screens begin to behave as an orifice as the slat height is increased which could cause significant jetting action of the fluid. The

vertical shift in the f_{EXP} plots are a direct result of changing the slat height. Therefore, it is possible to postulate a relationship between $f_{\exp}$, f_n, and D given as

$$f_{\exp} = f_n \alpha D \tag{4.8}$$

where α is a modification factor that is dependent on the arrangement of the slats and the screen location within the tank.

While the vertical shift in $f_{\exp}$ is attributed to the change in slat height, the increase in $f_{\exp}$ with amplitude is caused by the nonlinear free surface response η. Work done by Bauer (1969) was aimed at determining the shift, Δf, between f_{EXP} and f_{TLD} for different h/L values due to the free surface response. It is expressed in equation (4.9) and can be considered an implicit function of excitation amplitude since the fluid response is a function of *A/L*.

$$\Delta f = f_{TLD}\left(\frac{\eta}{L}\right)^2 \frac{\pi^2}{64}\left[\frac{9-12\tanh^2\left(\pi h/L\right)-5\tanh^4\left(\pi h/L\right)-2\tanh^6\left(\pi h/L\right)}{\tanh^4\left(\pi h/L\right)}\right] \tag{4.9}$$

The theoretical shift in f_{TLD} is plotted against η/L for various h/L ratios in Figure 4.27.

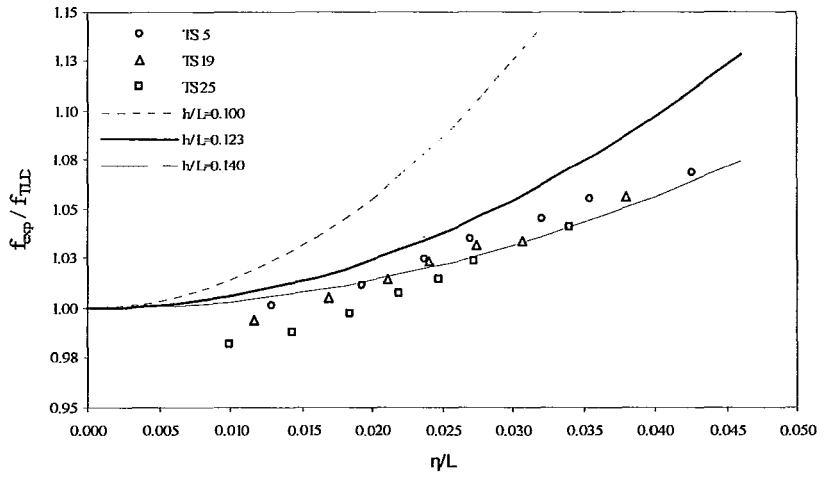

Figure 4.27 - Influence of η on f_{EXP} for Various h/L Ratios

Figure 4.27 compares the shift in the natural frequency of the TLD for three different h/L ratios. In addition, the experimental results for test TS5, TS19, and TS25 for a screen solidity of 42% are shown. As h/L increases the natural frequency of the TLD becomes closer to that predicted by potential flow theory over a greater range of response amplitudes.

4.2.5 Interaction of Free Surface Response and Base Shear Forces

From the experimental results the interaction of the free surface response, total base shear force, and sloshing base shear force can be assessed. Figure 4.28 compares the phase angle of the total base shear force, sloshing base shear force, and wave heights to the table displacement for the full range of excitation frequencies studied.

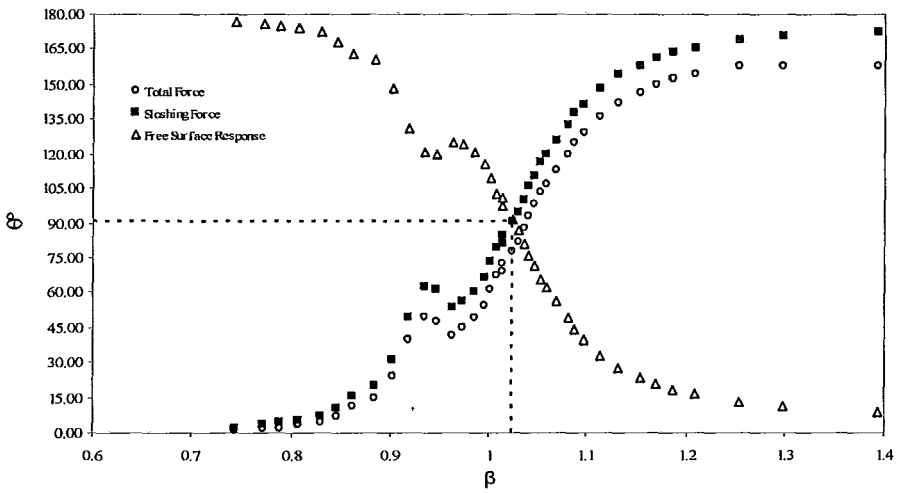

Figure 4.28 - Phase Angle Comparison, TS5, S=42%, *A/L*=0.0077

It is observed that the phase angle between the total base shear force and the table displacement lags the phase angle associated with the sloshing base shear force. Furthermore, the phase angle between the wave heights and the sloshing base shear forces start 180° out of phase and then intersect at a phase angle of 90°. This indicates that they are in phase when the TLD is at resonance $(\beta = 1.025)$ and shows that the sloshing base shear force is developed as a direct result of the free surface motion.

4.2.6 Influence of Slat Height on the Base Shear Forces

The total and sloshing base shear forces are low pass filtered in order to obtain the response of the fundamental mode. For each excitation frequency the maximum base shear forces are plotted versus β and are shown in Figure 4.29 to Figure 4.34.

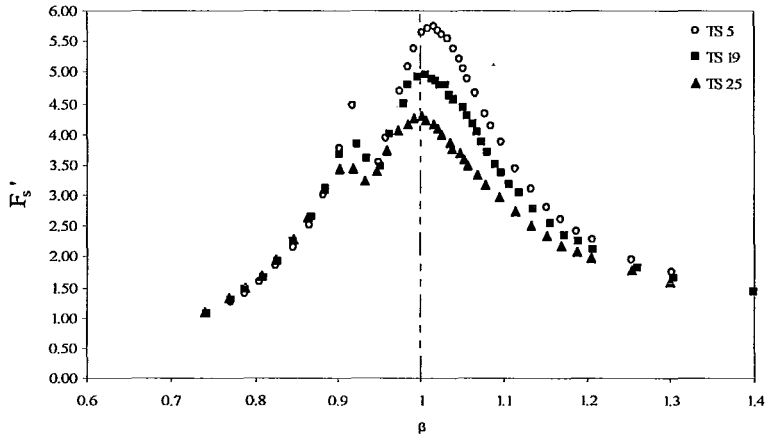

Figure 4.29 – Frequency-Response of F_S', S=42%, *A/L*=0.0052

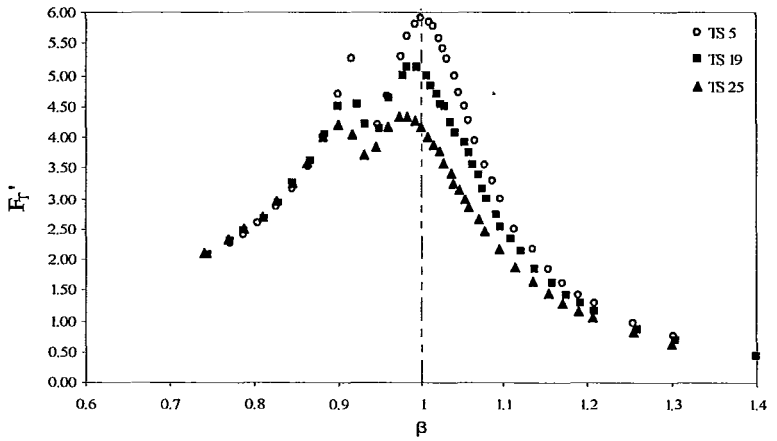

Figure 4.30 - Frequency-Response of F_T', S=42%, *A/L*=0.0052

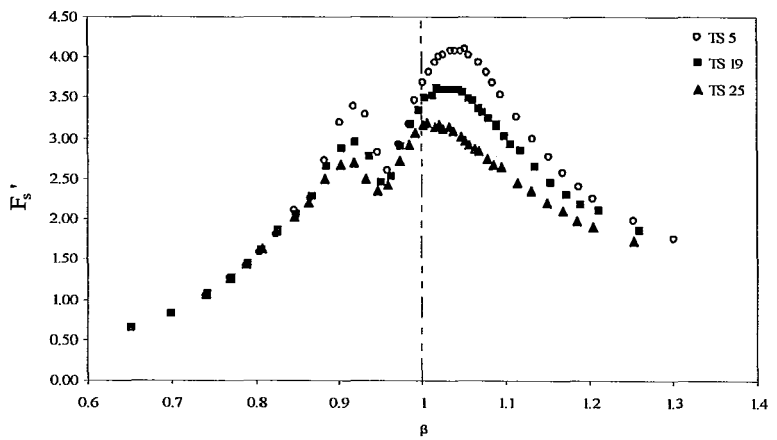

Figure 4.31 - Frequency-Response of F_S', S=42%, *A/L*=0.0104

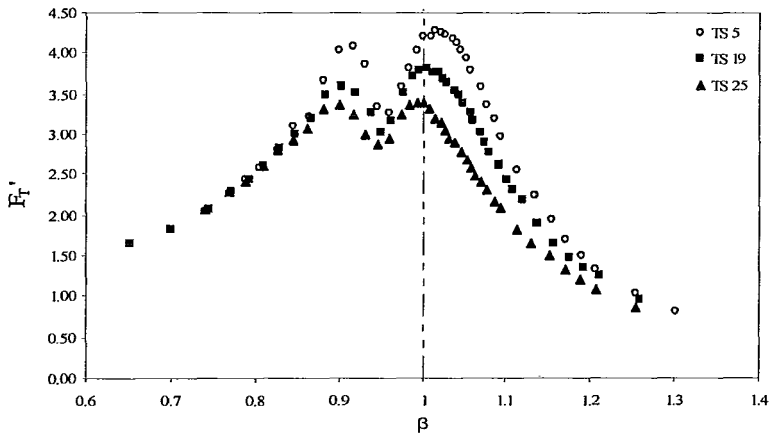

Figure 4.32 - Frequency-Response of F_T', S=42%, *A/L*=0.0104

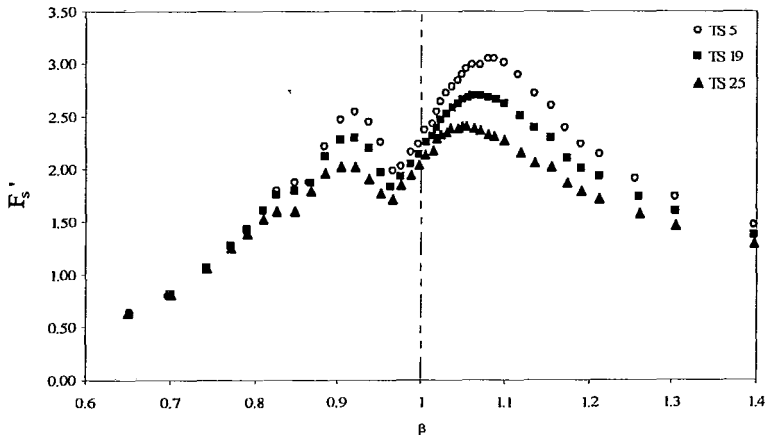

Figure 4.33 - Frequency-Response of F_S', S=42%, *A/L*=0.0207

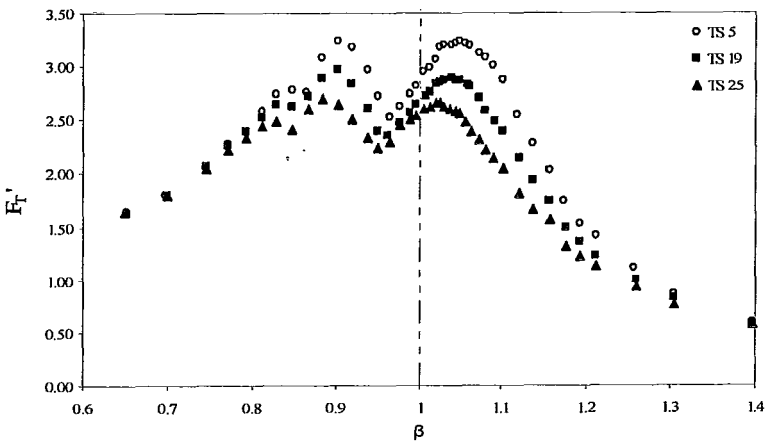

Figure 4.34 - Frequency-Response of F_T', S=42%, *A/L*=0.0207

The frequency-response plots shown compare the normalized total and sloshing base shear forces for slat heights of 5mm, 19mm, and 25mm. It is found that in all cases that peak value of $F_T^{'}$ is greater than the peak value of $F_S^{'}$. This is expected since $F_T^{'}$ is comprised of $F_S^{'}$ and the inertial force due to the non-participating mass. Therefore, at low β values $F_S^{'}$ is significantly lower than $F_T^{'}$ while at higher β values the opposite is true. In all cases it is evident that an increase in slat height leads to a reduction in the base shear forces, again showing that ζ_{TLD} increases with slat height.

4.2.7 Summary of Experimental Results for S=42%

The influence of slat height and amplitude on the response of a TLD has been shown in the previous sections. Energy dissipation plots were used as the main descriptor along with the TLD's free surface response and base shear forces. The following is a summary of the major findings at this screen solidity.

- An increase in slat height increases the damping of the TLD (ζ_{TLD}). This results in a reduction of the free surface response amplitude leading to a more linear response.
- This TLD acts as a hardening device and increasing the slat height does not reduce this phenomena.
- Increasing the slat height does cause a shift in $f_{\exp}$ for a given excitation amplitude indicating that an increase in slat height alters the flow path of

the fluid. A relationship between f_{exp} and slat height was suggested to be in the form of $f_{exp} = f_n \alpha D$

- The sloshing base shear force was shown to develop as a direct result of the free surface response

4.3 *Influence of Slat Height on the TLD Response for a Screen Solidity of 50%*

The influence that slat height has on the response of a TLD equipped with 50% solid slat screens is discussed in the following sections along with a comparison between the two screen solidities studied. Similar to the previous section, comparisons are made for *A/L* values of 0.0052, 0.0104, and 0.0207. The slat screens are installed at 0.4L and 0.6L and have slat heights of 5mm, 20mm and 25mm.

4.3.1 Influence of Slat Height on Free Surface Response

The free surface response of the TLD with 50% solid slat screens is low-pass filtered in order to obtain the response related to the fundamental mode. The frequency response of the wave heights at the tank end wall and centerline of tank are shown in Figure 4.35 to Figure 4.37.

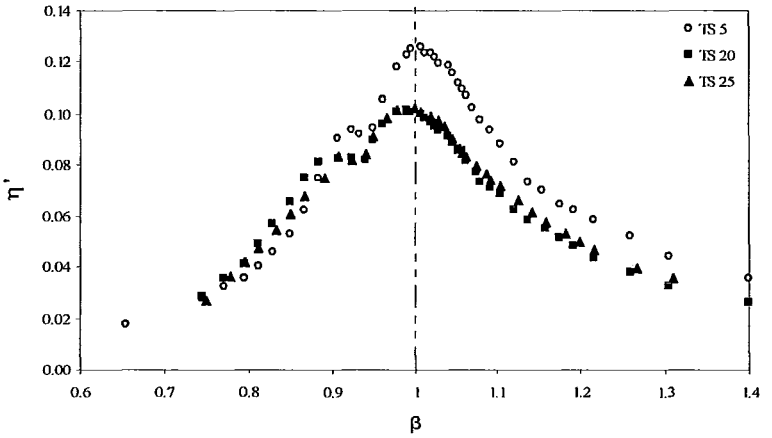

Figure 4.35 – Frequency-Response of η', S=50%, for A/L = 0.0052

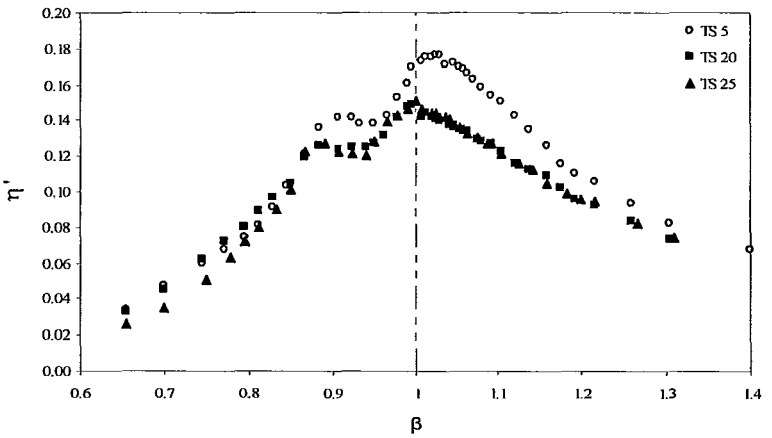

Figure 4.36 – Frequency-Response of η', S=50%, for A/L = 0.0104

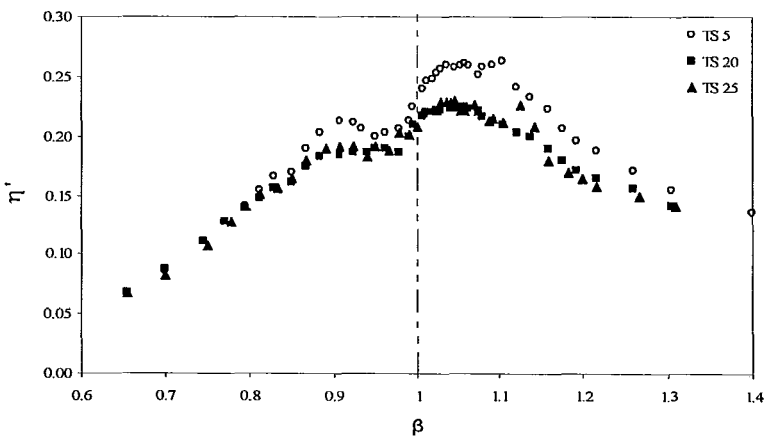

Figure 4.37 – Frequency-Response of η', S=50%, for A/L = 0.0207

The figures compare the normalized free surface response at the tank end walls for *A/L* values of 0.0052, 0.0104, and 0.0207. It is observed that increasing the slat height from 5mm to 20mm or 25mm reduces the free surface response by 22%, 20%, and 13% for the respective *A/L* values. This reduction in free surface response indicates an increase in ζ_{TLD} and is in agreement with the results from the 42% solid screens. Furthermore, it is seen that the response of the TLD with 20mm and 25mm slats is very similar. Both responses have the same maximum wave amplitude and typically have the same free surface response for a given excitation frequency. Similarities in the response are a result of using a mixture of slat heights in the construction of the 25mm-50% solid screens as discussed in Section 4.1. For this particular arrangement the D_{EFF} was calculated to be 19.8mm. Therefore, it is expected that the TLD will have the same response when using either the 20mm slats or the mixture of slats that comprise the 25mm slats. This is of practical importance to the design engineer because it shows a mixture of slat heights can be utilized as long as the effective slat height is used in analysis.

4.3.2 Influence of Slat Height on the Energy Dissipation

The amount of energy dissipated in one cycle of table motion is calculated from the force-displacement loops as described in Section 4.2.3. The frequency-response of the energy dissipated by the sloshing fluid is shown in Figure 4.38 to Figure 4.40 for the amplitudes tested at this screen solidity.

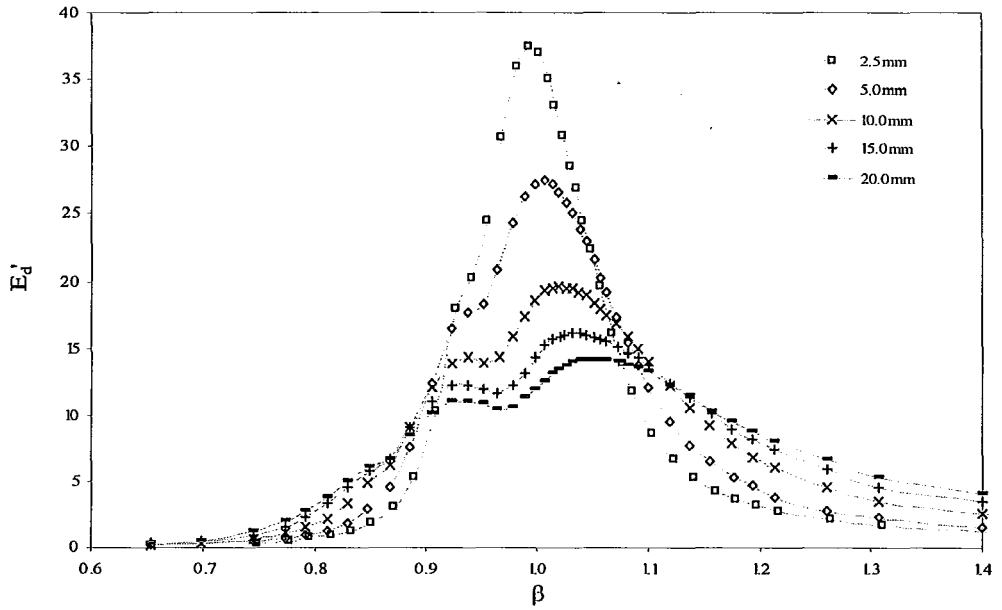

Figure 4.38 – $E_d^{'}$ Comparison, TS5, S=50%

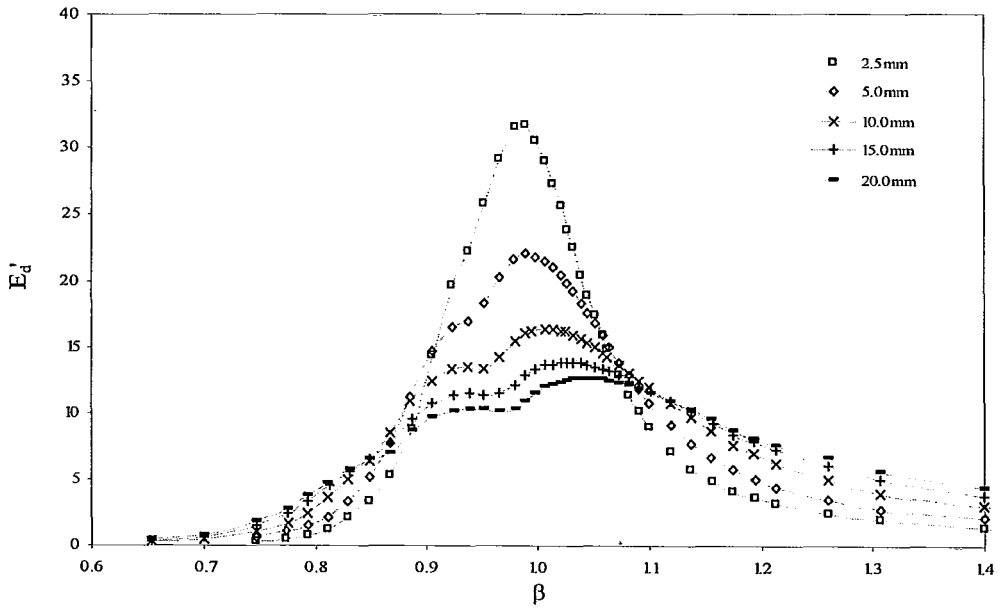

Figure 4.39 – $E_d^{'}$ Comparison, TS20, S=50%

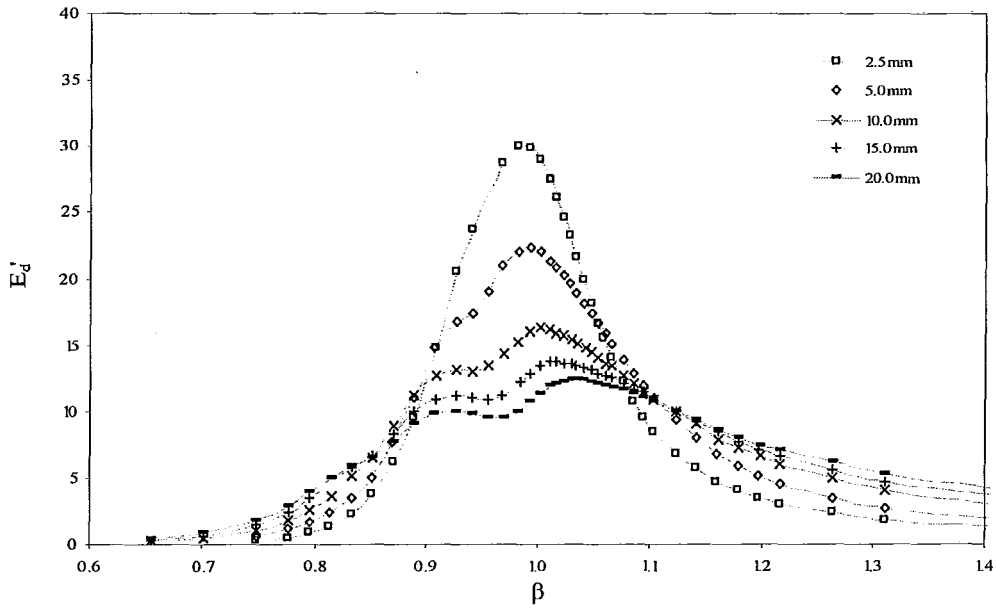

Figure 4.40 - $E_d^{'}$ Comparison, TS25, S=50%

The influence of slat height on the energy dissipating characteristics of the TLD with 50% solid screens is similar to that of the 42% solid screens. It is observed that the screen solidity does not influence the hardening type response of the device. An increase in slat height from 5mm to 20mm has reduced $E_d^{'}$ by 23%, 20%, and 15% for *A/L* values of 0.0052, 0.0104, and 0.0207, respectively. Furthermore, it is seen that an increase in slat height reduces the natural frequency of the device, a similar result was found for the 42% solid screens and was extensively discussed in Section 4.2.4.

4.3.3 Influence of Slat Height on Base Shear Forces

The experimental data is low-pass filtered in order to obtain the base shear forces that result from the fluid sloshing in its fundamental mode. The influence that slat

height has on the sloshing base shear force, $F_S^{'}$, is shown in figures Figure 4.41 to Figure 4.43 for A/L values of 0.0052, 0.0104, and 0.0207.

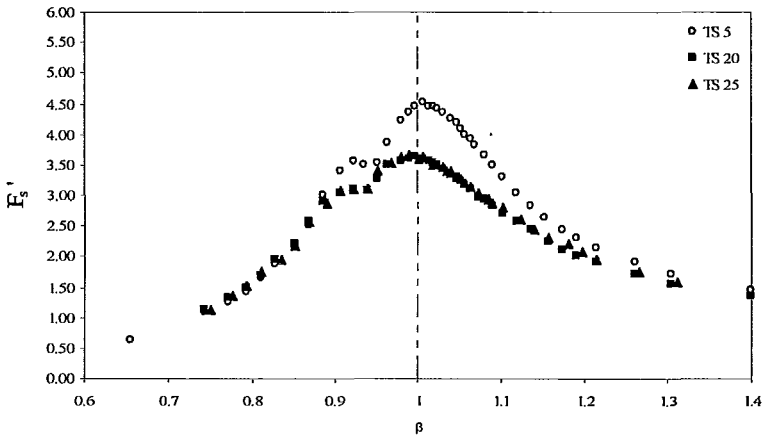

Figure 4.41 - Frequency-Response of $F_S^{'}$, S=50%, A/L=0.0052

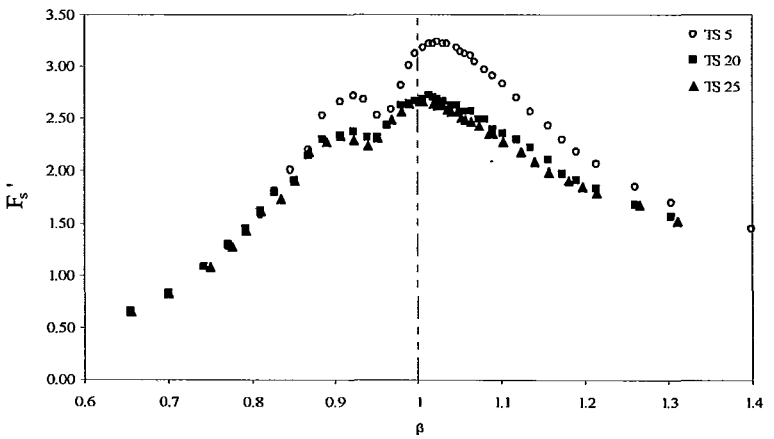

Figure 4.42 - Frequency-Response of $F_S^{'}$, S=50%, A/L=0.0104

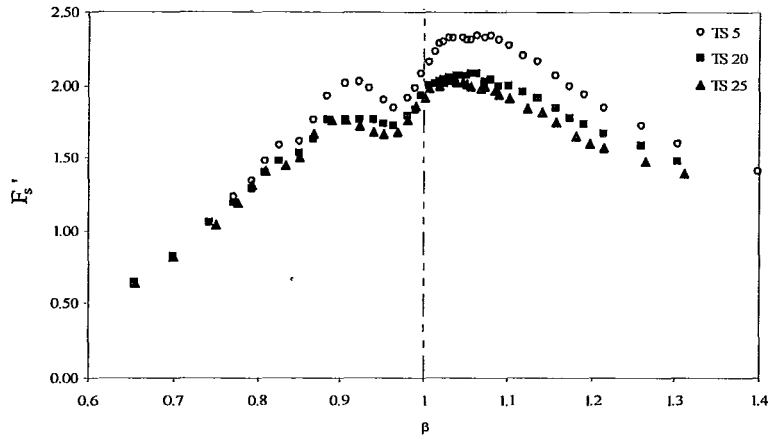

Figure 4.43 - Frequency-Response of F_S', S=50%, *A/L*=0.0207

It is observed that increasing the slat height from 5m to 20mm has reduced the normalized base shear force by 20%, 17%, and 10% for the respective *A/L* values. This trend is similar to that found for the 42% solid screens. Finally, the resultant base shear forces for the 20mm and 25mm slats show a very similar frequency-response for the three *A/L* values chosen. This result is expected and was discussed in Section 4.3.1.

4.4 *Influence of Corner Geometry on TLD Response*

A component of this experimental work was aimed at determining the influence that corner geometry, in particular, the corner radius (Figure 3.8) has on the fluid response of this TLD. This comparison is made between partial height screens with 20mm slats and a screen solidity of 50%. The sharp edged slat screens are referred to as test TS20 while the rounded edged slat screens are referred to as test TR20. The frequency-response of the energy dissipated by the sloshing fluid for test TR20 is shown in Figure 4.44.

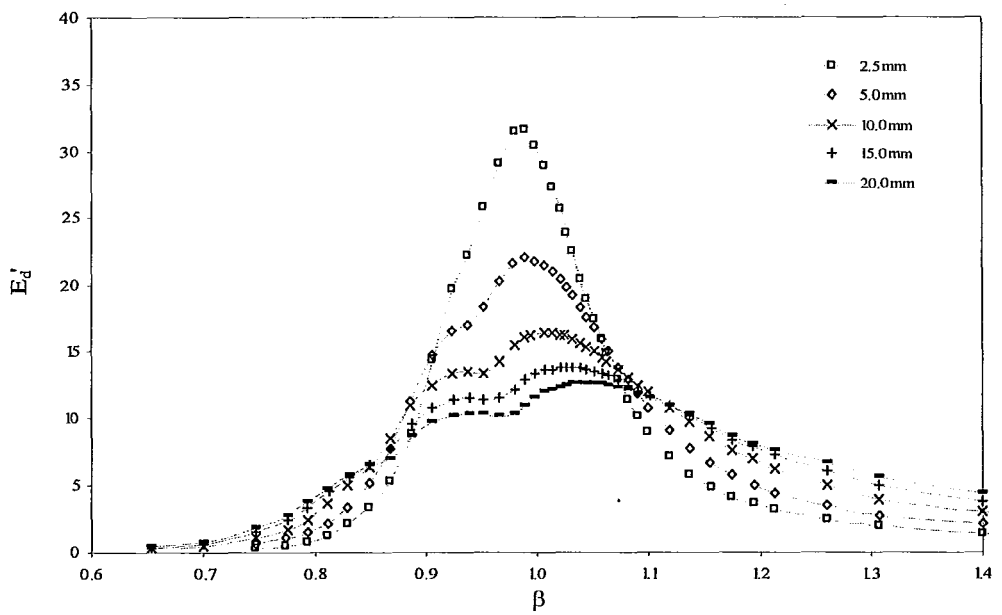

Figure 4.44 - $E_d^{'}$ Comparison for , TR20, S=50%

The response of the TLD with rounded edged slat screens exhibits the same behaviour as the TLD with sharp edged slat screens. Both the sharp and rounded edge slat screens result in a TLD that responds in a hardening manner and the presence of superharmonics is observed. On average the TLD with rounded edged slat screens dissipates between 12-16% more energy than the TLD with sharp edged slat screens.

The effect of flow around a submerged body is a topic in fluid mechanics that has been extensively studied. The main difference between flow around a sharp and round edge is that the flow separation and reattachment path is shorter for the rounded edge slats. This results in a higher fluid velocity compared to the sharp edged slats indicating a lower drag force and lower ζ_{TLD}. The response of the TLD with rounded edges slats is compared to the TLD with sharp edged slats

at A/L=0.0052, A/L=0.0104, and A/L=0.0207 and shown in Figure 4.45 to Figure 4.47.

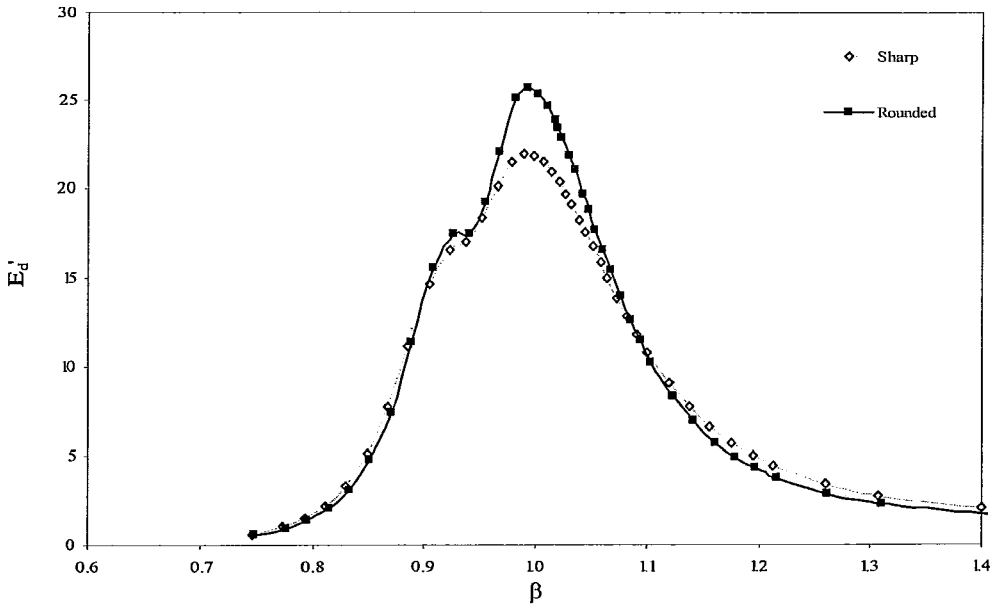

Figure 4.45 - E_d' Comparison between Sharp and Rounded Edges, S=50%, A/L=0.0052

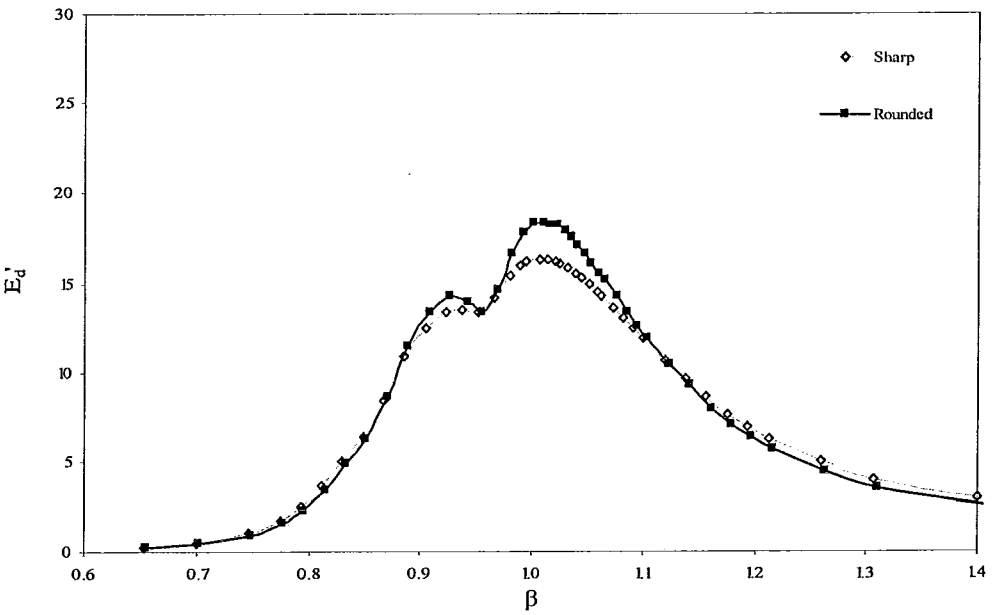

Figure 4.46 - E_d' Comparison between Sharp and Rounded Edges, S=50%, A/L=0.0104

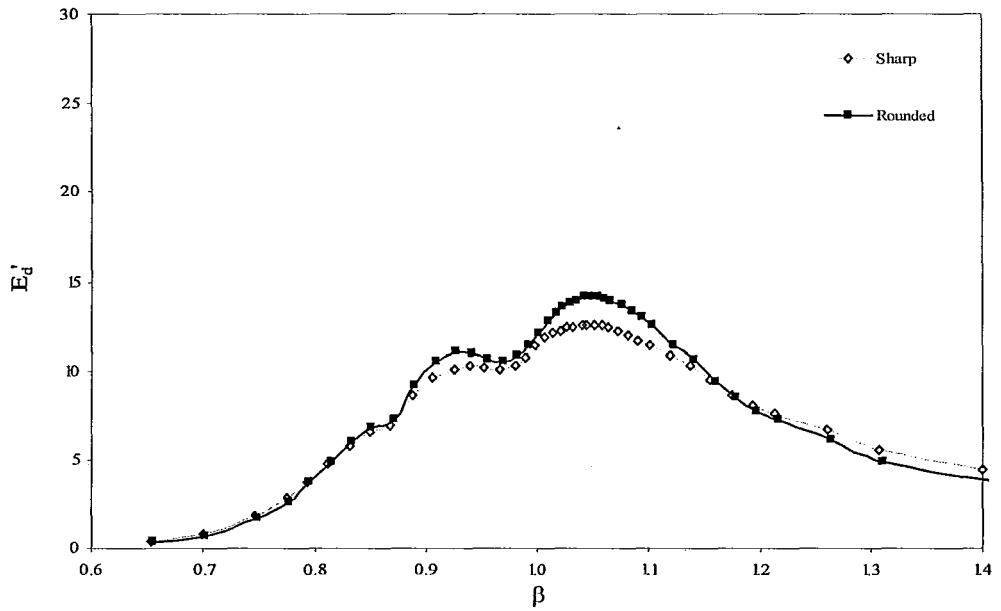

Figure 4.47 - $E_d^{'}$ Comparison between Sharp and Rounded Edges, S=50%, A/L=0.0207

At all three amplitudes the TLD with rounded edge slat screens dissipates more energy than the sharp edge slat screens. This is a result of the round edge slat screens having a lower loss coefficient than the sharp edged screens. This finding may be useful in the design of TLD's because it allows the screen loss coefficient to be modified once the screens have been installed. For example, if the TLD performance needs to be modified after installation, rather then installing new screens, the existing screens can be shaped (rounded) in order to achieve the desired response.

4.5 *Experimental Determination of C_L*

A component of this research study involves numerically modeling the response of a TLD subjected to sinusoidal excitation. The effect of slat screens is modelled

through a velocity loss coefficient, C_L, and is applied as a boundary condition at the screen locations (Chapter 5). In order to validate the model's ability to predict the response of the TLD it is necessary to determine the experimental values of C_L. The following procedure is used to estimate C_L for both solidities of slat screens. The forces exerted by the fluid on the screens are captured using load cells as outlined in Chapter 3. The time history variation of the free surface motion is captured by two wave probes located at 0.05L and 0.95L. Only the fundamental mode is retained to estimate the fluid velocity at the screen location. The horizontal component of particle velocity, $u(x,z,t)$, for a standing wave can be obtained from the free surface response as (Dean and Dalrymple, 1984)

$$u(x,z,t) = \eta\omega \frac{\cosh(k(z+h))}{\sinh(kh)} \cos\left(\frac{\pi x}{L}\right) \cos(\omega t) \tag{4.10}$$

where k is the wave number which is equal to π / L. The above equation is integrated through the fluid depth in order to obtain the average particle velocity

$$u(x,t) = \frac{\eta\omega L}{\pi h} \sin\left(\frac{\pi x}{L}\right) \tag{4.11}$$

The screens are located in oscillating flow where the along-wave force per unit length, f, acting on a submerged body is given by the Morrison equation (Morrison et al., 1950) as

$$F = C_m \rho_w \pi \frac{D^2}{4} \frac{\partial u}{\partial t} + \frac{1}{2} C_d D \rho_w u|u| \tag{4.12}$$

where C_m is the inertia component, ρ_w is the density of water, D is the slat height or equivalent slat height if partial slats are used, and C_d is the drag coefficient. The inertial component, C_m, is an added mass term that measures the amount of additional energy required to establish a flow field around a moving body (Tait, 2004) and is not considered in this study. Work by Keulegan and Carpenter (1958) provided the following relationship between C_d and the force F

$$C_d = -\frac{3}{4}\int_0^{2\pi} \frac{F\cos\theta d\theta}{\rho U_m^2 D} \tag{4.13}$$

where $\theta = \frac{2\pi}{T}$ and U_m is the amplitude of the velocity at the screen solved according to equation (4.11) for x=0.4L or 0.6L. The relationship between the drag coefficient, C_d, and the velocity loss coefficient, C_L, is given as

$$C_L = C_d S \tag{4.14}$$

Keulegan and Carpenter found a relationship between the drag coefficient and a parameter termed the Keulegan-Carpenter or KC number where the KC number is given as

$$KC = \frac{U_m T}{D} \tag{4.15}$$

This approach is used to determine the relationship between C_L and KC for all slat heights, solidities, and amplitudes. The results for S=42% are shown in Figure 4.48 and for S=50% in Figure 4.49.

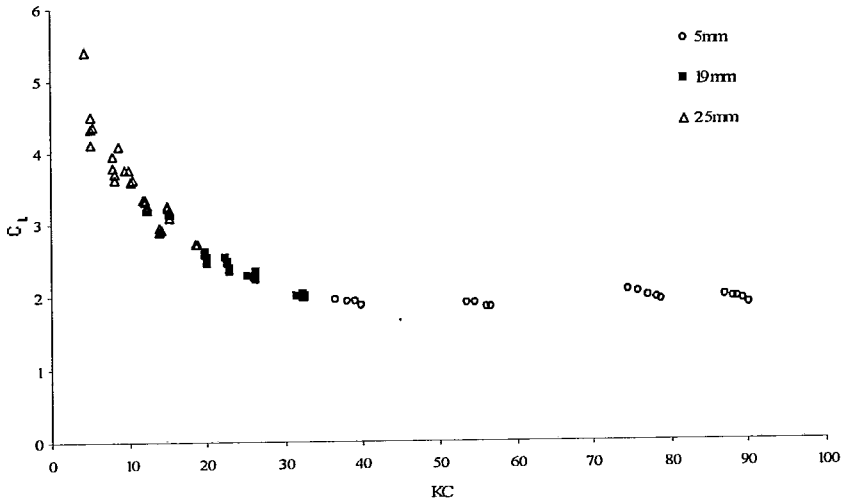

Figure 4.48 - Experimentally Determined C_L Values for S=42%

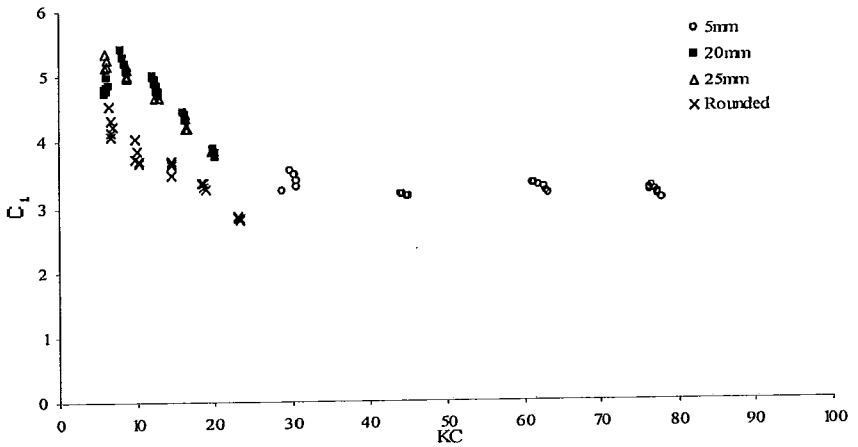

Figure 4.49 - Experimentally Determined C_L Values for S=50%

Figure 4.48 shows the relationship between C_L and KC for a screen solidity of 42%. There are two distinct regions observed in this plot, one where C_L is independent of KC and one where C_L is KC dependent. It is observed that as the slat height is increased the value of C_L also increases. Furthermore, for KC numbers greater than 30, C_L approaches a steady flow value of approximately 2.0

which is in agreement with studies by Tait (2004) and Fediw (1992). Figure 4.49 shows the relationship between C_L and KC for a screen solidity of 50% for both the solid and rounded edge slats. The overall trend is similar to that found in Figure 4.48. As the slat height increases the value of C_L also increases. However, for KC numbers greater than 30 the C_L value approaches a value of 3.1 with this difference being attributed to the difference in screen solidity.

4.6 *Conclusions*

The experimental results from the shake-table experiments have been presented for the TLD equipped with two damping screens at 0.4L and 0.6L having a screen solidity of 42% and 50%. Both time-history and frequency-response plots have been presented for A/L values covering the range of amplitudes tested. Comparisons of the TLD's hysteretic behavior, free surface response, and base shear forces have been presented and the influence of slat height on these responses assessed. The following are the major observations and conclusions that can be drawn from this work;

- An increase in slat height leads to a change in the loss coefficient C_L. The variation in C_L has been correlated to the KC number which is a function of fluid velocity and slat height
- An increase in slat height leads to a reduction in the natural frequency. This is postulated to occur due to the larger slats influencing the flow of

the fluid. A modification factor was suggested to account for this shift which is given as $f_{exp} = f_n \alpha D$

- A similar TLD response can be achieved by selecting a high solidity-small slat screen or a low solidity-large slat screen (i.e. TS5-50 vs. TS25-42). In addition, it provides the design engineer with an array of design alternatives since it allows the selection of screens based on screen solidity, slat height, and *KC*.
- Rounded edge slat screens were shown to exhibit a similar response compared to the sharp edged screens. However, for a given *KC* number the rounded edge screens have lower loss coefficients. This indicates that edge geometry is an important parameter in TLD design.

Chapter 5 – Numerical Model of a TLD with a Varying Loss Coefficient

Two numerical models are utilized in this chapter to simulate a TLD equipped with damping screens. A nonlinear model based on shallow water wave theory is presented and its ability to simulate the response of the shake table experiments is assessed. In addition a potential flow model, assuming a linearized free surface response, is also investigated. This chapter begins by presenting an overview of both numerical models utilized in this study. A curve fitting procedure is used to develop the relationship between the experimentally determined loss coefficient and the *KC* number. The influence of a varying loss coefficient is incorporated into the potential flow model and a comparison to the shake-table experiments is made. This is followed by incorporating the varying loss coefficient into the nonlinear numerical model and a comparison is made to the experimental results. The chapter concludes with an investigation into the influence that slat height has on the damping of the TLD.

5.1 Overview of Numerical Models

Two numerical models are utilized in the subsequent sections. The nonlinear model employed is based on work by Lepelletier and Raichlen (1988) who looked at linear and nonlinear oscillations in rectangular tanks assuming shallow water wave theory $(h/L \leq 0.1)$. Kaneko and Ishikawa (1999) used shallow water wave theory to model the response of a rectangular tuned liquid damper equipped with

submerged nets. Tait (2004) contributed to this body of work by incorporating the influence of flow damping devices (screens) through a loss coefficient (C_L) that was screen solidity dependent. Tait et al. (2005) validated his work for both the linear and nonlinear shallow water models under small (wind) and large (earthquake) amplitudes. Cassolato (2007) used linear shallow water wave theory to include the influence of screen angle on the fluid response and validated this model with shake table experiments.

Bauer (1964) developed a nonlinear numerical model for sloshing in a rectangular tank of infinite length using potential flow theory. Warnitchai and Pinkaew (1998) used potential flow theory to model the response of a rectangular tuned liquid damper with wire mesh screens. Isaacson and Premasiri (2001) investigated hydrodynamic damping due to baffles installed in a TLD subjected to earthquake excitation. Deng (2007) contributed to this body of research by modelling the response of the damper with various tank geometries. Cassolato (2007) introduced a screen angle dependent loss coefficient into this model and validated the results experimentally. All of the potential flow models described considered only the fundamental mode response and assume a linearized free surface response.

Shallow water wave theory and potential flow models have been used to model the response of a tuned liquid damper with slat screens by Tait et al. (2005). However, these models are developed for slat screens that have a constant loss coefficient. Tait showed that the loss coefficient could be estimated based on

the screen solidity for slat screens in the high KC number range $(KC \geq 30)$. The numerical models that are developed in the following sections add to this body of work by incorporating a loss coefficient that is dependent on both the KC number and the screen solidity.

5.2 Curve Fitting Procedure

The effect of having a KC number dependent loss coefficient has been illustrated throughout the presentation of the experimental results. The effect of an increase, or decrease, in slat height is that the C_L value will change accordingly until it reaches a steady state value ($KC > 30$). In Section 4.5 it has been shown that the 19mm, 20mm, and 25mm slat heights have KC number dependent loss coefficients. Conversely, the 5mm slat screens have a loss coefficient that is nearly independent of KC. In all cases, as the KC numbers increases, the C_L value approaches a steady state value where the losses become dependent on the screen solidity alone. The value of C_L under steady state conditions, C_L^{steady}, is given by Baines and Peterson (1951) as

$$C_L^{steady} = \left(\frac{1}{C_c(1-S)} - 1 \right)^2 \tag{5.1}$$

where C_c is the contraction coefficient. The value of C_c for a thin plate orifice was measured experimentally by Weisbach(1855) and is adapted by Tait (2004)

$$C_c = 0.405e^{-\pi S} + 0.595 \tag{5.2}$$

For the two screen solidities that were tested, S=0.42 and S=0.50, the respective C_L^{steady} values are 2.16 and 3.78. The relationship between KC and C_L has been presented in the previous chapter for both screen solidities (Figure 4.48 and Figure 4.49). In developing the numerical models it is required to express C_L as a function of the KC number. In order to extend the range of application of the numerical models C_L is expressed as a function of both KC and S. To accomplish this, the experimentally measured C_L value is normalized by the theoretical value of C_L at steady state, which is predicted by equation (5.1). A power curve is fitted to the experimental data using a least squares approach in order to determine the relationship between C_L, KC, and S. The equation of the experimentally fitted power curve is given as

$$C_L = \left(6.4KC^{-0.90} + 0.72\right) C_L^{steady} \tag{5.3}$$

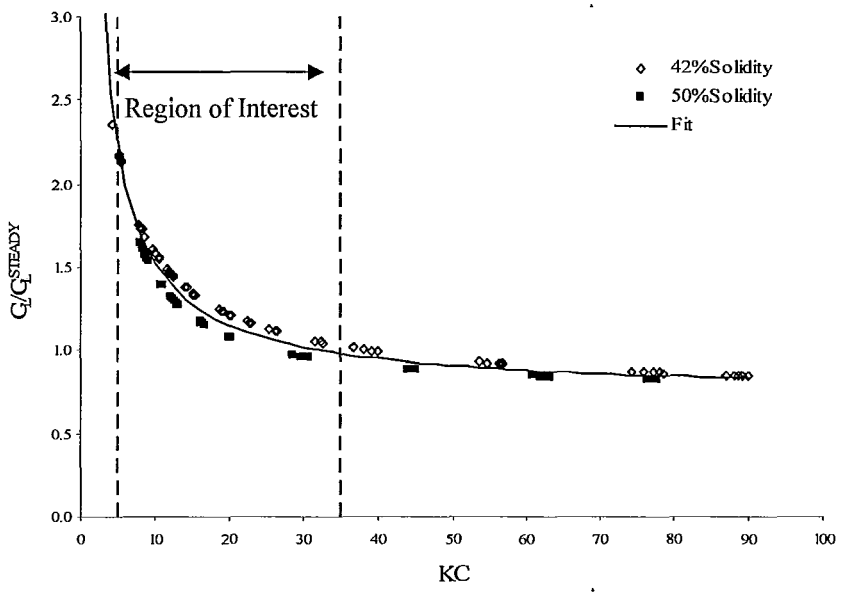

Figure 5.1 - Normalized Relationship between *KC* and C_L

Figure 5.1 compares the normalized experimentally measured loss coefficients and the fitted equation given by equation (5.3). A good fit is found between the experimental results and the C_L value calculated using equation (5.3). The largest discrepancy between the C_L values occurs for $15 \leq KC \leq 30$ where a 5% difference exists. This translates into a small difference in the C_L value that is used in the model and is not expected to reduce its applicability. The focus of this research is to assess the influence that screens with a varying loss coefficient have on the performance of a TLD. Therefore, the range of *KC* numbers that is of most interest is shown in Figure 5.1. In this region the loss coefficient varies significantly with changes in the *KC* number. For example, as the *KC* number increases from 6 to 30, the loss coefficient changes from $2 \bullet C_L^{steady}$ to C_L^{steady}. For

the 42% solid screens this leads to a change in C_L from 4.32 to 2.16. Conversely, as the KC number increases past 30, there is little change in the loss coefficient indicating that the losses are nearly KC number independent.

5.3 *Non-Linear Model*

The nonlinear numerical model utilized in this study is presented in the subsequent section.

5.3.1 Description of Nonlinear Model

The nonlinear model used in this study was developed by Kaneko and Ishikawa (1999) and is briefly described here. Figure 5.2 presents the definition sketch that is used in the development of this model.

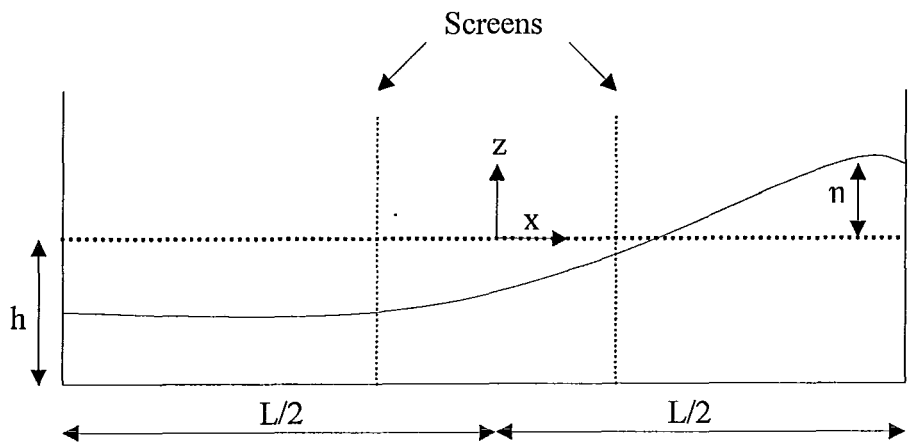

Figure 5.2 - Definition Sketch For Nonlinear Model

The nonlinear model is developed assuming shallow water wave theory (h/L<0.1) and unidirectional (1-D) motion. Additionally, it is assumed that the slat screens do not alter or influence the flow of the fluid. This assumption permits the use of theoretical work developed for a TLD without screens. The continuity and momentum equations that describe the sloshing response are given as (Lepelletier and Raichlen, 1988)

$$\frac{\partial \eta}{\partial t}+\frac{\partial (h+\eta)\bar{u}}{\partial x}=0 \tag{5.4}$$

$$\frac{\partial \bar{u}}{\partial t}+\bar{u}\frac{\partial \bar{u}}{\partial x}+g\frac{\partial \eta}{\partial x}-\frac{1}{3}(h+\eta)^2\frac{\partial^3 \bar{u}}{\partial x^2 \partial t}+\zeta_w \bar{u}+\ddot{X}_G=0 \tag{5.5}$$

where $\eta(x,t)$ is the free surface response, $\bar{u}(x,t)$ is the horizontal velocity averaged through the fluid depth, $\ddot{X}_G$ is the horizontal base acceleration, and ζ_w is a damping term introduced to account for viscous dissipation along the tank wall and free surface. In this model, a linear damping term proportional to the average velocity is assumed (Miles, 1967) and is given as

$$\zeta_w=\frac{2}{L}\sqrt{\upsilon_w \pi f}\left[\frac{L}{b}+1+\frac{\pi\left(1-\frac{2h}{L}\right)}{\sinh\left(\frac{2\pi h}{L}\right)}+\frac{\pi}{2}\coth\left(\frac{\pi h}{L}\right)\right] \tag{5.6}$$

where υ_w is the kinematic viscosity of the water. The above continuity and momentum equations can be solved numerically once the initial conditions are specified.

A one dimensional finite difference scheme is used for both $\bar{u}$ and η. The boundary conditions at the tank end walls are given as $\bar{u}(-0.5L,t) = \bar{u}(0.5L,t) = 0$. For a particular excitation amplitude, equations (5.4) and (5.5) are numerically integrated using the Runge-Kutta-Fehlberg method after imposing the initial conditions that $\eta(x,0) = 0$ and $\bar{u}(x,0) = 0$ (Tait, 2004).

At locations where damping screens are inserted inside the tank the velocity at the screen, $\bar{u}_{screen}$, is given as

$$\bar{u}_{screen} = \frac{\bar{u}_i + \bar{u}_{i+1}}{2} \tag{5.7}$$

The pressure drop across the screen, Δp, can be expressed as

$$\Delta p = C_L \frac{\rho \bar{u}_{screen}^2}{2} \tag{5.8}$$

and C_L is the KC number dependent loss coefficient provided by equation (5.3). The relationship between the pressure drop and the free surface wave height difference across the screen is given as (Kaneko and Ishikawa, 1999)

$$|\eta_L - \eta_R| = \Delta\eta = C_l \frac{\bar{u}_{screen}^2}{2g} \tag{5.9}$$

The resulting wave height to the left and right of the screen is then given as

$$\eta_L = \eta_i + sign[\bar{u}_{screen}]\frac{\Delta\eta}{2} \tag{5.10}$$

$$\eta_R = \eta_i - sign[\bar{u}_{screen}]\frac{\Delta\eta}{2} \tag{5.11}$$

An iterative procedure is used in the solution to this numerical model since the loss coefficient is velocity dependent. This iterative procedure it outlined below for the case of sinusoidal excitation;

- After one half cycle of table motion, the maximum fluid velocity at the screen and period of oscillation are calculated
- The KC number is determined and the corresponding C_L value is calculated using equation (5.3)
- The new loss coefficient is compared to the old loss coefficient. If the difference between the two is greater than 0.01 C_L is set equal to the new value of C_L and the current cycle of table motion is repeated
- If the difference is less than 0.01, the loss coefficient is considered to be correct and the simulation is continued
- The base shear forces, wave heights, and energy dissipated are determined for each excitation frequency
- This iterative procedure is continued for each frequency that is specified and a full frequency sweep is completed

5.3.2 Validation of Nonlinear Model

5.3.2.1 Frequency-Response of Energy Dissipated

The nonlinear model described in the previous section is used to model the effect of slat screens with KC number dependent losses on the response of a TLD. Figure 5.3 compares the results of the numerical model with KC number dependent losses to the model developed by Tait (2004) where C_L is constant (solely dependent on S). The normalized energy dissipated per cycle is plotted versus β for three different slat heights and for the steady state value of C_L corresponding to a screen solidity of 42%.

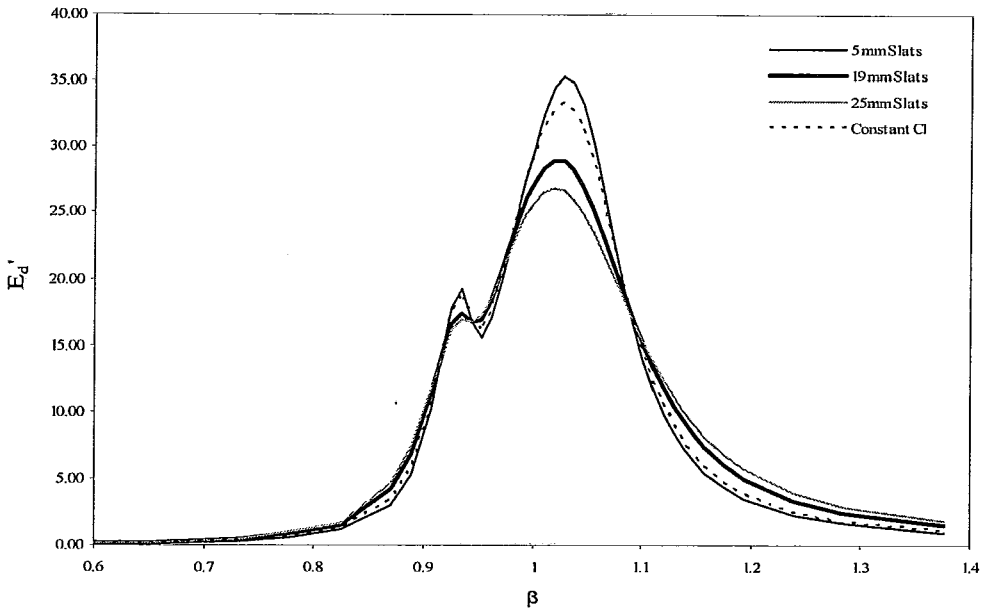

Figure 5.3 – Comparison Between Constant Loss Coefficient Numerical Model and the Varying Loss Coefficient Model

Tait (2004) developed a model for the case of a constant loss coefficient, shown by the dashed line in Figure 5.3. As a result, the influence of slat height was not considered. In the proposed modified model, the influence of slat height has been incorporated and is plotted for slat heights of 5mm, 19mm, and 25mm. All four responses shown correspond to a screen solidity of 42%. This comparison illustrates that the peak value of E_d' changes as the slat height is increased thus indicating that the nonlinear model described in the previous section correctly incorporates the *KC* number effect on the screen loss coefficient. In addition, a double peak response is observed in the E_d' plots indicating that the proposed model is capable of capturing the nonlinearities associated with the fluid response. Figure 5.4 and Figure 5.5 compare the normalized energy dissipated per cycle

from the experimental tests to those predicted by the nonlinear model for an *A/L* value of 0.0026.

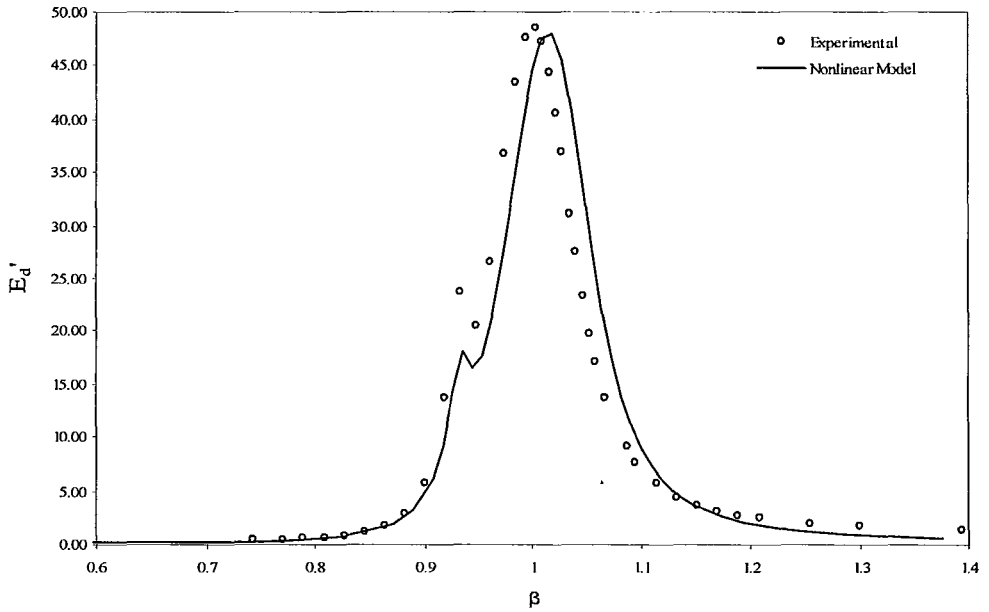

Figure 5.4 - Comparison Between Nonlinear Model and Experimental Results, TS5, *A/L*=0.0026, S=42%

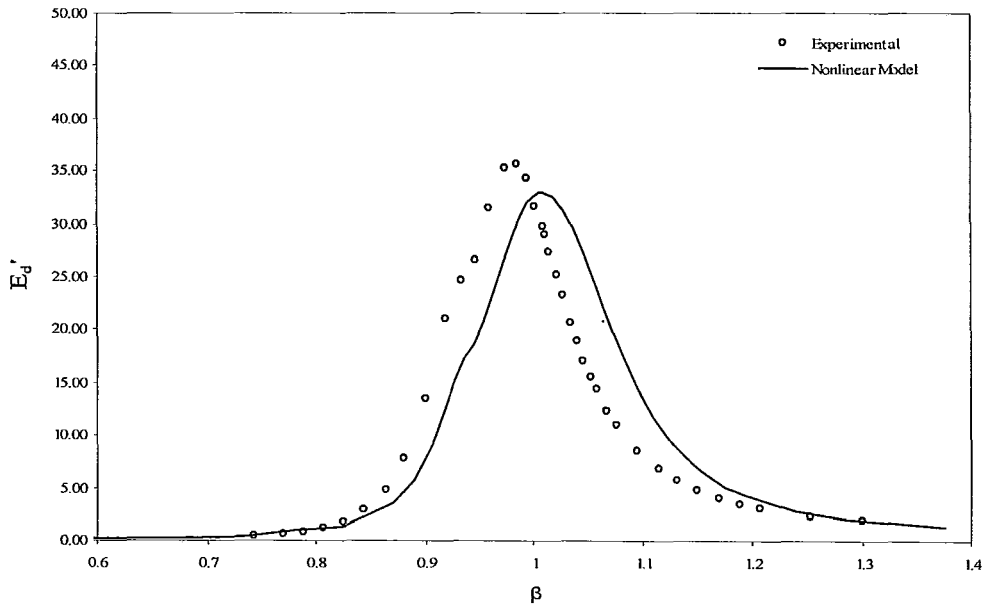

Figure 5.5 - Comparison Between Nonlinear Model and Experimental Results, TS25, *A/L*=0.0026, S=42%

The numerical model predicts the peak response of $E_d^{'}$ for the 5mm slat screens to within 1%. The natural frequency is slightly (1.5%) over-predicted by the numerical model which agrees with findings by Tait (2004). The numerical model over-predicts the peak value of $E_d^{'}$ by 10% for the 25mm slats. The discrepancy observed for the 25mm slats is due to the sensitivity of small changes in the *KC* number at low values ($KC<8$) as illustrated in Figure 5.1. Therefore, a small error in the predicted *KC* number from the model is amplified as this results in a significant error in the estimated loss coefficient. This discrepancy is not observed for the 5mm slats because the loss coefficient is nearly constant for this range of *KC* numbers.

There is a discrepancy in the natural frequency predicted by the numerical model at this amplitude of excitation. One of the assumptions in the development of this model is that the screens do not alter the overall flow of the fluid. However, as the slat height increases this assumption may no longer be valid. It is postulated that as the slat height is increased the effective tank length increases resulting in a reduction in the natural sloshing frequency of the fluid. Therefore, at this excitation amplitude the numerical model is unable to capture the natural frequency of the TLD when the larger slat screens are installed.

Figure 5.6 to Figure 5.8 compare the normalized energy dissipated per cycle from the experimental tests to those predicted by the nonlinear model for an *A/L* value of 0.0077.

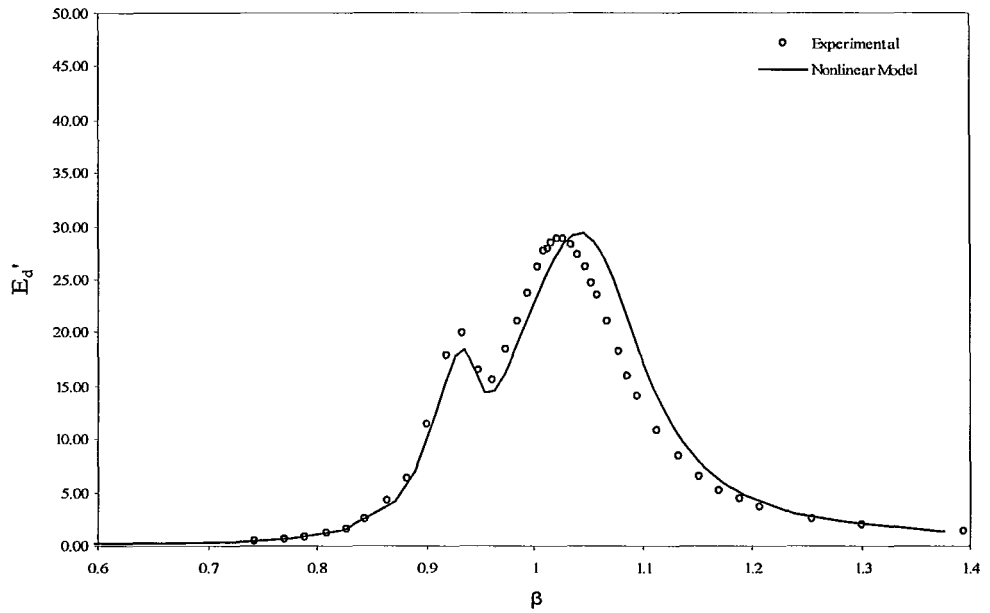

Figure 5.6 - Comparison Between Nonlinear Model and Experimental Results, TS5, *A/L*=0.0077, S=42%

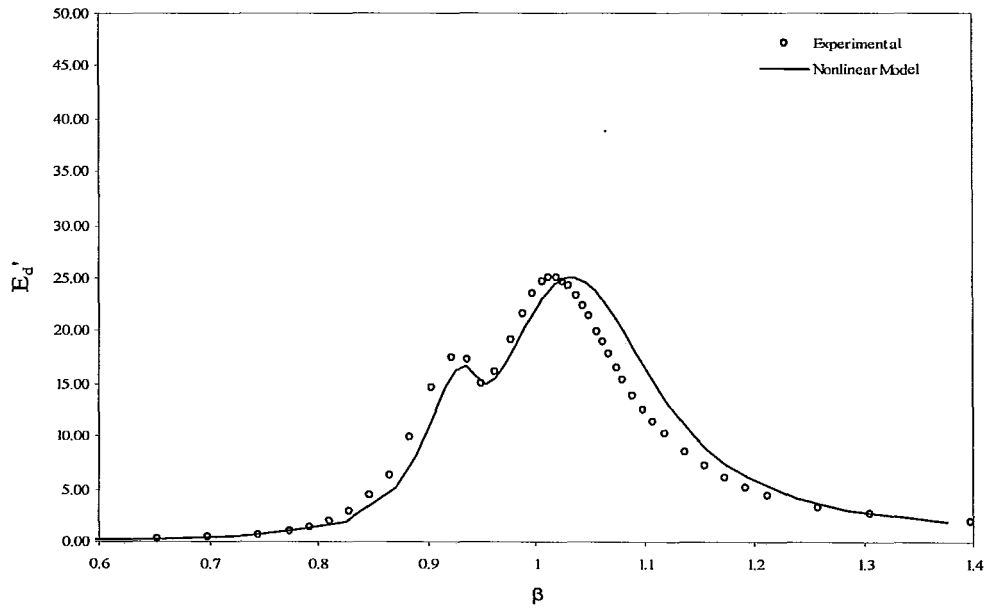

Figure 5.7 - Comparison Between Nonlinear Model and Experimental Results, TS19, *A/L*=0.0077, S=42%

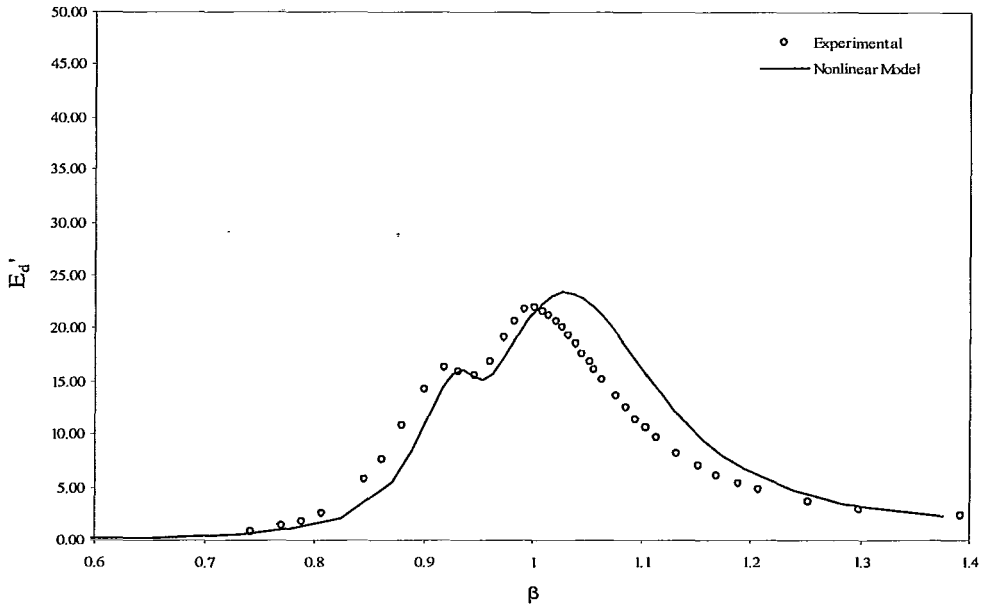

Figure 5.8 - Comparison Between Nonlinear Model and Experimental Results, TS25, *A/L*=0.0077, S=42%

Good agreement between the model and experimental results is observed for both the 5mm and 19mm slat screens. The model over-predicts the peak response of $E_d^{'}$ by 6% for the 25mm slats and in all three cases the predicted natural frequency is higher than the value found in experiment. The ability of the model to predict the presence of superharmonics is indicated by the double peak response in the $E_d^{'}$ plot. The frequency at which the superharmonic is excited is accurately predicted by the model for the 5mm slat screens. However, the model over-predicts this frequency for the larger slats. Finally, the numerically predicted natural frequencies observed in the $E_d^{'}$ plots from Figure 5.6 to Figure 5.8 are higher than those observed for *A/L* equal to 0.0026 (Figure 5.4 to Figure 5.5). This indicates that the numerical model predicts an increase in the natural frequency

with amplitude and reinforces that the proposed nonlinear model adequately captures the nonlinear effects of the sloshing fluid.

5.3.2.2 Frequency-Response of Free Surface Amplitude

The ability of the numerical model to predict the free surface response is illustrated in the following figures. Both frequency-response and time-histories are shown for select amplitudes and slat heights. Figure 5.9 to Figure 5.12 compare the numerical results to the experimental results at a screen solidity of 50%. This comparison further validates the numerical model at a different screen solidity.

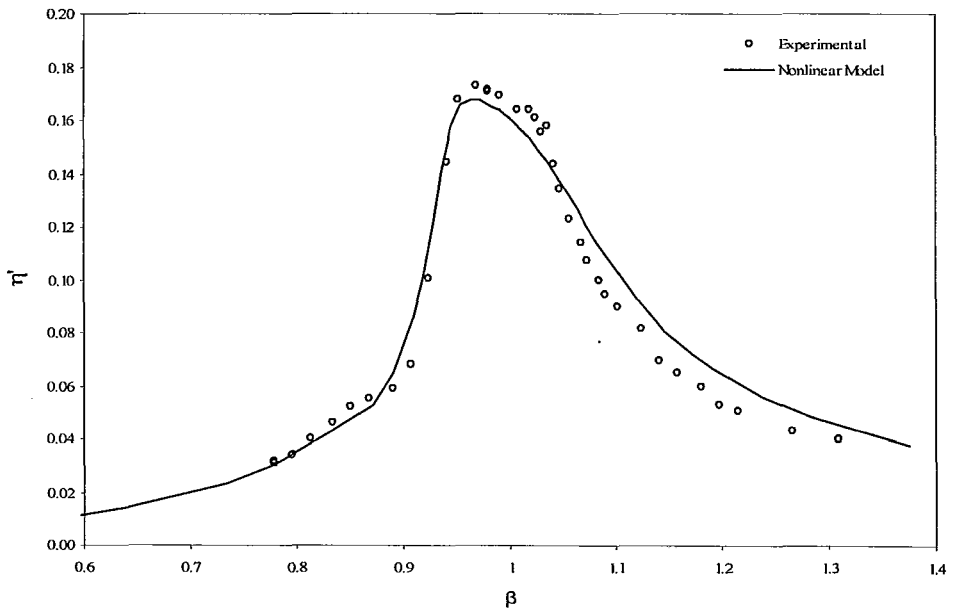

Figure 5.9 - Frequency-Response of η' : Experimental vs. Nonlinear Model, TS5, A/L=0.0026, S=50%

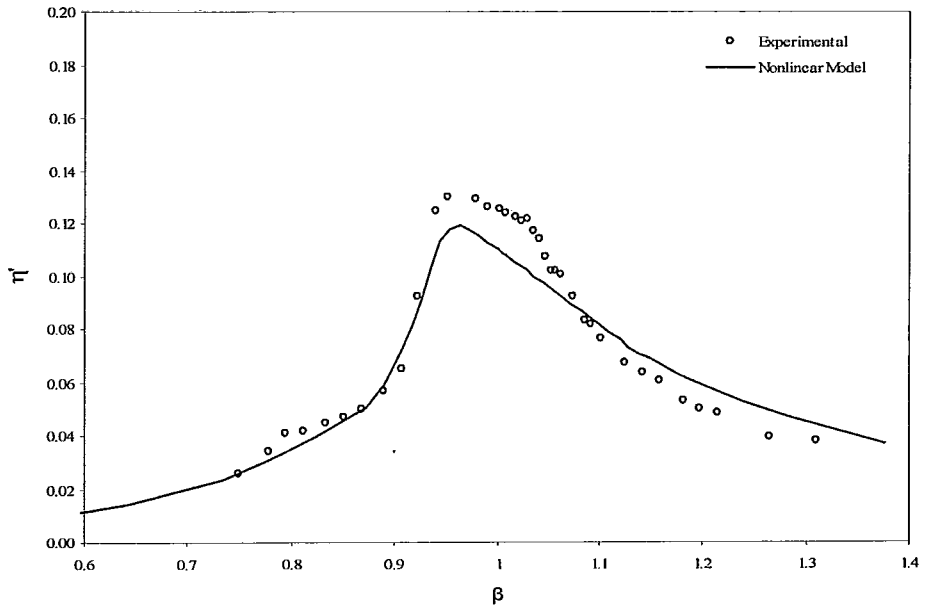

Figure 5.10 - Frequency-Response of η' : Experimental vs. Nonlinear Model, TS20, *A/L*=0.0052, S=50%

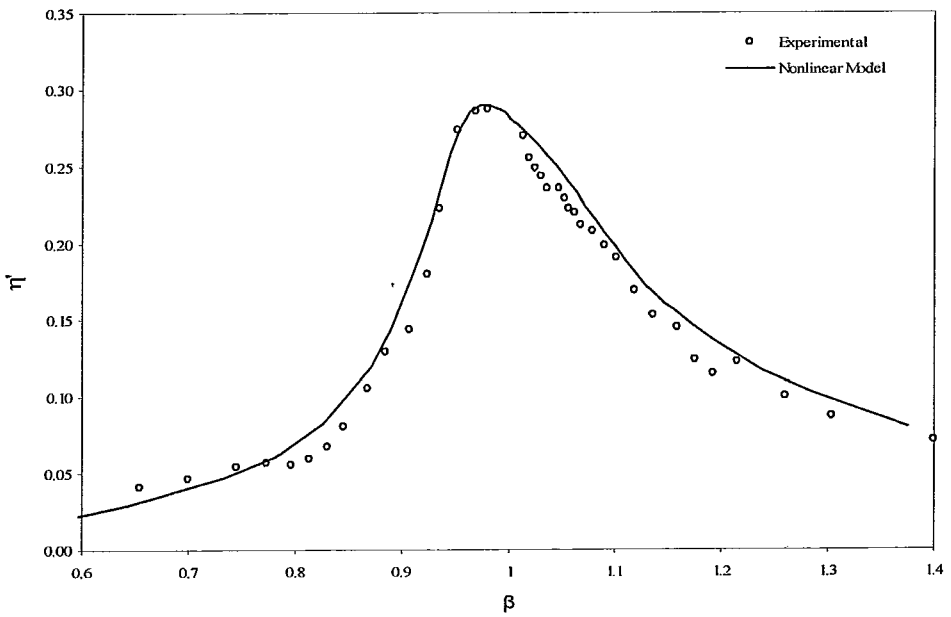

Figure 5.11 - Frequency-Response of η' : Experimental vs. Nonlinear Model, TS5, *A/L*=0.0010, S=50%

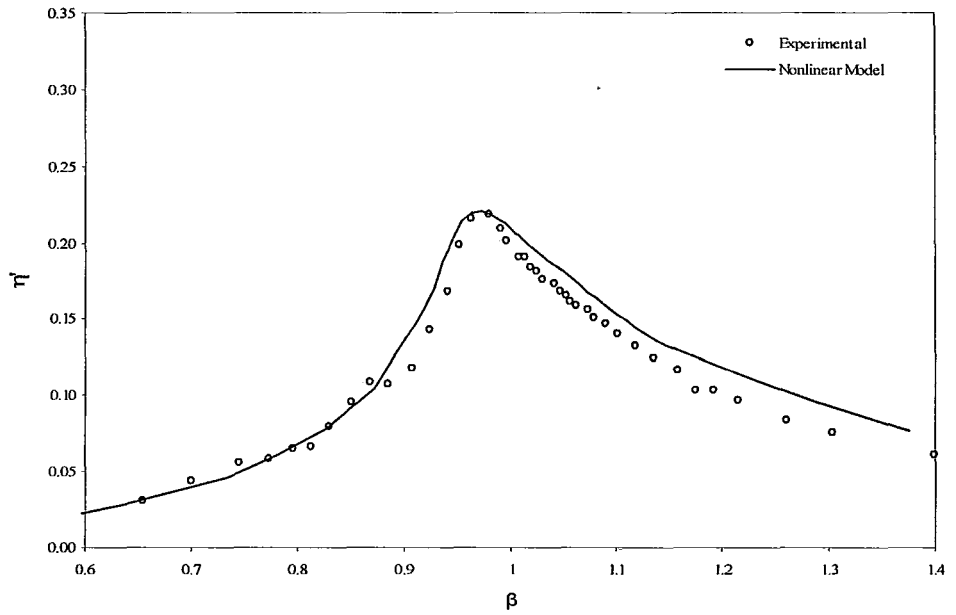

Figure 5.12 - Frequency-Response of η' : Experimental vs. Nonlinear Model, TS20, *A/L*=0.0010, S=50%

Comparisons are made between tests TS5 and TS20 having a screen solidity of 50% and excited at *A/L* values of 0.0052 and 0.0104. Figure 5.9, Figure 5.11, and Figure 5.12 illustrate that the model accurately predicts the fluid response for both small and large excitation amplitudes. A small discrepancy, observed in Figure 5.10, is found to occur when the loss coefficient predicted by the model is approximately 4% less than the experimental value.

5.3.3 Time-History Response

The ability of the nonlinear numerical model to simulate the time-history response is verified in this section. Although the frequency-response comparisons show good agreement with the experimental tests, it is important to verify the

numerical model in the time domain to ensure that the model adequately predicts the amplitude and phase angle of the response.

Figure 5.13 to Figure 5.15 compare the predicted free surface time-history response from the nonlinear numerical model to the experimental results at the tank end wall (x=0.05L and x=0.95L). Comparisons are made for tests TS5 and TS25 with a solidity of 42%.

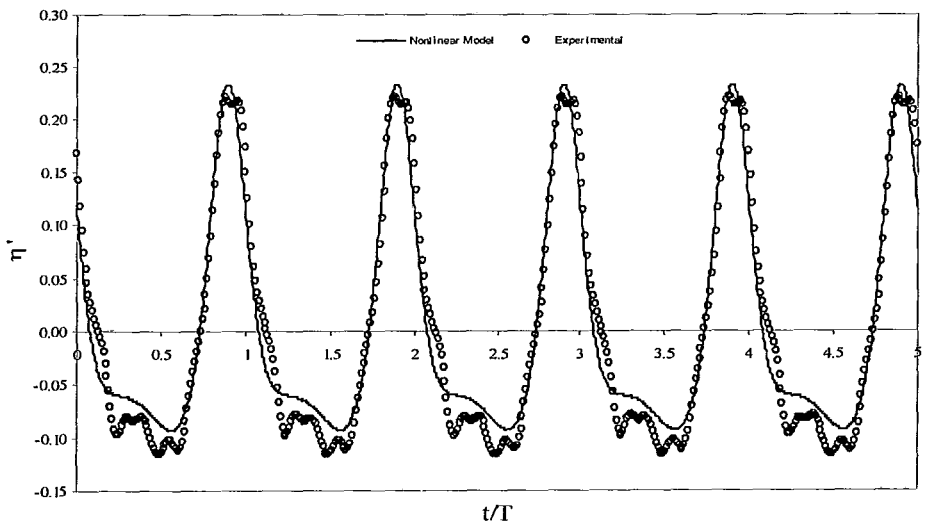

Figure 5.13 – Time-History Response of η', TS5, A/L = 0.0052, S=42%, β =1.0

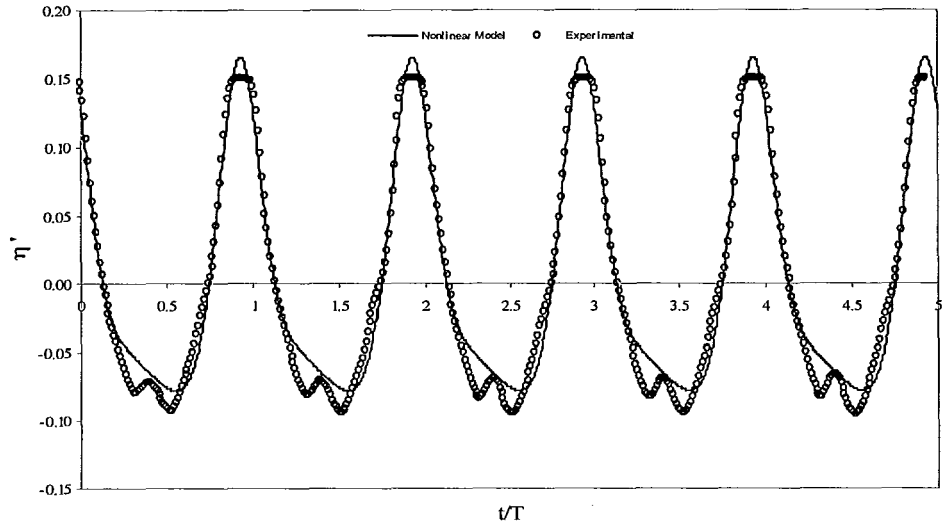

Figure 5.14 - Time-History Response of η', TS25, A/L = 0.0052, S=42%, β=1.0

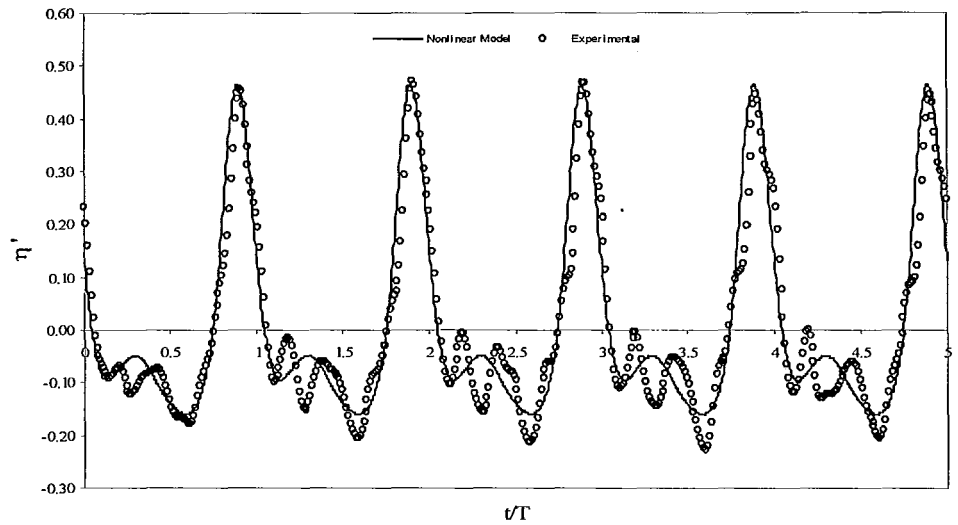

Figure 5.15 - Time-History Response of η', TS25, A/L = 0.0155, S=42%, β=1.0

The TLD is excited at A/L values of 0.0052 and 0.0155 with β=1.0. Good agreement is found between the maximum free surface amplitude predicted by the model and measured results. The model does not capture the higher harmonics present at the minimum free surface response or wave trough. This is also found

in work by Reed et al. (1998) and Tait (2004) who attribute this discrepancy to the presence of high frequency trailing waves observed in experiments.

5.3.4 Summary of Findings Utilizing the Nonlinear Model

The nonlinear numerical model developed in this section shows good agreement with the experimental test results. The largest differences in the model's prediction (10%) occurred at low excitation amplitudes where C_L is highly sensitive to small changes in the *KC* number. As a result, small errors in the predicted velocity at the screen are magnified. A discrepancy between the predicted natural frequency and the experimental natural frequency was observed. It is postulated that this is attributed to the influence that the larger slat heights have on the flow of the fluid. Lastly, time-history comparisons of the free surface response showed good agreement indicating the model can be used to predict the response of a TLD subjected to random excitation.

5.4 *Linear Potential Flow Model*

5.4.1 Description of Linear Potential Flow Model

In this section an analytical model describing the sloshing motion of a tuned liquid damper with damping screens is presented using potential flow theory. Consider the rectangular tank shown in Figure 5.16 having a length *L*, quiescent fluid depth *h*, and tank width *b* (out of the plane of the page) subjected to a base displacement *X(t)*.

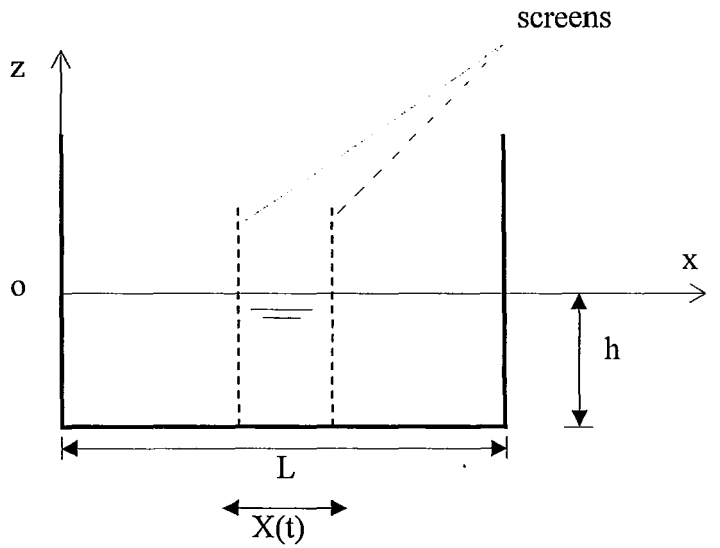

Figure 5.16 - Definition Sketch For Liquid Sloshing in a Rectangular Tank Using Potential Flow Theory (Deng, 2007)

The assumptions of inviscid, incompressible, irrotational flow, and negligible surface tension are made. It is assumed that the fluid response amplitude is small compared to the water depth ($\eta << h$) and that the screens do not significantly influence the flow of the sloshing liquid. For this type of problem, the velocity of a particle relative to the tank walls can be expressed as a gradient $\Phi(x,z,t)$. By the condition of kinematic continuity of incompressible flow it is required that

$$\frac{\partial^2 \Phi}{\partial x^2} + \frac{\partial^2 \Phi}{\partial z^2} = 0 \tag{5.12}$$

and the boundary conditions are given as

$$u(x,z,t) = \frac{\partial \Phi}{\partial x} = 0 \text{ at x=0, L} \tag{5.13}$$

$$w(x,z,t) = \frac{\partial \Phi}{\partial z} = 0 \text{ at z=-h} \tag{5.14}$$

where $u(x,z,t)$ and $w(x,z,t)$ are the x and z components of liquid velocity relative to the tank at the point (x,z) and time t. The solution satisfying equation (5.12) with boundary conditions from equations (5.13) and (5.14) is obtained in a general form as a sum of infinite sloshing modes, n, as (Warnitchai, 1998)

$$\Phi(x,z,t)=\sum_{n=1}^{\infty}\dot{q}_n(t)\frac{\cosh\left(\frac{n\pi(z+h)}{L}\right)\cos\left(\frac{n\pi x}{L}\right)}{\frac{n\pi}{L}\sinh\left(\frac{n\pi h}{L}\right)} \tag{5.15}$$

The amplitude of the sloshing motion is assumed to be sufficiently small so that the linearized free surface condition

$$\left[\frac{\partial\Phi}{\partial z}\right]_{z=0}=\frac{\partial\eta}{\partial t} \tag{5.16}$$

is satisfied. Introducing equation (5.15) into equation (5.16) the free surface response can be expressed as

$$\eta(x,t)=\sum_{n=1}^{\infty}q_n(t)\cos\left(\frac{n\pi x}{L}\right) \tag{5.17}$$

Therefore, $q_n(t)$ is physically described as the free surface sloshing amplitude of the n^{th} sloshing mode at $x=0$. Since the free surface response is completely described by the set of $q_n(t)$ for $n=1,2,3...\infty$ it is used in this model as the set of generalized coordinates (Warnitchai and Pinkaew, 1998).

Based on the above equations the gravitational potential (V) and kinetic energy (T) of the liquid sloshing are given as

$$V = \frac{1}{2}\rho b g \int_0^L \eta^2(x,t)dx \tag{5.18}$$

$$T = \frac{1}{2}\rho b \int_{-h}^{0}\int_0^L \left[\left(\dot{X} + \frac{\partial \Phi}{\partial x}\right)^2 + \left(\frac{\partial \Phi}{\partial z}\right)^2\right] dxdz \tag{5.19}$$

Equations (5.15) and (5.17) are substituted into equations (5.18) and (5.19) and the Lagrange equations are applied leading to the equation of motion of the system given as

$$m_n \ddot{q}_n(t) + m_n \omega_n^2 q_n(t) = \gamma_n \ddot{X}(t) \tag{5.20}$$

where the generalized mass, natural frequency, and excitation factor are given respectively as

$$m_n = \frac{1}{2}\frac{\rho b L^2}{n\pi \tanh\left(\frac{n\pi h}{L}\right)} \tag{5.21}$$

$$\omega_n^2 = \frac{n\pi g}{L}\tanh\left(\frac{n\pi h}{L}\right) \tag{5.22}$$

$$\gamma_n = \frac{\rho b L^2 \left(1 - \cos(n\pi)\right)}{(n\pi)^2} \tag{5.23}$$

The above derivation assumes ideal fluid behaviour which does not consider the influence of flow damping devices. The influence of flow damping devices (screens) on the sloshing response of the fluid has been accounted for in the potential flow model using virtual work by Tait (2007) and Deng (2007). For

sinusoidal excitation, the linear generalized damping coefficient value is given as (Tait, 2007)

$$c_n^{eq} = C_L \frac{4\rho bL}{3\pi^2} \Delta_n \Xi_n q_n \omega \tag{5.24}$$

and the generalized damping ratio for the fundamental sloshing mode $(n=1)$ is expressed as (Tait, 2007)

$$\zeta^{eq} = C_L \frac{4}{3\pi} \tanh\left(\frac{\pi h}{L}\right) \Delta \Xi \frac{q}{L} \tag{5.25}$$

where

$$\Delta = \left(\frac{1}{3} + \frac{1}{\sinh^2\left(\frac{\pi h}{L}\right)} \right) \tag{5.26}$$

$$\Xi = \sum_{j=1}^{ns} \sin\left(\frac{\pi x_j}{L}\right)^3 \tag{5.27}$$

In this research study, *ns* is the number of screens which is equal to 2, x_j is the location of the screens (0.4L and 0.6L), and C_L is the loss coefficient that is Keuelegean-Carpenter number dependent (Section 4.5). The resulting equation of motion that describes the response of the sloshing fluid and incorporates the influence of flow damping devices is given as

$$m_n \ddot{q}_n(t) + c_n^{eq} \dot{q}(t) + m_n \omega_n^2 q_n(t) = \gamma_n \ddot{X}(t) \tag{5.28}$$

Equation (5.28) is derived assuming ideal fluid behaviour and small wave amplitude. Once the solutions of $q_n(t)$ are obtained, the free surface response, base shear forces, and energy dissipating characteristics of the TLD can be easily determined (Warnitchai and Pinkaew, 1998).

5.4.2 Validation of Potential Flow Model

This section compares the predicted response of the TLD using potential flow theory to the experimental results obtained from shake table tests. The potential flow model used for this comparison considers only the response of the fundamental mode (n=1) and assumes small wave amplitudes. Figure 5.17 to Figure 5.24 compare the results from the potential flow model to the experimental results from shake table tests. The figures plot the normalized energy dissipated per cycle versus β for A/L values of 0.0026, 0.0077, and 0.0152, respectively. The slat screens used for comparison are partial height screens with a screen solidity of 42% and slat heights of 5mm, 19mm, and 25mm. Figure 5.17 and Figure 5.18 compare the predicted and measured results of E_d' for an A/L value of 0.0026.

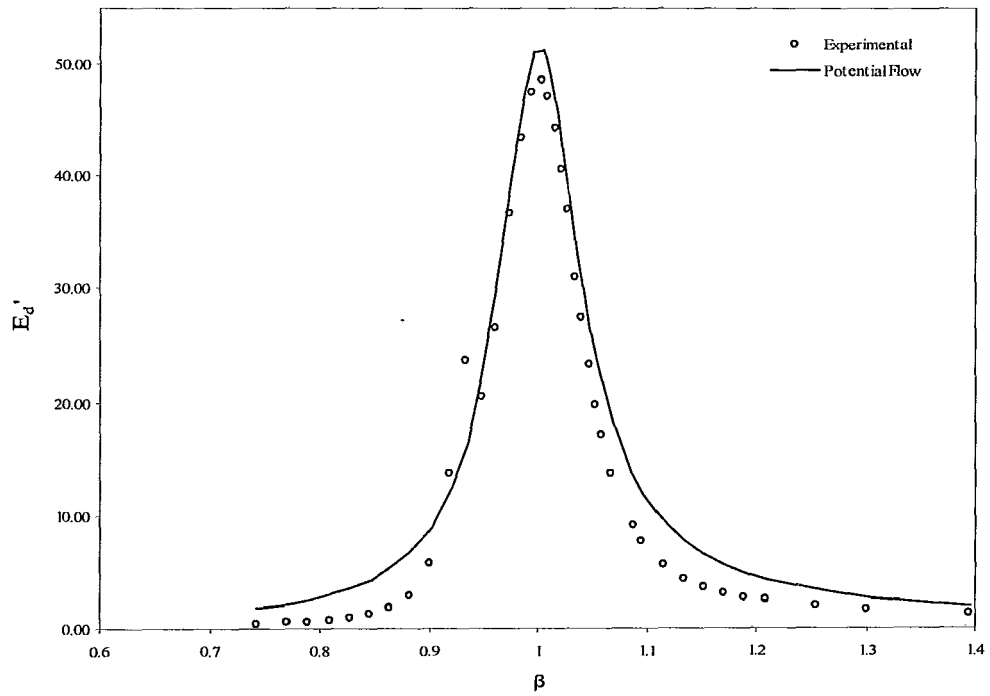

Figure 5.17 - Comparison Between Potential Flow Model and Experimental Results, TS5, *A/L*=0.0026, S=42%

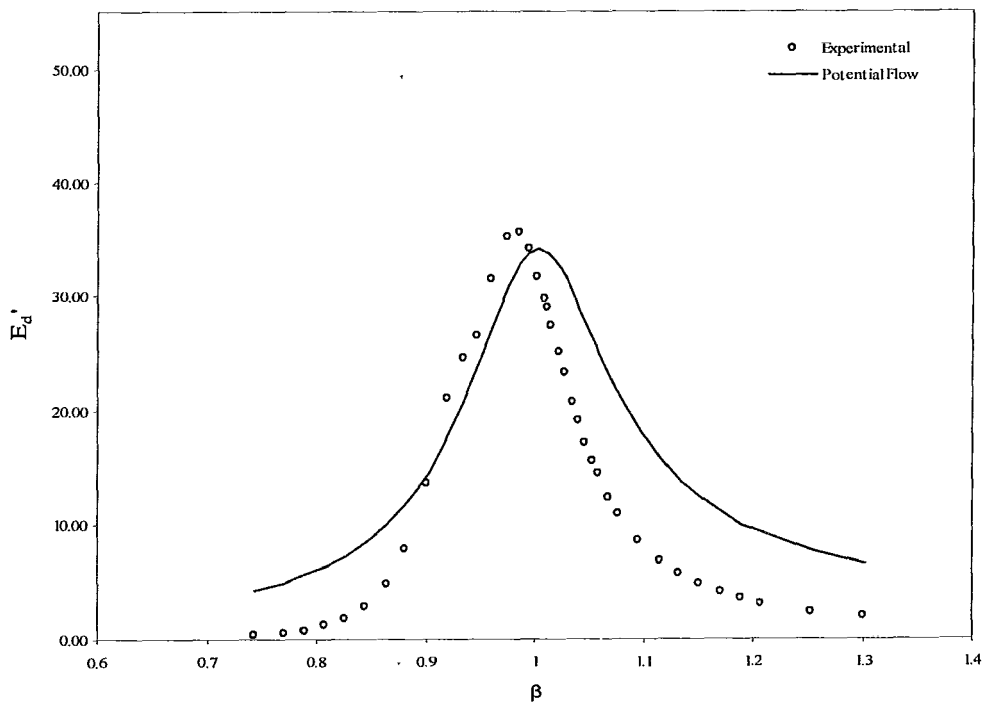

Figure 5.18 - Comparison Between Potential Flow Model and Experimental Results, TS25, *A/L*=0.0026, S=42%

The model accurately predicted both the natural frequency and peak value of $E_d^{'}$ for the 5mm slats where the peak value of $E_d^{'}$ is over-predicted by 5% by the numerical model and the natural frequency is within 1%. However, larger discrepancies are observed for the 25mm slats where the peak value of $E_d^{'}$ is under-predicted by 5%. The natural frequency predicted by the numerical model is higher than that observed during experimental testing. This occurs because an underlying assumption in the potential flow model is that the slat screens do not alter the flow of the fluid. As discussed in Section 4.2.4, it is postulated that the larger slats alter the flow of the fluid in such a way that the effective tank length is increased resulting in a reduction in the natural frequency. Since this is not accounted for in this model it is expected that the natural frequency would not be accurately predicted over the range of excitation amplitudes. Furthermore, since this is a linear model it is unable to capture the nonlinearities in the fluid response represented by the double peaked response in the $E_d^{'}$ plot.

Figure 5.19 to Figure 5.21 compare the results predicted by the potential flow model to the experimental results for A/L value of 0.0077.

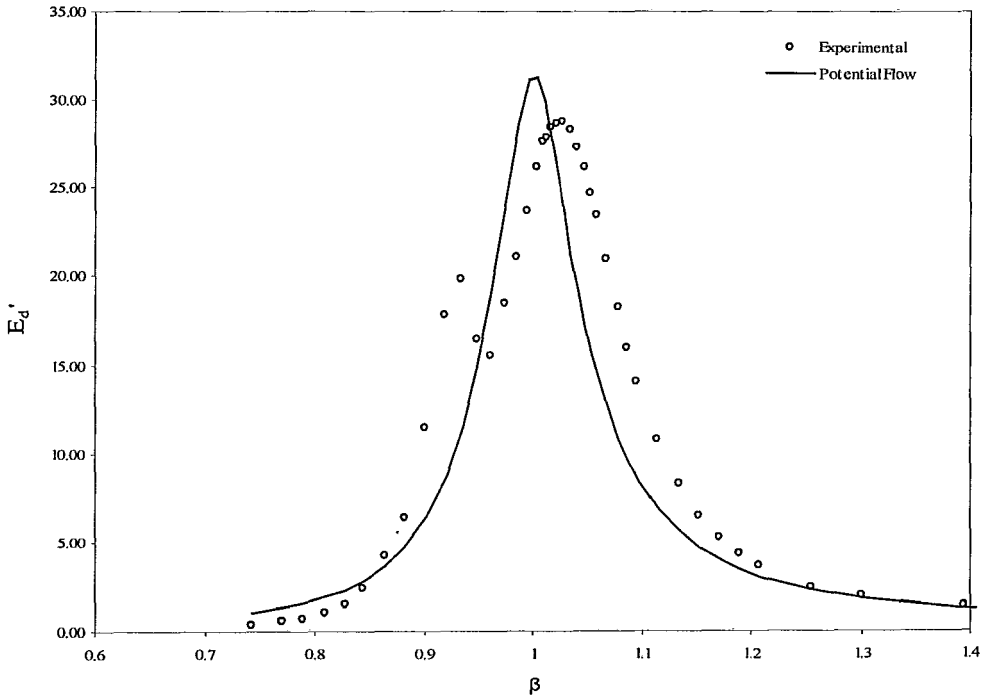

Figure 5.19 - Comparison Between Potential Flow Model and Experimental Results, TS5, *A/L*=0.0077, S=42%

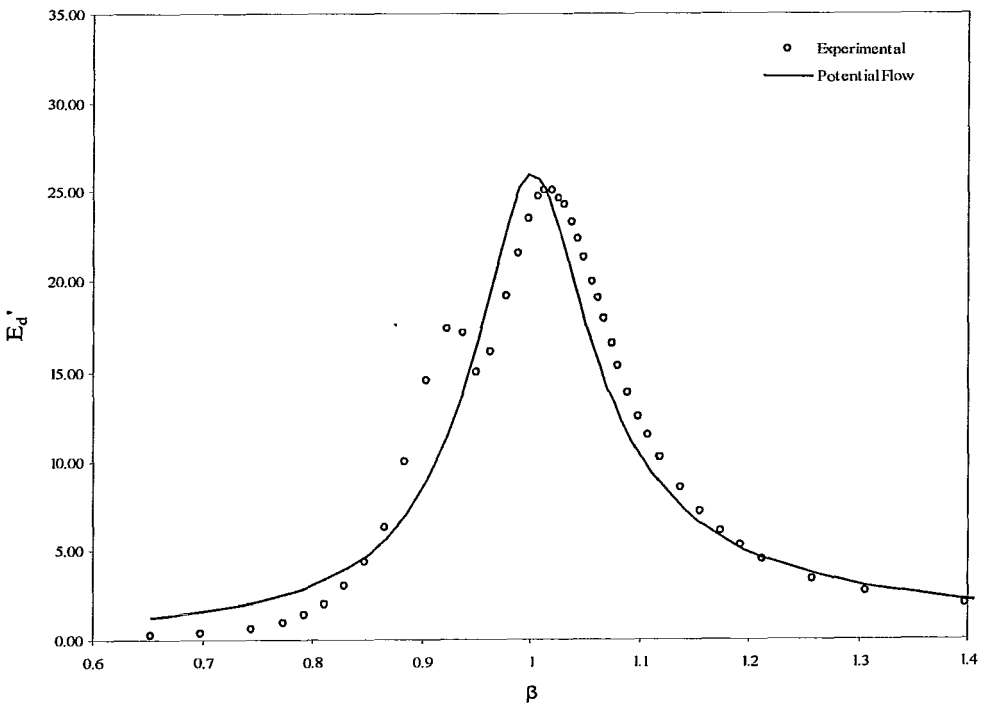

Figure 5.20 - Comparison Between Potential Flow Model and Experimental Results, TS19, *A/L*=0.0077, S=42%

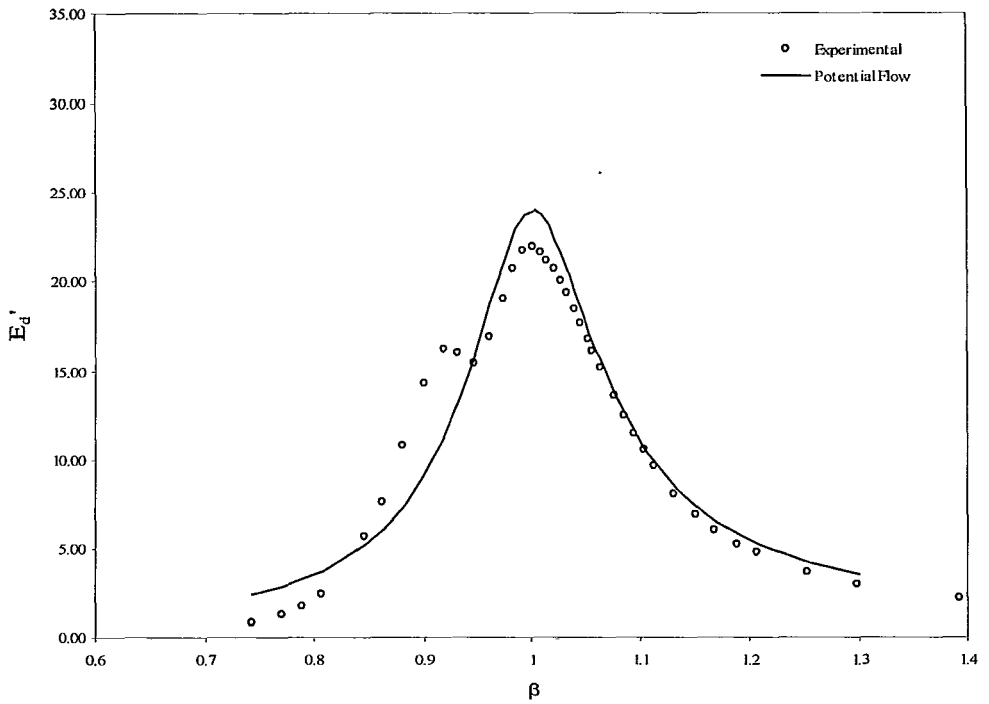

Figure 5.21 - Comparison Between Potential Flow Model and Experimental Results, TS25, *A/L*=0.0077, S=42%

The numerical model over-predicts the peak value of $E_d^{'}$ by 9% for the 5mm and 25mm slat screens. However, the model does a good job of predicting the peak response of $E_d^{'}$ for the 19mm slats with a difference of 2%. At this excitation amplitude the model does a suitable job of predicting the natural frequency of the sloshing fluid. However, since this is a linear model, it is unable to accurately predict the increase in natural frequency with amplitude.

Figure 5.22 to Figure 5.24 compare the results predicted by the potential flow model to the experimental results for an *A/L* value of 0.0152.

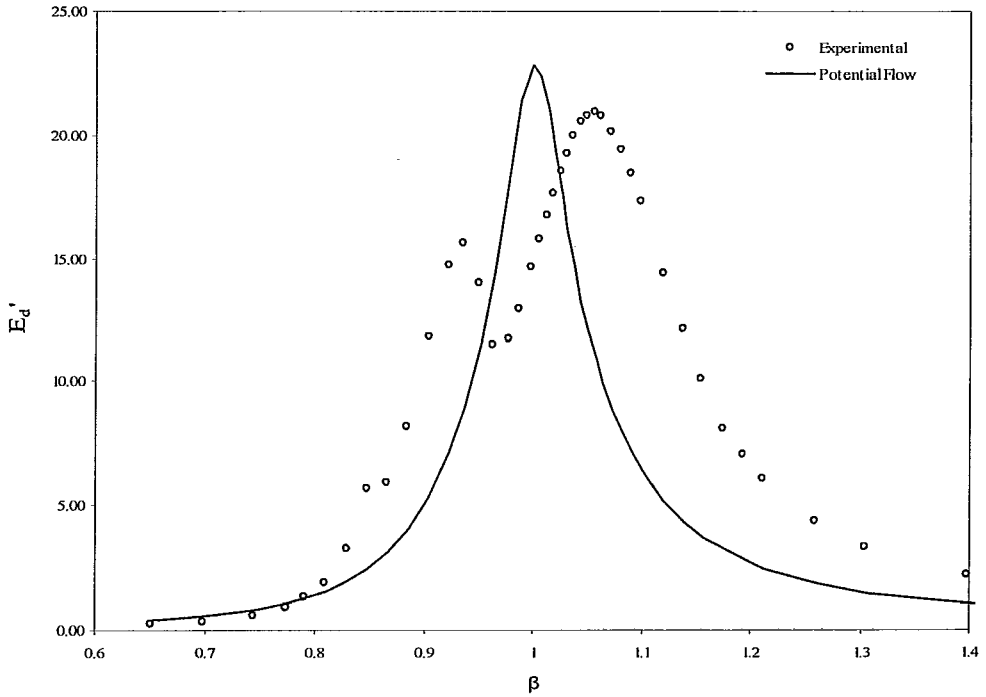

Figure 5.22 - Comparison Between Potential Flow Model and Experimental Results, TS5, *A/L*=0.0152, S=42%

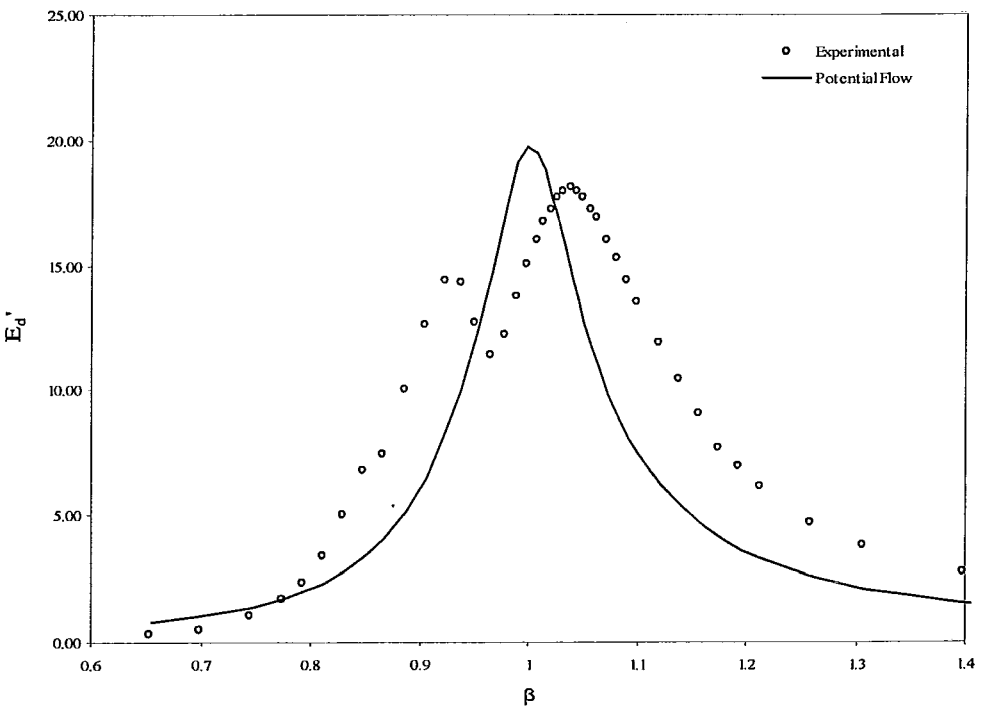

Figure 5.23 - Comparison Between Potential Flow Model and Experimental Results, TS19, *A/L*=0.0152, S=42%

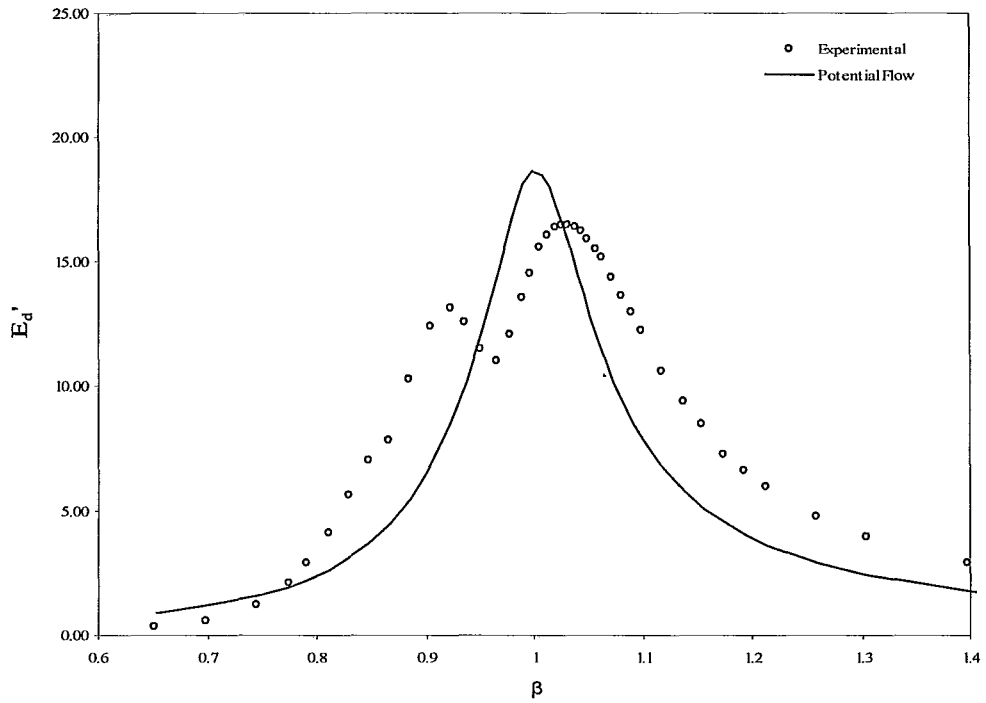

Figure 5.24 - Comparison Between Potential Flow Model and Experimental Results, TS25, *A/L*=0.0152, S=42%

In all three cases the numerical model over-predicts the peak value in E_d'. For the 5mm, 19mm, and 25mm slats the model over-predicts E_d' by 10%, 8%, and 13%, respectively. Furthermore, the natural frequency is not accurately predicted for any of the three tests with an average error of 3%. A greater discrepancy in the E_d' plots is expected to occur at large excitation amplitudes since the TLD response becomes highly nonlinear as *A/L* increases. The inability of the linear potential flow model to predict the response of the TLD at large free surface amplitudes is consistent with findings from Tait et al. (2005).

The potential model is validated for a screen solidity of 50% in Figure 5.25 to Figure 5.28 by comparing the predicted response of F_S' to the

experimental test results. Two comparisons are made at A/L values of 0.0052 and 0.0155 for slat heights of 5mm and 20mm.

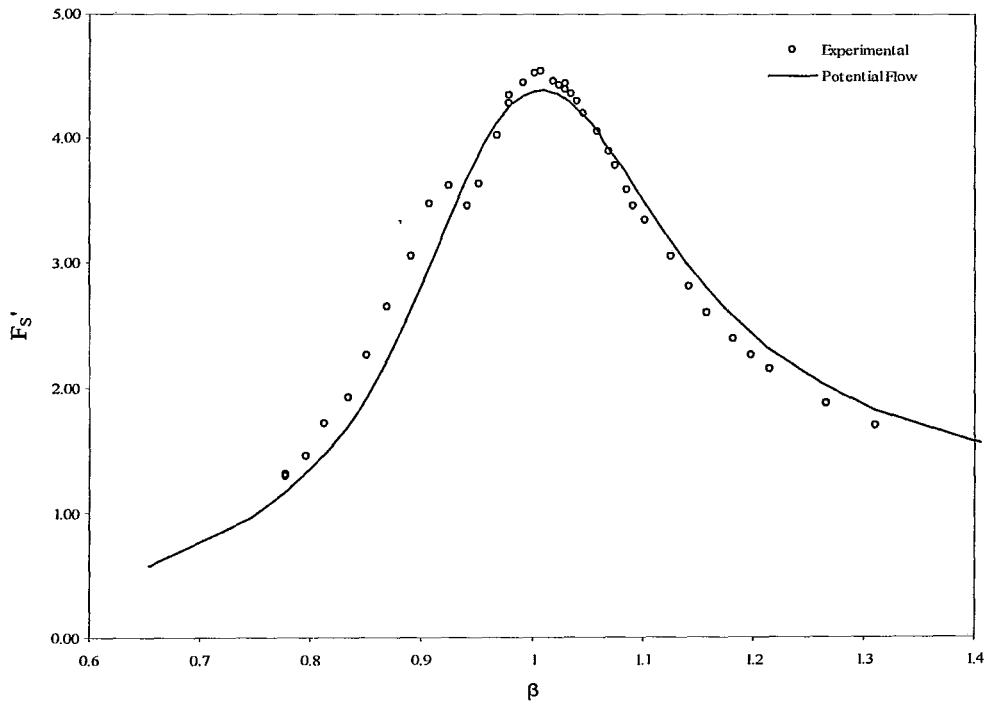

Figure 5.25 – Experimental and Numerical Results of F_S', TS5, S=50%, A/L=0.0052

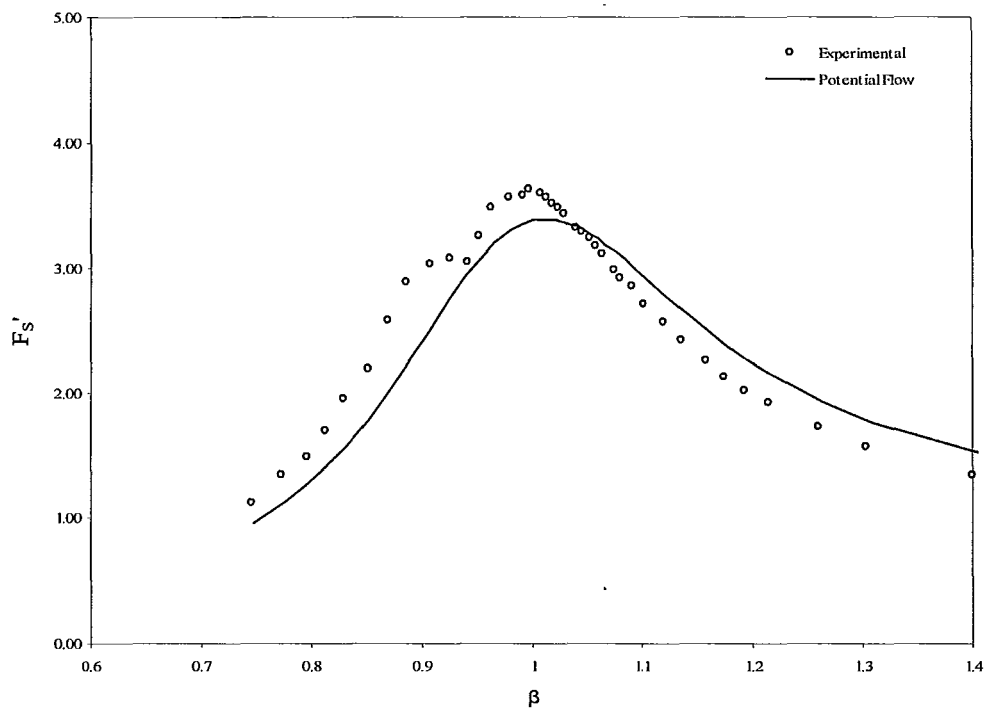

Figure 5.26 - Experimental and Numerical Results of F_S', TS20, S=50%, *A/L*=0.0052

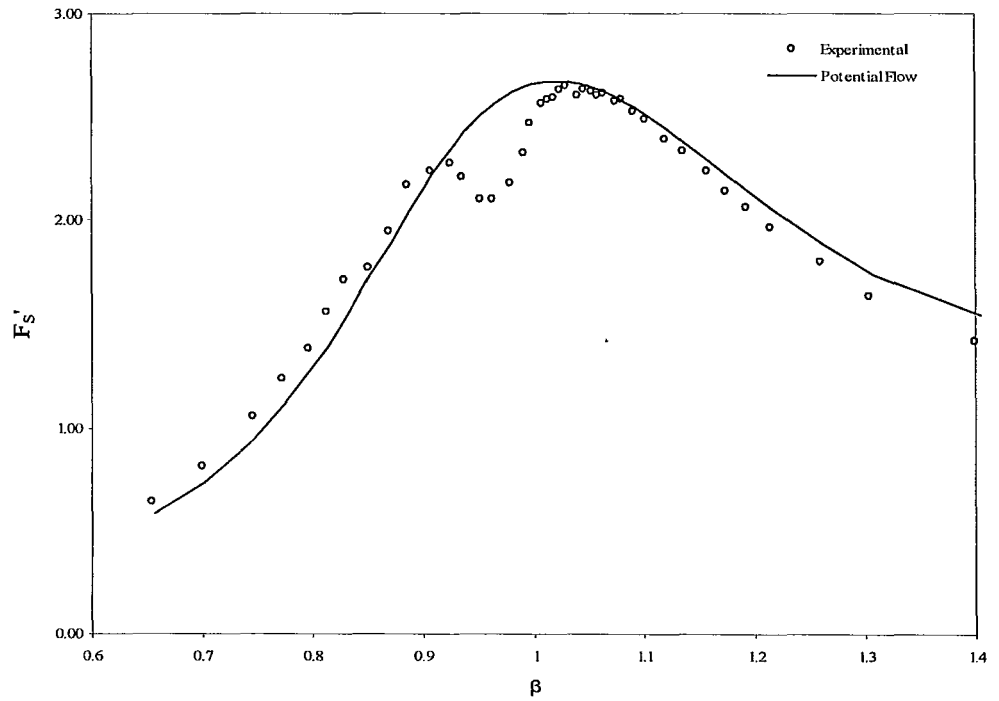

Figure 5.27 - Experimental and Numerical Results of F_S', TS5, S=50%, *A/L*=0.0155

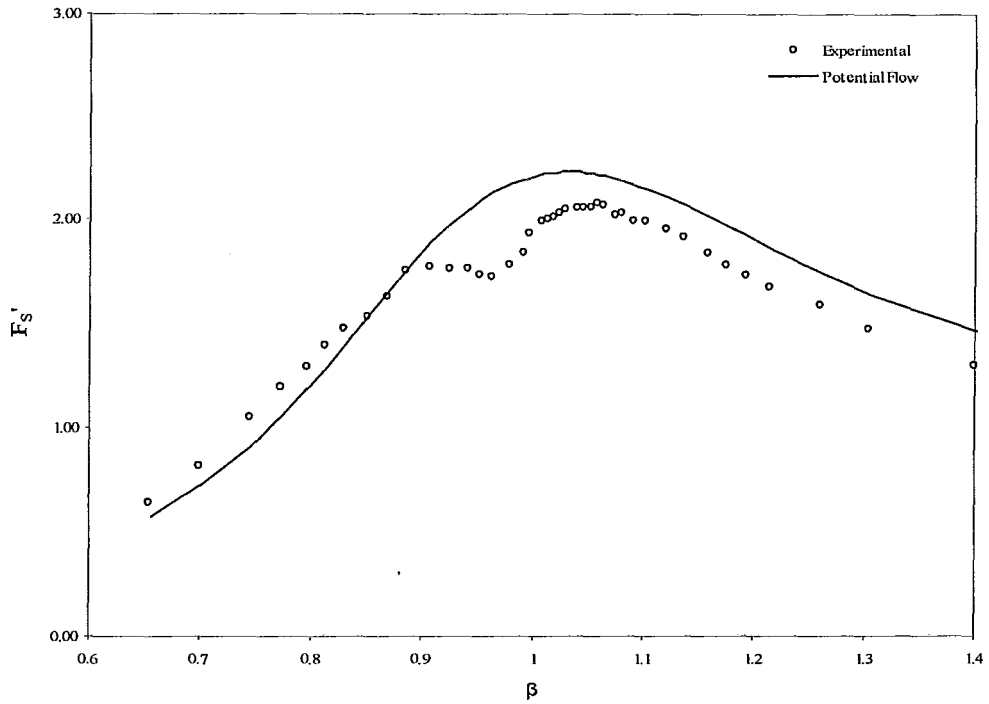

Figure 5.28 - Experimental and Numerical Results of F_S', TS20, S=50%, A/L=0.0155

Figure 5.25 and Figure 5.26 compare the predicted free surface response from the potential flow model to the experimental test results for an A/L value of 0.0052. Both slat heights investigated, TS5 and TS20, under-predicted the peak value of F_S' by approximately 6%. The natural frequency is adequately captured for test TS5 while a slight difference (2%) is observed for test TS20. A comparison at this amplitude shows that the proposed model adequately captures the response of the TLD for both slat heights.

Figure 5.27 and Figure 5.28 compare the predicted response from the potential flow model to the experimental test results for an A/L value of 0.0155. Good agreement in the peak value of F_S' is observed between the predicted and

experimental test results for the 5mm slats. The predicted natural frequency is lower than the experimental value because the numerical model does not capture the hardening characteristics of the TLD. The numerical model over-predicts the peak value of $F_S^{'}$ by 8% indicating that the $C_L^{'}$ value is under estimated. This discrepancy between the experimental and numerical response is not considered to be significant when the underlying assumptions used to develop this model are considered. Therefore, the potential flow model can be employed to predict the TLD response at this screen solidity $(S = 0.50)$ for small (wind) amplitudes.

5.4.3 Summary of Findings Utilizing the Potential Flow Model

In general, the proposed potential flow model predicts the response of $E_d^{'}$ satisfactorily for small free surface amplitudes. The largest discrepancy is 9% while other tests show a difference in the range of 2% to 5%. At larger free surface amplitudes the discrepancy is more significant since the assumption of small amplitude wave response does not apply. There is a discrepancy between the natural frequency predicted by the model and the experimentally determined natural frequency. This is associated with the influence that the large slats have on the flow path of the fluid. Additionally, the potential flow model employed in this study is unable to capture the hardening effects of the TLD. As a result, at excitation amplitudes larger than 5mm the predicted natural frequency will be lower than the experimentally observed natural frequency.

5.5 *Influence of KC Number Dependent Screens on* ζ_{TLD}

The major objective in this study is to determine the influence that slat screens with *KC* number dependent losses have on the overall performance of the TLD and a structure-TLD system. The potential flow model utilized in this section is used to determine the relationship between the fluid response (η) and the damping of the TLD (ζ_{TLD}). Figure 5.29 compares the changes in ζ_{TLD} that occur as the fluid response increases.

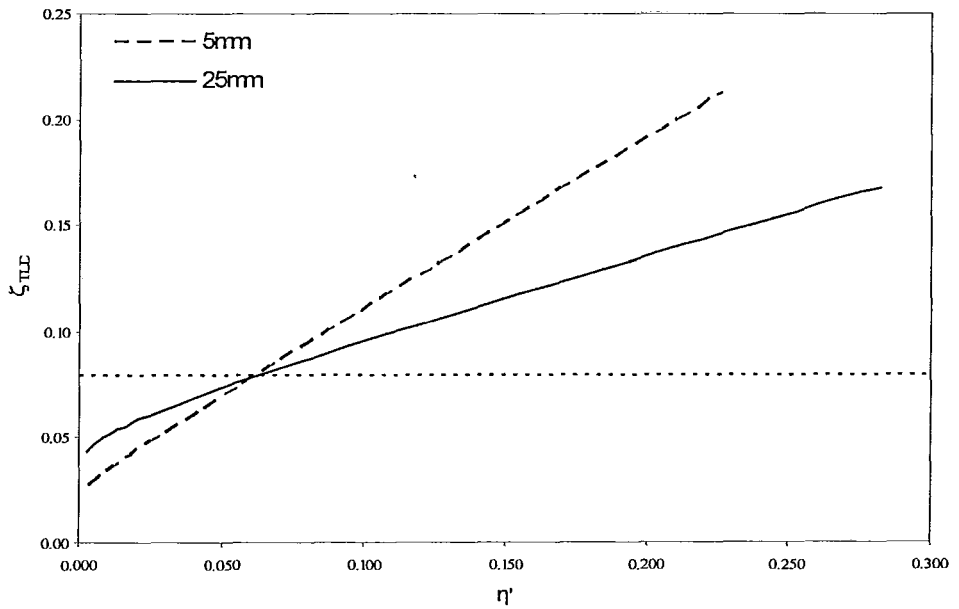

Figure 5.29 - Influence of Slat Height on ζ_{TLD}

Figure 5.29 illustrates that at a specific response amplitude both the 5mm and 25 mm slat screens can be used to provide the desired level of damping. However, as the free surface response amplitude increases the 5mm slat screens cause ζ_{TLD} to

deviate significantly from this value. Conversely, the damping provided by the TLD with 25mm slats remains more constant as η' increases. This illustrates that slat screens with *KC* number dependent losses reduce the amplitude dependency of the TLD which theoretically will result in a more efficient structure-TLD system. The influence that *KC* number dependent slat screens have on the performance of a structure-TLD system will be assessed in the following chapter.

5.6 *Conclusions*

In this chapter a nonlinear numerical model and a potential flow model have been utilized. The nonlinear model was modified in order to simulate response of a TLD with *KC* number dependent losses. Frequency-response comparisons between the experimental results and the numerical model showed excellent agreement at *A/L* of 0.0077 or greater. At low excitation amplitudes larger discrepancies were observed for slat heights of 19mm and 25mm. This occurs because the loss coefficient changes vary rapidly with the *KC* number. Excellent agreement was found for the 5mm slat screens at all excitation amplitudes because these screens are *KC* number independent in the range of *KC* values tested. For the larger slats, the model did not accurately predict the natural frequency of the TLD. In addition to the frequency-response comparisons, the time-history response of the free surface amplitude showed good agreement with the numerical results. These findings indicate that the proposed nonlinear model is

able to capture the influence of nonlinearities in the sloshing fluid and can account for slat screens that have *KC* number dependent losses.

The proposed potential flow model predicts the peak response of $E_d^{'}$ satisfactorily for low excitation amplitudes. At larger amplitudes the discrepancy is more significant since the assumption of small amplitude wave response does not apply. In addition, the potential flow model assumes a first mode response which does not account for nonlinearities in the fluid response. Therefore, the hardening characteristics of the TLD are not captured with the potential flow model utilized in this study.

The influence that screens with *KC* number dependent losses have on the damping of the TLD (ζ_{TLD}) was assessed using the potential flow model. Both *KC* number dependent and *KC* number independent screens provided the target level of damping at a specified free surface response amplitude. However, slat screens with *KC* number dependent losses showed less deviation from the target damping level compared to the constant loss coefficient screens. This shows that velocity dependent slat screens reduce the amplitude dependency of the TLD and should improve the efficiency of the structure-TLD system.

Chapter 6 - Performance of a Structure-TLD System with Varying Loss Coefficient Slat Screens

6.1 *Introduction*

Traditionally, flow damping screens with constant loss coefficients have been used to increase the inherent damping of the TLD. The drawback with these screens is that they perform optimally at a given target response but lose efficiency as the excitation amplitude deviates from the target value.

The previous chapters have focused on the influence that screen geometry, in particular slat height, has on the fluid response. The objective of this chapter is to assess the influence of screens with a varying loss coefficient on the efficiency of a structure-TLD system. This chapter begins by introducing the mechanical model of a structure-TLD system. This is followed by a presentation of the equivalent mechanical model which represents a TLD as an equivalent TMD. The second numerical model investigated utilizes the nonlinear TLD model presented in the previous section attached to a structure. The structure-TLD models are validated with experimental results from Tait (2004). The chapter concludes with an investigation into the influence of slat height on the efficiency of a structure-TLD system.

6.2 *Mechanical Model of a Structure-TLD System*

A mechanical model that represents a structure-TLD system is proposed in this section. It is desirable to represent the structure-TLD system as an equivalent

mechanical system that is analogous to a TMD. This permits the use of well established analysis techniques and optimization parameters. Figure 6.1 presents the step by step process that simplifies a multi-degree of freedom (MDOF) structure-TLD system into an equivalent two-degree of freedom mechanical model.

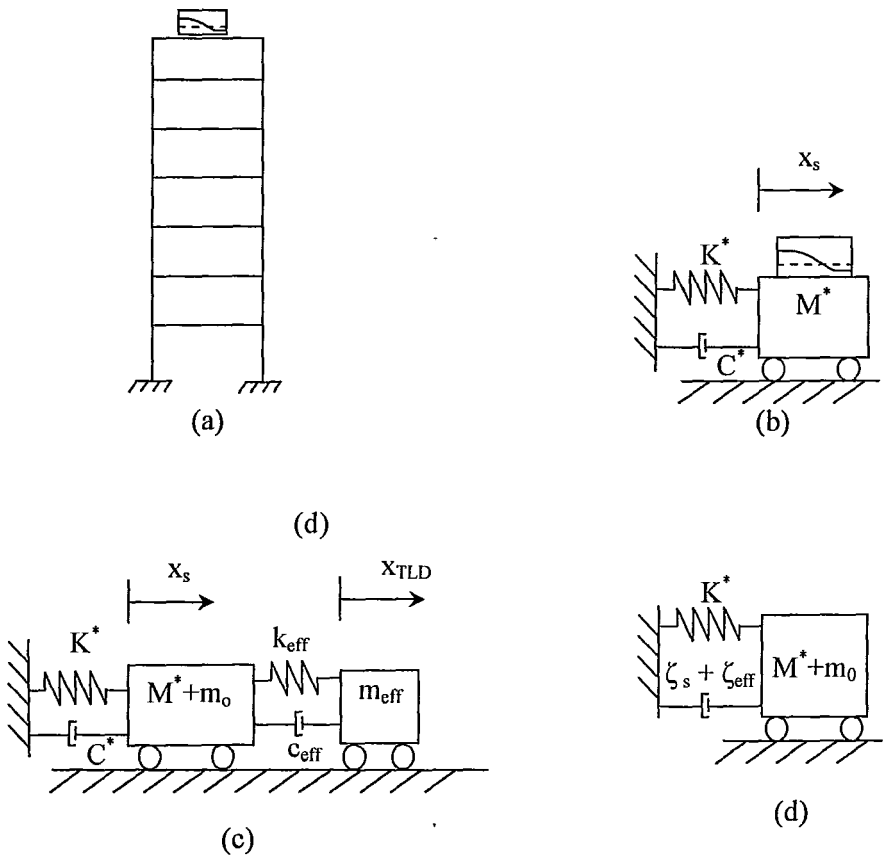

Figure 6.1 - Representation of a Structure-TLD System

A tall building with an attached tuned liquid damper is shown in Figure 6.1(a). This system is represented as a two degree of freedom structure (Figure 6.1(b)), where M^*, C^*, and K^* corresponds to the generalized mass, damping, and stiffness in the mode of vibration that is to be suppressed. The TLD is represented

as an equivalent SDOF system (Figure 6.1(c)) as presented in Section 2.8.1. This permits the application of TMD theory and well known analysis techniques applicable to two-degree of freedom structures. Vickery and Davenport (1970) illustrated that a structure-DVA system can be modelled as a SDOF system (Figure 6.1(d)) with the addition of an effective damping term ζ_{eff} due to the absorber. The concept of effective damping has been defined in Section 2.8.3 and is expressed mathematically as

$$\zeta_{eff} = \frac{\pi}{4} f_s \frac{1}{\int_0^\infty |H_s(f)|^2 \, df} - \zeta_s \tag{6.1}$$

where $|H_s(f)|$ is the frequency response function of the structure-TLD system and ζ_s is the damping ratio of the structure. McNamara (1977) developed a closed form solution for ζ_{eff} assuming a damped structure subjected to white-noise (random) excitation

$$\zeta_{eff} = \frac{(1+\mu)^2\left(\Omega^4\zeta_s\zeta_{TLD}\right)+(1+\mu)\left(2\Omega\zeta_s\zeta_{TLD}+2\zeta_{TLD}^2-1\right)\left(2\Omega^2\zeta_s\zeta_{TLD}\right)+(\Omega\mu)\left(\Omega^2\zeta_s^2+2f\Omega\zeta_s\zeta_{TLD}+\zeta_{TLD}^2\right)+(\zeta_s\zeta_{TLD})(4\Omega\zeta_s\zeta_{TLD}+4\Omega\zeta_s\zeta_{TLD}+1)}{(1+\mu)^2\left(\Omega^4\zeta_{TLD}\right)+(1+\mu)\left(2\Omega\zeta_s\zeta_{TLD}+2\zeta_{TLD}^2-1\right)\left(2\Omega^2\zeta_{TLD}\right)+\left(\Omega^2\mu\right)(f_r\zeta_s+\zeta_{TLD})+(\zeta_{TLD})\left(4\Omega^2\zeta_s^2+4\Omega\zeta_s\zeta_{TLD}+1\right)} - \zeta_s \tag{6.2}$$

where Ω is the tuning ratio defined as the natural frequency ratio between the absorber and the main mass. If damping in the main mass is neglected then (6.2) simplifies to (Luft, 1979)

$$\zeta_{eff} = \frac{\Omega\mu\zeta_{TLD}}{(1+\mu)^2\,\Omega^4 + 2(1+\mu)\left(\Omega^2\right)\left(2\zeta_{TLD}^2-1\right)+\Omega^2\mu+1} \tag{6.3}$$

6.3 *Factors Affecting the System's Performance*

There are four main parameters that influence the performance of the structure-TLD system. These parameters are the mass ratio μ, the tuning ratio Ω, the TLD damping ratio ζ_{TLD}, and the structural damping ratio ζ_s.

- TLD Mass Ratio

$$\mu = \frac{\phi^2 m_{eff}}{M_s} \tag{6.4}$$

$$M_s = M^* + m_o \tag{6.5}$$

where ϕ is the mode shape value at the damper location. In this investigation it is assumed that the damper is located at the rooftop level and that the generalized coordinates correspond to the displacement of the rooftop resulting in a ϕ value of unity. The effective mass m_{eff} is given by equation (2.19) with n=1 and M_s is the total mass of the system which accounts for the mass of the inactive fluid, m_o.

- Tuning ratio

$$\Omega = \frac{f_{TLD}}{f_s} \tag{6.6}$$

where f_{TLD} is given by equation (4.3) and f_s is the natural frequency of the structure given as

$$f_s = \frac{1}{2\pi}\sqrt{\frac{K^*}{M^*}} \tag{6.7}$$

- TLD Damping Ratio

$$\zeta_{TLD} = \frac{c}{4\pi m_{eff} f_{TLD}} \tag{6.8}$$

For random excitation Tait (2007) provides the equivalent damping coefficient and damping ratio as

$$c_{eq} = C_L \frac{16\rho BL}{\pi^3}\sqrt{\frac{32}{\pi^3}}\tanh^3\left(\frac{\pi h}{L}\right)\Delta\Xi\omega\sigma_r \tag{6.9}$$

$$\zeta_{TLD} = C_L\sqrt{\frac{32}{\pi^3}}\tanh^2\left(\frac{\pi h}{L}\right)\Delta\Xi\frac{\sigma_r}{L} \tag{6.10}$$

where Δ and Ξ are given by equations (5.26) and equations (5.27) and σ_r is the relative motion between the TLD and structure. The ratio of the relative motion between the absorber and the structures displacement (σ_s) is given as (Tait, 2007)

$$R = \frac{\sigma_r}{\sigma_s} \tag{6.11}$$

The relationship between the free surface response of the fluid and the structure is given as (Tait, 2007)

$$R_\eta = \gamma R = \frac{\sigma_n}{\sigma_s} \tag{6.12}$$

where γ is the modal participation factor given as (Tait, 2007)

$$\gamma = \frac{4}{\pi}\tanh\left(\frac{\pi h}{L}\right) \tag{6.13}$$

For the case of random excitation, McNamara (1977) provide the relative motion of an optimally design absorber as

$$R_{opt} = \frac{1+\mu}{\sqrt{2\mu + \frac{3\mu^2}{2}}} \tag{6.14}$$

- Structural Damping ratio

$$\zeta_s = \frac{C^*}{4\pi M^* f_s} \tag{6.15}$$

Structural damping has been discussed in detail in Section 2.1 and its influence on the performance of an absorber is often negligible (Warburton, 1982).

Optimization of absorber parameters Ω and ζ_A (ζ_{TLD} in this application) were first determined by Den Hartog (1956) for an undamped system subjected to harmonic excitation. In this discussion, optimization is defined as the values of Ω and ζ_{TLD} that make the slope of the fixed points zero in the R_d vs β plots (Soong and Dargush, 1997). Damping in the main mass was considered by Randall et al. (1981) who optimized Ω and ζ_{TLD} by minimizing the larger of the two peaks in Figure 2.7. Ioi and Ikeda (1978) provided empirical values for Ω and ζ_{TLD} that are valid for $0.03 \le \mu \le 0.40$ and $0.0 \le \zeta_s \le 0.15$ which is the practical range of interest. A detailed analysis was carried out by Warburton (1982) who provided optimal absorber parameters for a system subjected to random excitation assuming light damping in the main mass $(\zeta_s \le 0.10)$. The optimal absorber parameters are given as

$$\Omega_{opt} = \frac{\sqrt{1+\frac{\mu}{2}}}{1+\mu} \tag{6.16}$$

$$\zeta_{TLD-opt} = \sqrt{\frac{\mu\left(1+\frac{3\mu}{4}\right)}{4(1+\mu)(1+\mu/2)}} \tag{6.17}$$

If equation (6.16) and (6.17) are substituted into equation (6.3) then $\zeta_{eff-opt}$ for a lightly damped system is given as

$$\zeta_{eff-opt} = \frac{1}{4}\sqrt{\frac{\mu(1+\mu)}{1+0.75\mu}} \tag{6.18}$$

6.4 *Design Methodology of a Structure-TLD System Using the Equivalent Mechanical Model*

The design of an optimal structure-TLD system is based on the selection of the mass ratio μ and screen loss coefficient C_L. Initially, a mass ratio is selected in order to provide the specified amount of effective damping ζ_{eff}, from equation (6.2), required to reach a target structural response, σ_s. Once the mass ratio has been selected, optimum parameters Ω and ζ_{TLD} can be calculated from equations (6.16) and (6.17). The tuning ratio Ω will dictate the h/L value of the TLD. The relative response between the structure and the TLD is given by equation (6.11) with $R = R_{opt}$. Once the relative motion between the damper and structure is calculated, σ_r is substituted into equation (6.10) where $\zeta_{TLD} = \zeta_{TLD-opt}$ and the screen amount, location, and solidity can be determined. It is evident that this design procedure is an iterative process that may require several repetitions in order to determine the optimal mass ratio and screen geometry. Furthermore, the

outlined design process is limited to the preliminary design and sizing of the TLD and screen configuration. Since the procedure utilizes an equivalent linear mechanical model it does not take into account the nonlinear behaviour of the fluid. Therefore, shake-table experiments or the nonlinear model described in Section 5.3 should be used to validate the design.

6.5 *Validation of Structure-TLD Mechanical Model*

The equivalent mechanical model that was described in Section 6.2 is validated with the experimental testing of a structure-TLD system. Two different numerical models are used to simulate the influence of the TLD on the main mass.

The potential flow model that was validated in Section 5.4 is used along with the design procedure outlined in the previous section to predict the response of the system. This model is an efficient tool to utilize since all equations have closed form solutions and can be tabulated within a spreadsheet. The drawback of this model is that only the fundamental response is considered.

The nonlinear model that was validated in Section 5.3 is used in a slightly different manner to simulate the response of the structure-TLD system. A random force time-history is used to simulate the wind forces for a given return period. The forces are sampled at a rate of 150Hz. A time-stepping procedure is used where the displacement of the structure is first calculated. This displacement is used as the excitation amplitude for the TLD. The resulting base shear force is calculated from the TLD and is added to the next applied force from the time-history. This procedure is continued until the end of the time-history. This model

is of interest because it captures the nonlinearities associated with the sloshing fluid. Its drawbacks are that it requires slightly more time to obtain results when compared to the potential flow model and a computer program is a necessity.

6.5.1 Experimental Set-Up

A systems test on a SDOF structure-TLD was conducted by Tait (2004). A schematic of the experimental set-up is shown in Figure 6.2.

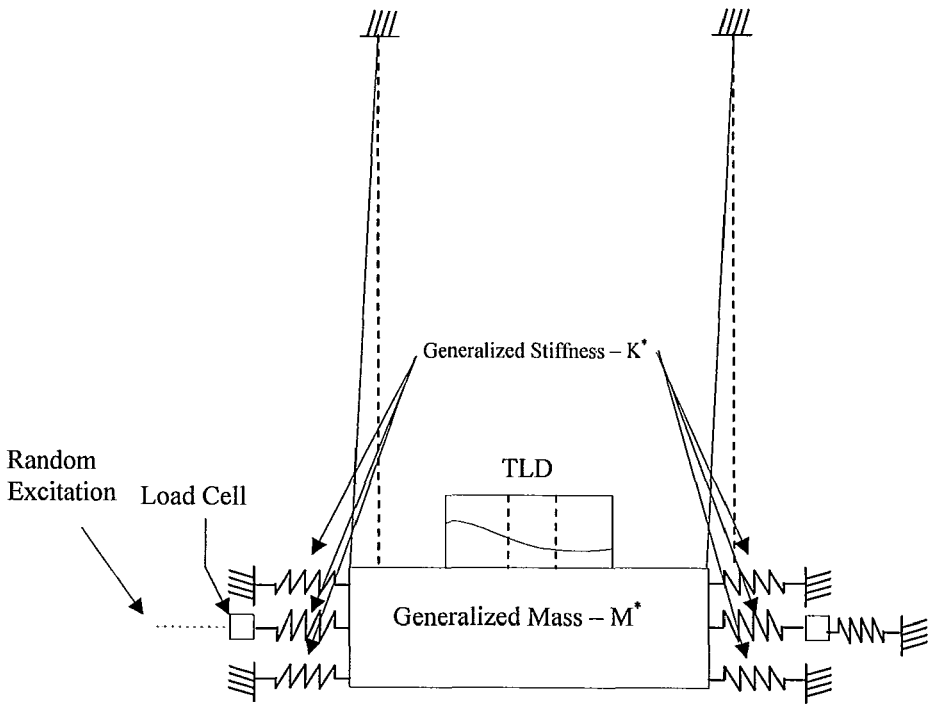

Figure 6.2 - Experimental Set-Up of Two Degree of Freedom System (Adapted From Tait, 2004)

The schematic shows the proposed building modelled as an equivalent SDOF system representing the fundamental mode of vibration of the structure. Free decay tests of the structure without a TLD were completed to determine the

natural frequency and damping ratio of the system. The system was excited randomly through a pre-tensioned driving spring which allowed the structure to be excited directly without influencing the structure-TLD response. A more detailed discussion on the experimental set-up can be found in Tait (2004).

6.5.2 Experimental Results

The structure that was tested has a mass M^*=4040 kg, stiffness K^*=49656 N/m and a coefficient of damping C^*=14 kg/s $(\zeta_s = 0.05\%)$. A rectangular tank of length L=966mm, width b=874mm and a still water depth h=119mm was used. The tank was equipped with two damping screens having a slat height of 5mm and a solidity ratio of 42%. They were located at 0.4L and 0.6L. The structure-TLD system was subjected to RMS excitation amplitudes of 11.7N, 23.8N, 47.8N, and 70.0N. These amplitudes result in peak hourly structural accelerations of 5milli-g, 8.4milli-g, 15.8milli-g, and 23.6milli-g which cover the range of NBCC recommended target response accelerations.

6.5.2.1 Equivalent Mechanical Model

The closed form solution of the structure-TMD system (McNamara, 1977) and equation (6.9) are used to determine the value of σ_r for a given RMS excitation force σ_F. The frequency-response functions for the structure $|H(f)|$ and free surface response $|H_\eta(f)|$ can then be calculated using the equivalent damping ratio (equation (6.10)) , the calculated value of σ_r, and the equations developed for a structure-TMD system (McNamara, 1977). Figure 6.3 compares the

experimental and predicted maximum structural response for the range of target RMS excitation forces.

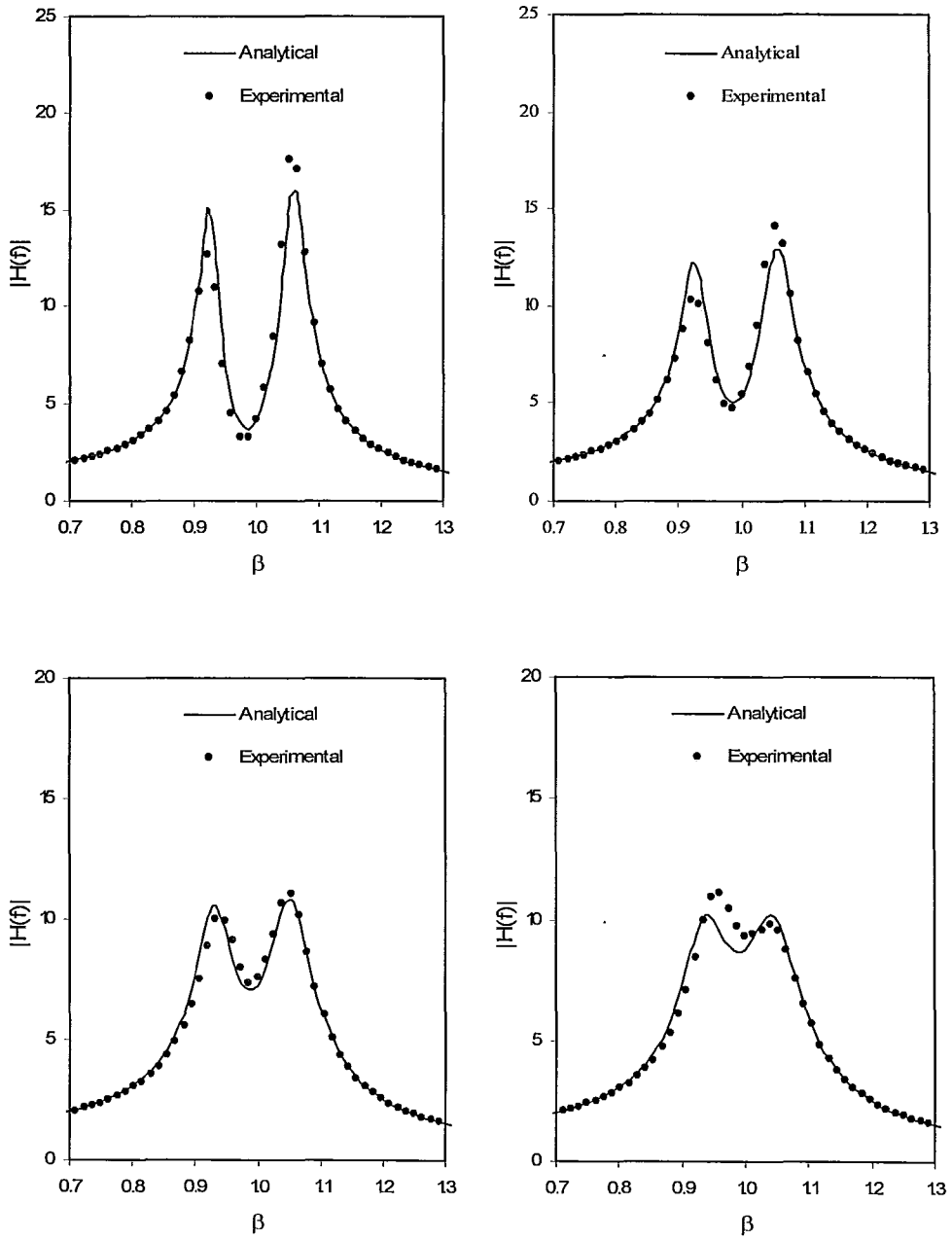

Figure 6.3 - Comparison of Measured and Predicted Normalized Structural Displacement for Random Excitation Based on Equivalent Mechanical Model a) σ_F =11.7N b) σ_F =23.8N c) σ_F =47.8N d) σ_F =70.0N

Figure 6.3 shows suitable agreement between the experimental and predicted structural displacement for all values of σ_F investigated. The double peaked response is indicative of a coupled system. It is observed that at low excitation amplitudes the nonlinear TLD response causes the predicted structural displacement to over-predict the value observed in experiment, this is indicated with the first peak in the frequency-response plot. In all four cases the area under the curve, which is an indicator of the effective damping, is well predicted. The value of $|H(f)|$ at $\beta = 0.98$ is found to increase as the excitation force increases. This is a direct result of the nonlinear response of the sloshing fluid.

Figure 6.4 compares the experimental and predicted normalized free surface response for the target range of RMS excitation forces. Good agreement between the experimental and predicted free surface response amplitude is observed for the range of RMS excitation forces investigated. The predicted free surface response is slightly over-predicted (8%) at low excitation amplitudes due to the sensitivity of C_L to small changes in the KC number. At larger force amplitudes the predicted and experimental free surface responses are within 4%.

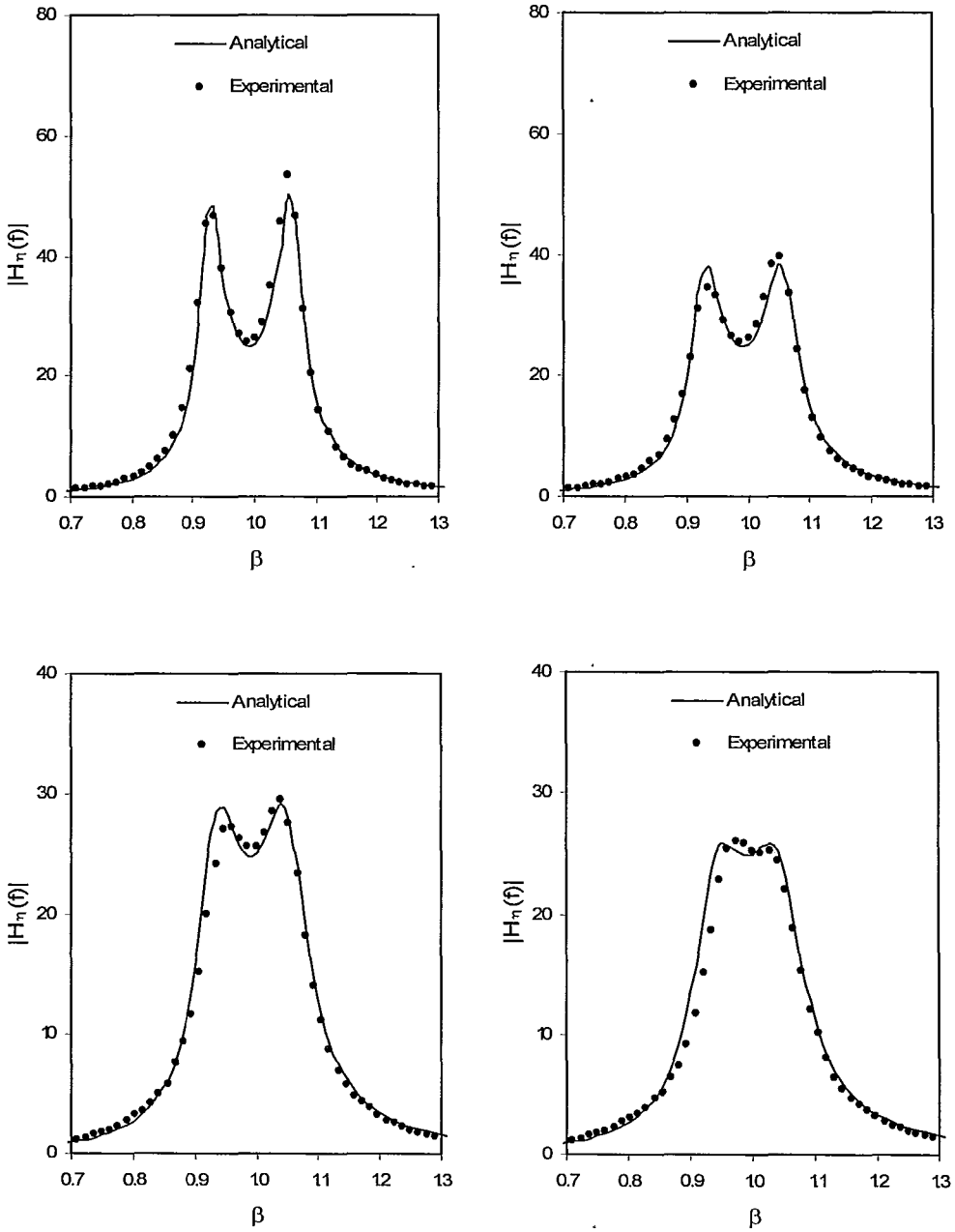

Figure 6.4 - Comparison of Measured and Predicted Normalized Free Surface Response Amplitude for Random Excitation Based on Equivalent Mechanical Model a) σ_F =11.7N b) σ_F =23.8N c) σ_F =47.8N d) σ_F =70.0N

Both Figure 6.3 and Figure 6.4 have demonstrated the ability of the potential flow model to predict the structural response and free surface response amplitude of a structure-TLD system. This model can now be utilized to assess the influence that screen geometry has on the efficiency of a structure-TLD system.

6.5.2.2 Nonlinear Model

The time-stepping procedure previously mentioned is used to simulate the interaction of a structure-TLD system. The structure and TLD properties along with the RMS excitation forces were described in Section 6.5.2. Figure 6.5 compares the predicted and experimental normalized structural displacement for the four excitation forces investigated.

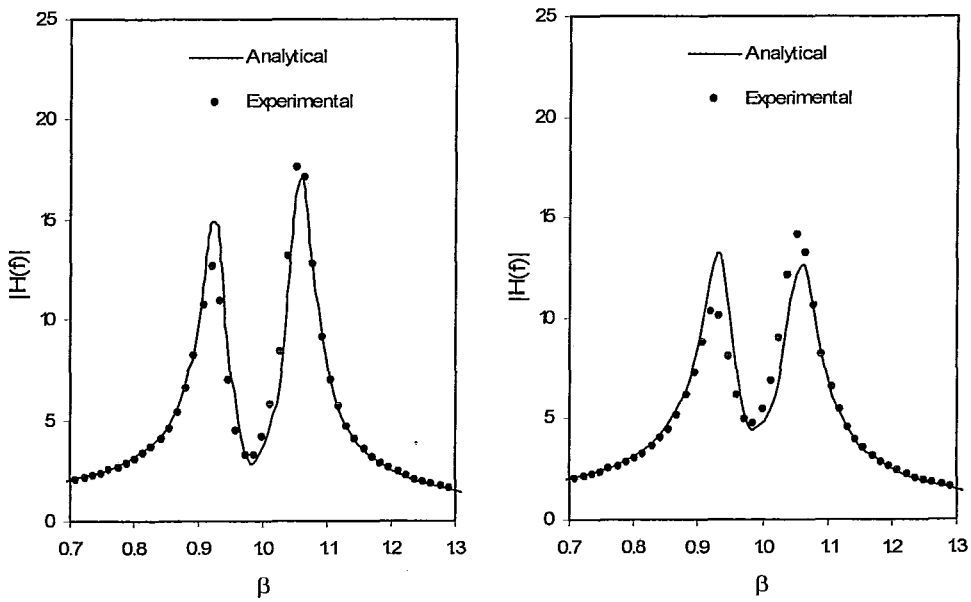

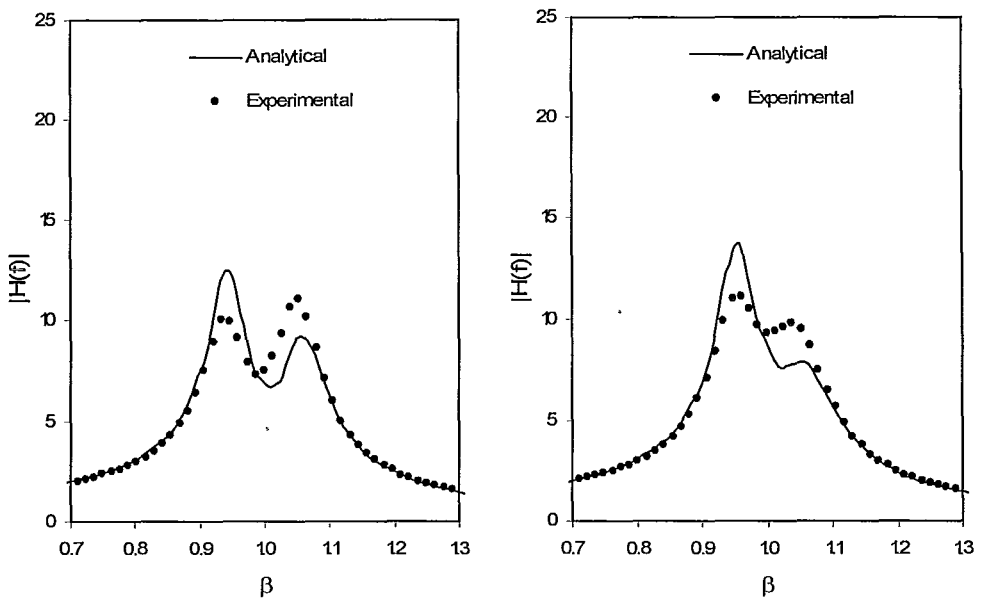

Figure 6.5 - Comparison of Measured and Predicted Normalized Structural Displacement for Random Excitation Based on Nonlinear Numerical Model a) σ_F =11.7N b) σ_F =23.8N c) σ_F =47.8N d) σ_F =70.0N

Figure 6.5 shows that the nonlinear structure-TLD model does not accurately predict the peak response of the structure's displacement. In all four cases the model over-predicts the first peak in the response which is dominated by the response of the fluid. Conversely, the model under-predicts the second peak in the response which is dominated by the structure. The model does not accurately capture the value of the peak response because it overestimates the hardening of the TLD. Since the natural frequency of the TLD is overestimated, the tuning ratio deviates from its optimal design value. Tait (2004) has shown through performance charts that the peak response of the frequency-response function, $|H(f)|$, is sensitive to small changes in Ω. However, Figure 6.5 does show that

the model correctly predicts the general response of the structure and appears to enclose the same amount of area under the curve as the experimental $|H(f)|$ plots. The area under the $|H(f)|$ curve is related to the effective damping that the TLD provides and a comparison between the predicted and experimental β_{eff} is shown in Figure 6.6.

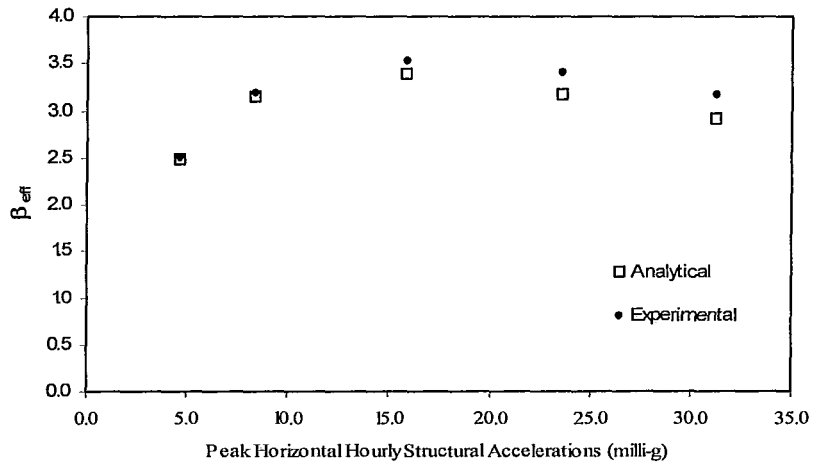

Figure 6.6 - Comparison of Predicted and Experimental Values of β_{eff}

Figure 6.6 shows that the model is capable of accurately predicting the value of β_{eff} for the range of peak hourly structural accelerations investigated. The model is most accurate at low accelerations because the TLD response is close to linear. As the acceleration increases the model over-predicts the natural frequency of the TLD which causes mistuning and an under prediction in the effective damping. The ability of the numerical model to predict the free surface response of the TLD is compared to the experimental results in Figure 6.7.

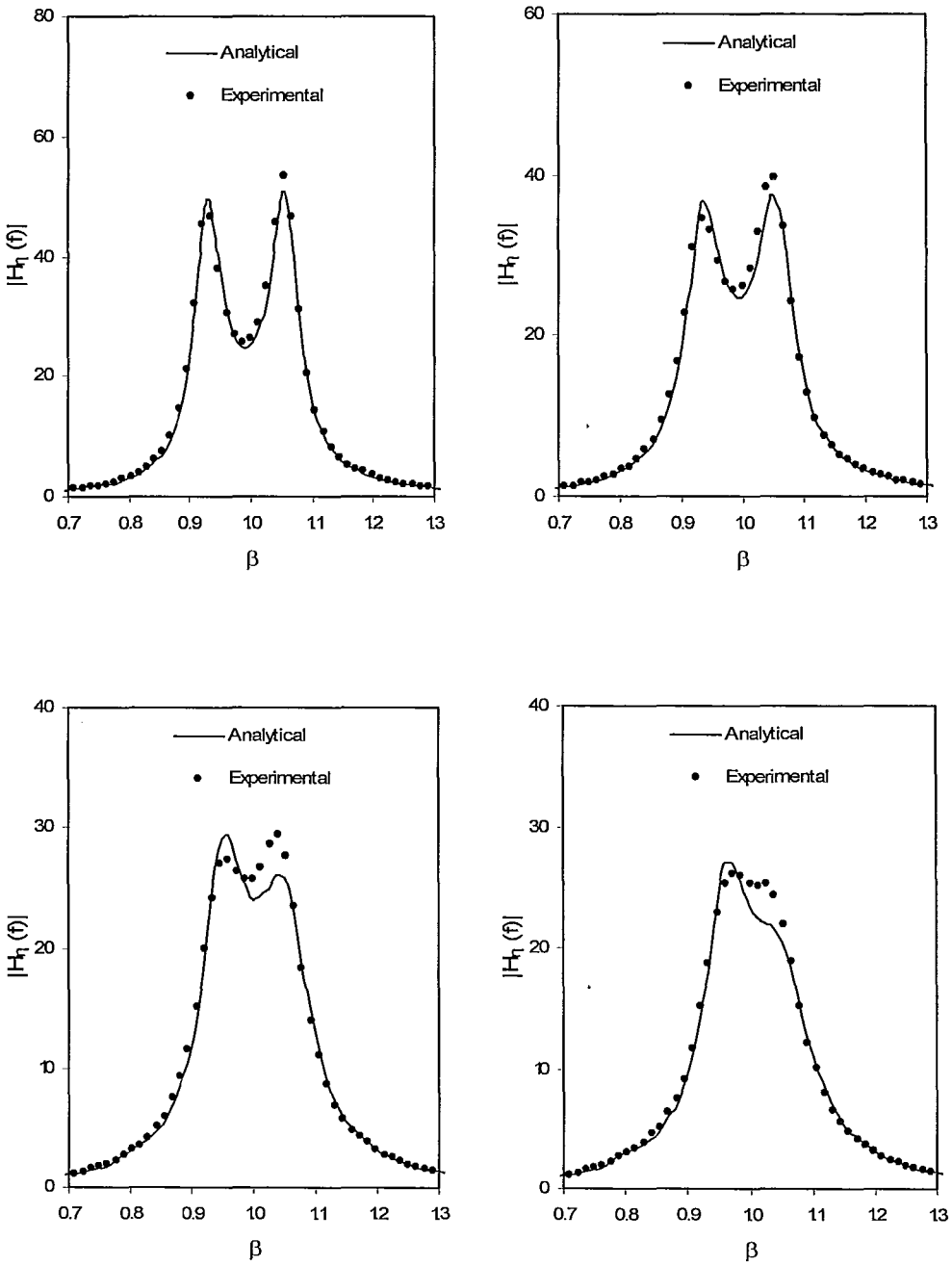

Figure 6.7 - Comparison of Measured and Predicted Normalized Free Surface Response Amplitude for Random Excitation Based on Nonlinear Numerical Model a) σ_F =11.7N b) σ_F =23.8N c) σ_F =47.8N d) σ_F =70.0N

Figure 6.7 illustrates that the nonlinear structure-TLD model is able to capture the free surface response of the TLD. At the two lowest values of σ_F the model captures the peak response of the fluid to within 5%. At larger values of σ_F the model over-predicts the first peak of the fluid response and under-predicts the second peak. This occurs because the natural frequency of the TLD is over-predicted at these excitation forces.

Figure 6.5 to Figure 6.7 have demonstrated the ability of the numerical model to predict the response of the structure-TLD system. It has been shown that while the model does not accurately predict the peak value of the frequency-response function it does accurately predict the effective damping.

6.6 *Influence of Slat Height on the Efficiency of a TLD*

The primary objective of this study is to assess the effect that slat height has on the efficiency of a TLD. To date, no TLD study has considered the *KC* number influence on C_L in the context of slat screens and TLD efficiency. In this comparison both the equivalent mechanical model and nonlinear numerical model will be used to illustrate the influence that slat height has on the efficiency of the structure-TLD system. The structure that is utilized for comparisons in the following sections was introduced in 6.5.1.

6.6.1 Equivalent Mechanical Model

The response of a structure-TLD system is compared for peak hourly structural accelerations from 5milli-g to 20milli-g. A TLD equipped with damping screens having slat heights of 5mm and 25mm are installed at 0.4L and 0.6L. A mass ratio of 1.9% and tuning ratio of 0.986 is selected as it corresponds to the mass ratio and tuning ratio used in experimental work (Tait, 2004). The screen solidity is selected such that the TLD performs at 100% efficiency (optimized) at a target response of 15milli-g. The response of the system for a range of structural accelerations is shown in Figure 6.8 .

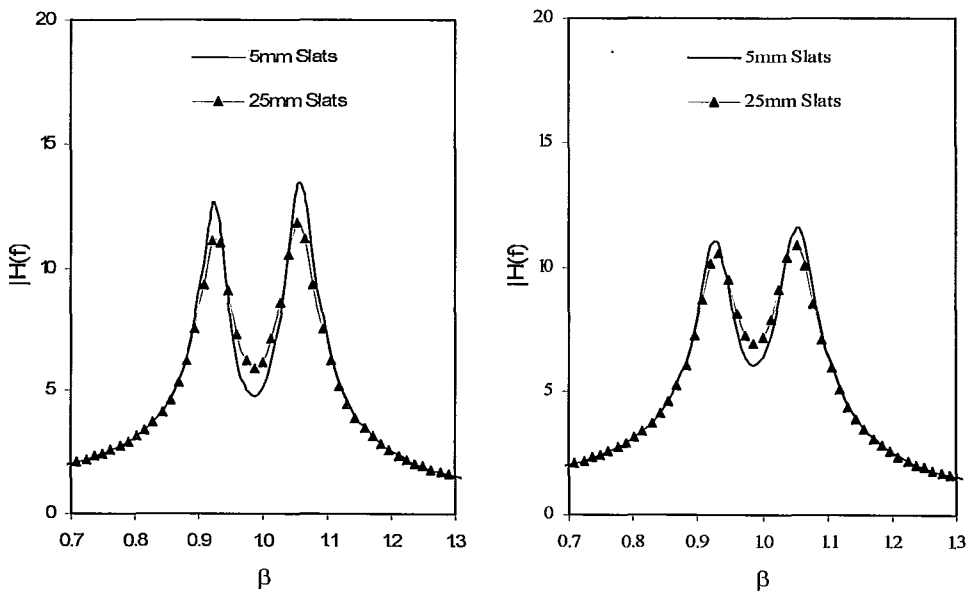

(a) $\ddot{\sigma}_s = 5milli - g$ (b) $\ddot{\sigma}_s = 10milli - g$

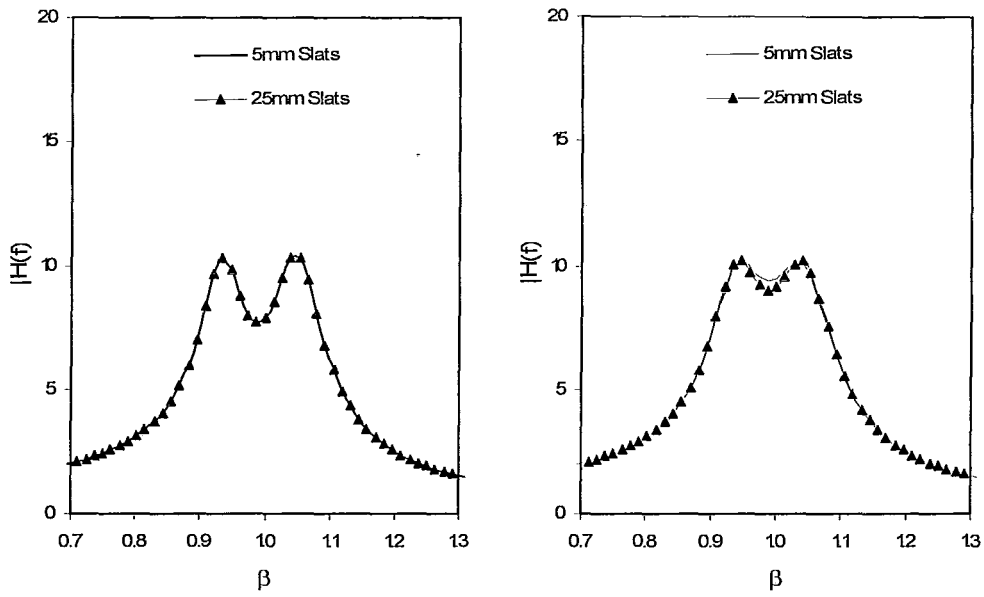

(c) $\ddot{\sigma}_s = 15milli - g$ (d) $\ddot{\sigma}_s = 20milli - g$

Figure 6.8 – Comparison of Structure-TLD Response for a TLD with Slat Screens of 5mm and 25mm Heights

The mechanical admittance function of the structure-TLD system is compared in Figure 6.8. It is observed that the response of the system with 5mm and 25mm slat screens is identical at 15milli-g excitation. This is expected since the screen solidities are optimized for this response. The influence of *KC* number dependent slat screens is best observed by comparing the system's response as the peak hourly structural acceleration deviates from the target value of 15milli-g. The TLD with larger slat heights maintains a more constant $|H(f)|$ compared to the TLD with 5mm slats. This indicates that the larger slats are reducing the amplitude dependency of the damping. The area under the $|H(f)|$ plots is related to the efficiency of the structure-TLD system. It is observed that as the

acceleration increases there is more deviation in the area under the curve corresponding to the 5mm slats screens. This indicates that the efficiency of the structure-TLD system is affected by the slat height.

In order to gain a better understanding of the performance of a structure-TLD system with various slat heights, the equivalent mechanical model is used to predict the efficiency of the system over a range of full scale peak hourly accelerations. This approach is very practical for use in a design office because it allows a quick estimate of the systems efficiency based upon the mass ratio and screen properties (S and C_L). The efficiency of the structure-TLD system is investigated for a building with an attached TLD having a 1.0% mass ratio. Slat screens with heights of 5mm, 15mm, and 25mm are installed at 0.4L and 0.6L. The solidity of each screen is selected such that it provides 100% efficiency (optimal) at the target response acceleration. Target response accelerations of 10milli-g, 15milli-g, and 20milli-g are selected for comparison and are shown in Figure 6.9 to Figure 6.11.

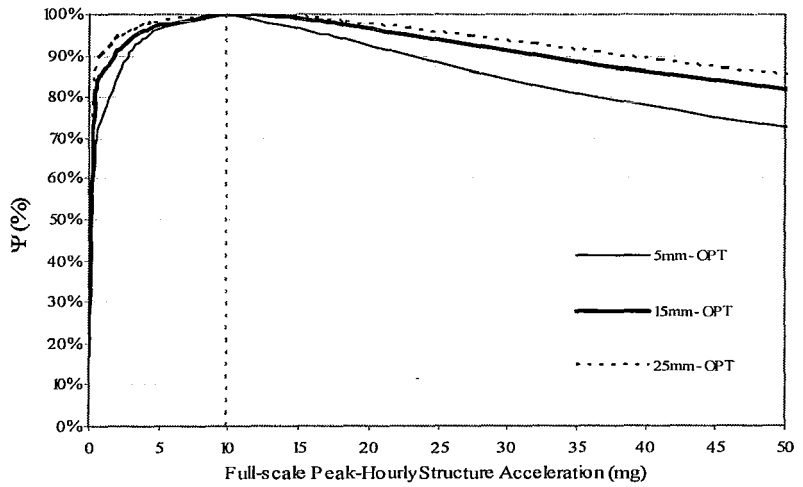

Figure 6.9 – TLD Efficiency vs $\ddot{\sigma}_s$, $\ddot{\sigma}_{s-target}$ = 10mg, μ =1.0%, $\zeta_s = 0$

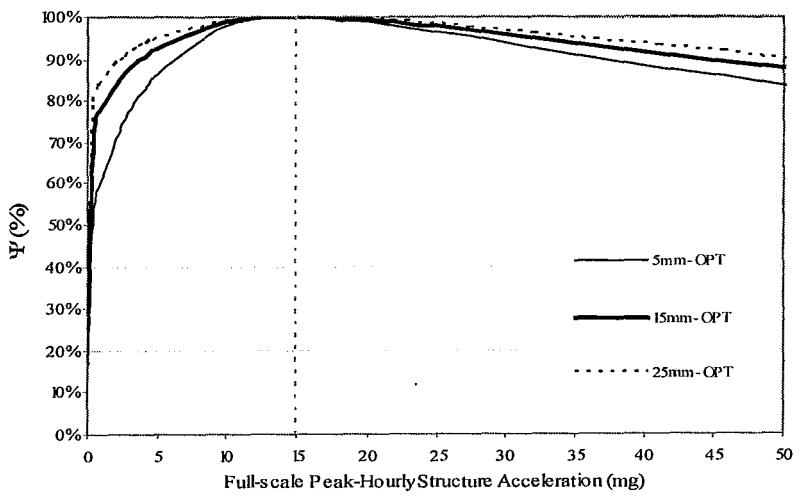

Figure 6.10 - TLD Efficiency vs $\ddot{\sigma}_s$, $\ddot{\sigma}_{s-target}$ = 15mg, μ =1.0%, $\zeta_s = 0$

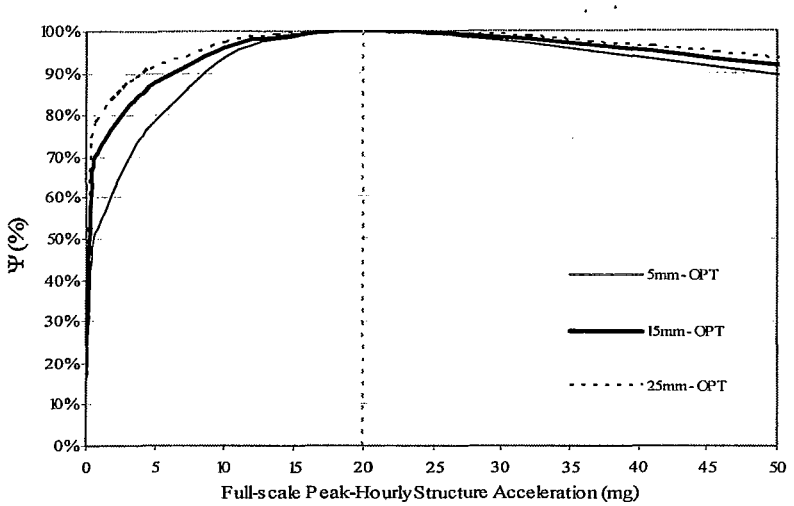

Figure 6.11 - TLD Efficiency vs $\ddot{\sigma}_s$, $\ddot{\sigma}_{s-target} = 20$mg, μ =1.0%, $\zeta_s = 0$

It is observed in all three cases that the use of larger slats increases the efficiency range of the TLD-structure system. For example, a TLD equipped with 25mm slat screens that is optimized to have 100% efficiency at 10milli-g's of acceleration maintains a 90% efficiency for $1 \leq \ddot{\sigma}_s \leq 37$ (milli-g). Conversely, the 5mm slat screens, optimized for 100% efficiency at 10 milli-g's only operates above 90% efficiency for $5 \leq \sigma_s \leq 20$ (milli-g). The largest difference in the efficiency range is observed for low target response accelerations. This is due to small amplitude wave response resulting in small *KC* numbers and slat screens with a varying loss coefficient. In general, the observed increase in the efficiency range occurs because the *KC* number dependent slat screens reduce the amplitude dependency of TLD damping.

Figure 6.12 to Figure 6.14 are used to compare the influence that the mass ratio has on the efficiency of the structure-TLD system. It is known that a larger

mass ratio improves the robustness of the system leading to a more efficient structure-TLD system (Tait, 2004). However, this often means an increased cost to the owner and in some instances is neither practical nor possible.

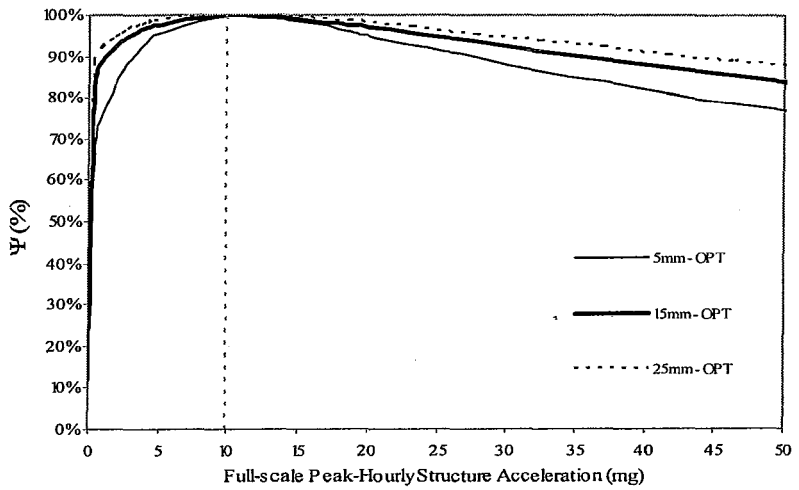

Figure 6.12 - TLD Efficiency vs $\ddot{\sigma}_s$, $\ddot{\sigma}_{s-target} = 10mg$, $\mu = 2.0\%$, $\zeta_s = 0$

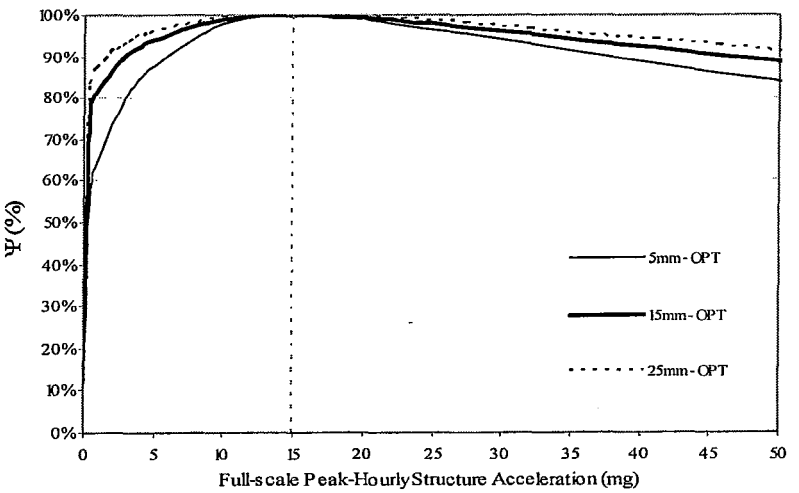

Figure 6.13 - TLD Efficiency vs $\ddot{\sigma}_s$, $\ddot{\sigma}_{s-target} = 15mg$, $\mu = 2.0\%$, $\zeta_s = 0$

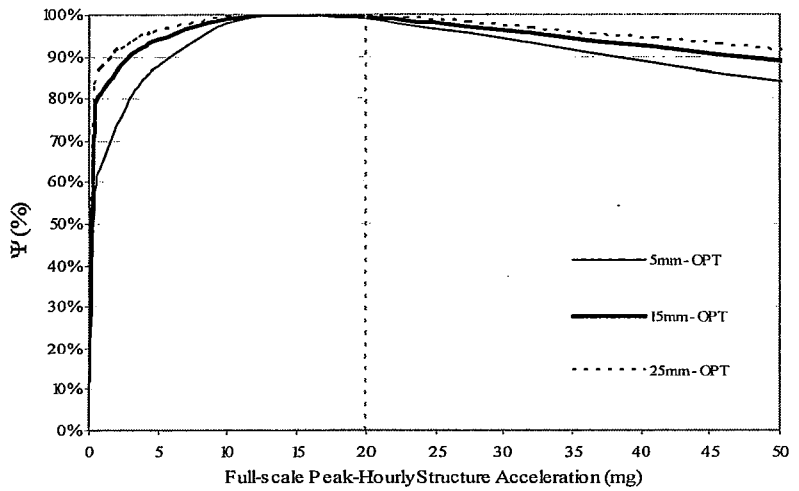

Figure 6.14 - TLD Efficiency vs $\ddot{\sigma}_s$, $\ddot{\sigma}_{s-target}$ = 20mg, μ =2.0%, $\zeta_s = 0$

By comparing the figures presented for μ=1% and 2% it is observed that an increase in the mass ratio increases the efficiency range of the TLD. For example, Figure 6.12 illustrates that at μ=2% the 5mm slat screens maintain a 90% efficiency level for $5 \leq \sigma \leq 25$ (milli-g), an improved efficiency compared to the case where μ=1.0%. In addition, it is observed in all three cases that an increase in slat height results in an increase in the efficiency range.

6.6.2 Nonlinear Structure-TLD Model

The nonlinear numerical model verified in Section 6.5.2.2 is used to investigate the influence that slat height has on the response of a structure-TLD system. Figure 6.15 compares the effective damping provided by the TLD for different slat heights. The screens have a solidity of 42%, the mass ratio is 2.5%, and the tuning ratio is 0.98.

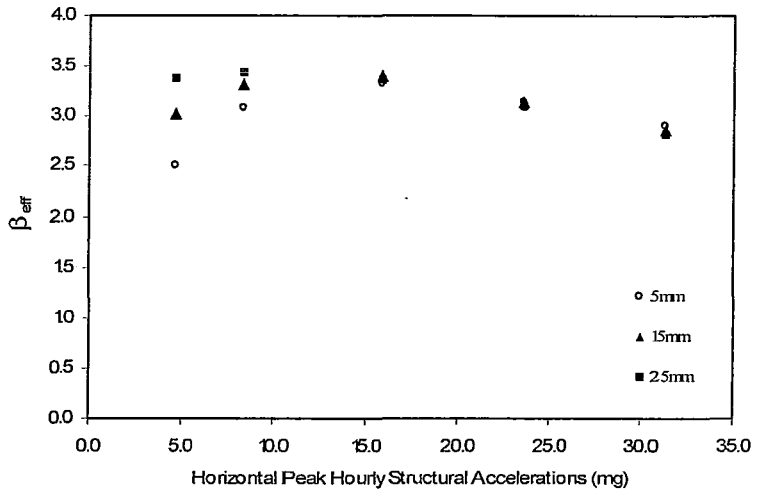

Figure 6.15 - Influence of Slat Height on Effective Damping, μ =0.025, S=42%

Figure 6.15 shows that all three slat heights provide the same amount of effective damping to the structure at accelerations greater than 15milli-g. At lower structural accelerations the KC number influence on C_L allows the system to maintain a higher effective damping level then what could be achieved by using the 5mm slat screens. Observe that both the 15mm and 25mm slat screens provide a larger amount of effective damping to the system at a response level of 8 milli-g then compared to 15 milli-g. This indicates that a screen solidity of 42% is not an optimal choice for a target response of 15milli-g. However, these screens still provide and maintain a wider efficiency range than the 5mm slat screens. A screen solidity of 42% is the optimal solidity for a target response of 8 milli-g, $\mu = 2.5\%$, and $\Omega = 0.98$. A comparison between optimally designed 5mm slat screens and 25mm slat screens for a target response of 8 milli-g's is shown in Figure 6.16.

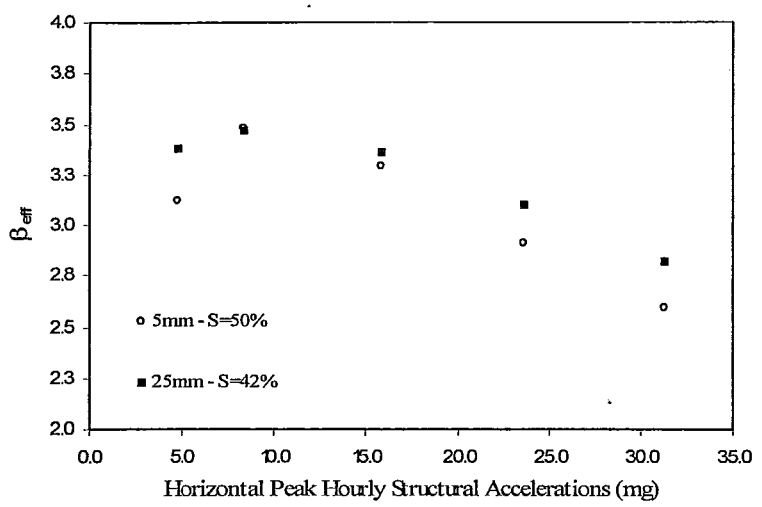

Figure 6.16 - Comparison of Optimally Designed Slat Screens, μ =0.025

Similar to the comparisons made with the equivalent mechanical model it is observed that for a given target response, 8 milli-g's in this case, both the 5mm and 25mm slat screens are capable of providing the required level of effective damping. However, as the structural acceleration deviates from the target value the 5mm slat screens have a significant reduction in the amount of effective damping they can provide. This results in a lower efficiency level when $\ddot{\sigma}_S$ deviates from $\ddot{\sigma}_{S-target}$. Conversely, the 25mm slat screens provide a more consistent level of effective damping across the $\ddot{\sigma}_S$ range. This means that the system is able to maintain a higher level of efficiency when $\ddot{\sigma}_S$ deviates from $\ddot{\sigma}_{S-target}$. As mentioned in the previous section this is a direct result of using slat screens that have a varying loss coefficient.

6.6.3 Optimized Design of Structure-TLD System

In the two previous sections the focus has been placed on determining the efficiency of a structure-TLD system for three specific slat heights. In this section, the efficiency of the system is optimized over a range of structural accelerations ranging from $5 \leq \ddot{\sigma}_s \leq 35$ with 20 milli-g being the target response. The screen properties S and C_L are selected such that the efficiency level remains above 95% over the range of structural accelerations and is optimized (100%) at 20milli-g.

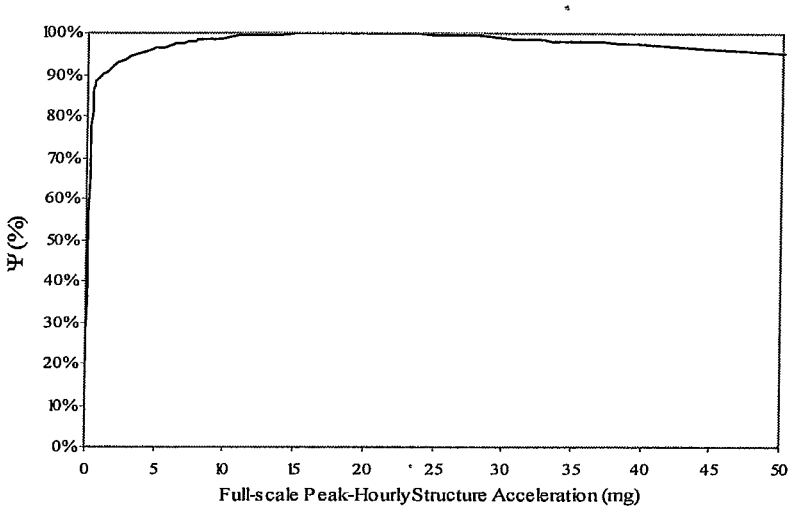

Figure 6.17 - Optimized Structure-TLD System, μ =1.0%, ζ_s = 0

Figure 6.17 shows the predicted efficiency of a structure-TLD system equipped with 21% solid screens having a slat height of 39mm utilizing the equivalent mechanical model. It illustrates that the screen properties S and C_L can be selected so that a consistently high efficiency level is achieved over a range of structural response accelerations. It is important to note that this is a theoretical

comparison and does not consider the influence that a large slat height (39mm) will have on the flow of the fluid.

6.7 *Conclusions*

A structure-TLD system has been investigated in this chapter with the use of an equivalent mechanical model and nonlinear shallow water wave theory. The objective was to determine the influence that screen geometry has on the efficiency of the system. Comparisons were made at peak hourly structural accelerations ranging from 5 milli-g to 30milli-g which covers the practical range of interest for wind-induced accelerations at a serviceability limit state. The prototype structure investigated corresponds to a 1:10 scale model of the 73 storey and 253m tall Highcliff Towers in Honk Kong. For all target peak hourly accelerations it was determined that the required amount of effective damping could be provided by the TLD if parameters μ, S, and C_L are properly selected. However, the TLD with 5mm slat screens (constant loss coefficient) loses efficiency as the structural acceleration deviates from its design value. This lack of efficiency was attributed to velocity squared losses at the screens. Conversely, the TLD with larger slat screens, in particular the 25mm slat screens, maintained a consistent level of efficiency over the entire range of structural accelerations. This is attributed to the KC number influence on C_L.

Chapter 7 - Conclusions and Recommendations

7.1 *Summary and Conclusions*

The research conducted in this study focuses on the dynamic response and performance of a 1-D tuned liquid damper equipped with two damping screens at 0.4L and 0.6L. The main objective of this investigation was to assess the influence that slat height has on the performance of a TLD. A series of shake-table experiments were completed under sinusoidal excitation over a range of amplitudes of practical importance. The performance of the TLD was assessed by comparing both frequency-response and time histories of the base shear forces, free surface response, and energy dissipation. The experimentally measured screen forces were used to determine the relationship between the *KC* number and the loss coefficient C_L.

Theoretical work was conducted to incorporate the influence of a varying loss coefficient into the numerical models. Two models were investigated: nonlinear shallow water wave theory and linearized potential flow theory. The numerical models were used to study the efficiency of a structure-TLD system over a range of target response amplitudes. This investigation demonstrated that slat screens with a varying loss coefficient improve the efficiency of the damper over the range of structural response accelerations studied.

7.2 *Research Findings*

The major conclusions that stem from this body of research are summarized here.

7.2.1 Experimental Study of TLD with Various Slat Heights

- An increase in slat height leads to a change in the loss coefficient C_L. The variation in C_L has been correlated to the KC number which is a function of fluid velocity and slat height
- An increase in slat height leads to a reduction in the natural frequency. This is believed to occur because the larger slats influence the flow of the fluid. A modification factor was suggested to account for this shift which is given as $f_{exp} = f_n \alpha D$
- A similar TLD response can be achieved by selecting a high solidity-small slat screen or a low solidity-large slat screen (i.e. TS5-50 vs. TS25-42). In addition, it provides the design engineer with an array of design alternatives since it allows the selection of screens based on solidity, slat height and KC
- Rounded edge slat screens were shown to exhibit a similar response compared to the sharp edged screens. However, for a given KC number the rounded edge screens have lower loss coefficients. This indicates that edge geometry is an important parameter in TLD design.

7.2.2 Numerical Modeling of a TLD with a Varying Loss Coefficient

- The loss coefficient is highly sensitive to small variations in the *KC* number. As a result, errors that occur in the estimation of *KC* are magnified with larger errors in C_L. Therefore, the model under-predicts the TLD response at small excitation amplitudes.
- The linearized potential flow model assumes a first mode response and small amplitude wave response. It shows good agreement for excitation amplitudes up to *A/L*=0.0077. However, as *A/L* increases these assumptions are no longer valid and the model shows a discrepancy in the predicted and measured responses.
- A comparison between ζ_{TLD} and η' showed that both the 5mm and 25mm slat screens were able to provide a specified level of damping for a target free surface response. However, as the response deviated from the target value, the 25mm slat screens were more efficient at maintaining the required level of damping.

7.2.3 Performance of a Structure-TLD System with Varying Loss Coefficient Slat Screens

- The equivalent mechanical model was primarily used to assess the influence that slat screens with a varying loss coefficient have on the efficiency of a tuned liquid damper
- It was found that the peak hourly structural acceleration can be reduced to a given target value if the mass ratio and screen properties (slat height & solidity) are properly selected.
- The TLD with screens having a varying loss coefficient maintained a higher efficiency level than the same TLD with screens having a constant loss coefficient. This ensures that the efficiency of the TLD is maintained as the structural acceleration deviates from the target design value

7.3 *Recommendations for Further Research*

This study focused on the performance of a 1-D tuned liquid damper. The major objective of this work was to determine the influence that slat screens with a varying loss coefficient have on the performance of a TLD. The damper was investigated for sinusoidal excitation at amplitudes indicative of wind-induced accelerations. The following is a list of recommendations on future work in the area of tuned liquid dampers. In all cases it is implied that damping screens with varying losses will be utilized:

- The performance of tuned liquid dampers has been thoroughly studied for small response amplitudes indicative of wind-induced vibrations. The response of tuned liquid dampers under larger excitations that are representative of earthquake loads should be investigated through shake-table experiments and numerical modeling.
- The major focus of tuned liquid damper research has been on their applicability to reduce the wind-induced accelerations at a serviceability limit state. An investigation into the ability of tuned liquid dampers to reduce the strength demands on the primary structural members should be considered.
- The response of this tuned liquid damper has shown to have a natural frequency that increases with the free surface response. The concern with this behaviour is that the tuning ratio between the structure and the TLD will change as the excitation amplitude increases. As a result, the concept of using multiple mode TLD's should be investigated. This approach utilizes a number of TLD's that all have different natural frequencies but are distributed equally around the natural frequency of the structure.
- Work recently completed by Deng (2007) focused on utilizing various tank geometries. A full experimental program validating his proposed models should be undertaken. In addition, both constant loss and varying loss slat screens should be installed.

- The influence of edge geometry was briefly investigated in this study. While this showed some positive results in terms of a varying loss coefficient a more rigorous experimental study should be completed where the corner radius is varied and the performance of the TLD is assessed. In addition, other slat shapes such as circular should be considered.
- An experimental program that investigates the performance of a structure-TLD with various slat heights should be undertaken in order to confirm the results of Chapter 6 and the numerical models utilized.

References

Baines, W.D. and Peterson, E.G. (1951). "An Investigation of Flow Through Screens", *Transactions of the ASME,* Vol. 73, pp. 467-479.

Bauer, H.F. (1964), "Nonlinear Propellant Sloshing in a Rectangular Container of Infinite Length", *Developments in Theoretical and Applied Mechanics*, Vol. 3, pp 725-759.

Bishop, R.E.D. and Welbourn, D.B. (1952). "The Problem of the Dynamic Vibration Absorber", *Engineering*, London,174, 769.

Blevins, Robert D. (1977). *"Flow-Induced Vibrations"*, 2nd Edition, Van Nostrand Reinhold Company: New York.

Boggs, D. (1995). "*Acceleration Indexes for Human Comfort in Tall Buildings-Peak or RMS?*", Submitted for publishing in CTBUH Monograph Chapter 13: Motion Perception Tolerance and Mitigation.

Campbell, R. (1995). *"Builder* Faced Bigger Crisis Than Falling Windows*"*, *The Boston Globe*, March 3, 1995.

Cassolato (Casson), M. and Tait, M., (2005) "A Preliminary Study of a Tuned Liquid Damper with Smart Screens", *Proceedings of the 1st Canadian Conference on Effective Design of Structures,* McMaster University, Canada, pp. 227-236.

Cassolato, M. (2007). *"The Performance of a TLF with Inclined and Oscillating Screens",* M.A.Sc. Thesis, McMaster University, Hamilton, Canada.

Cement Association of Canada (2006).
<www.cement.ca/cement.nsf/e/92A318A5EE9F672F852572F2005EF5AC/$FILE/KING%20WEST%20BUILDING.pdf> Accessed: 20 July 2007

Chopra, Anil K. (2000). "*Dynamics of Structures: Theory and Applications to Earthquake Engineering*", 2nd Edition, Prentice-Hall Inc.: Upper Saddle River, NJ.

Clough, R.W. and Penzien, J. (1975). *"Dynamics of Structures"*, 1st Edition, McGraw-Hill College.

Davenport, A.G. (1964). "Note on the Distribution of the largest Value of a Random Function with Application to Gust Loading". *Institute for Civil Engineers,* Vol. 28, pp.187-196.

Dean, R.G. and Dalrymple, A.D. (1984). *"Water Wave Mechanics for Engineers and Scientists"*, 1st Edition, Prentice-Hall Inc.: Upper Saddle River, N.J.

Den Hartog, J.P. (1956). *"Mechanical Vibrations"*, 4th Edition, McGraw-Hill:New York, NY.

Deng, X. (2007). *"The Performance of Tuned Liquid Dampers with Different Tank Geometries"*, M.A.Sc. Thesis, McMaster University, Hamilton, Canada.

Fediw, A.A. (1992). *"Performance of a One Dimensional Tuned Sloshing Water Damper"*, M.E.Sc. Thesis, University of Western Ontario, London, Canada.

Fediw, A.A. (1995). "Performance of a Tuned Sloshing Water Damper", *Journal of Wind Engineering and Industrial Aerodynamics.* Vol. 57, pp. 237-247.

Fujino, Y., Pacheco, B.M., Chaiseri, P., and Sun, L.M. (1988). "Parametric Studies on Tuned Liquid Dampers (TLD) Using Circular Containers by Free Oscillations Experiments", *Structural Engineering/Earthquake Engineering*, JSCE, Vol. 5, pp. 318-391.

Graham, E.W. and Rodriguez, A.M. (1952). "The Characteristics of Fuel Motion Which Affect Airplane Dynamics:, *Journal of Applied Mechanics,* Vol. 19, No.3, pp.381-388.

Hansen, R.J., Reed, J.W., and Vanmarcke, E.H., (1973). "Human Response to Wind-Induced Motion of Buildings", *J. Struct. Div.,* ASCE, V99.

Holmes, J.D. (1995). "List of Installations", *Engineering Structures,* Vol 17, No.9, pp. 676-677.

Ioi, T. and Ikeda, K. (1978). "On the Dynamic Vibration Damped Absorber of the Vibration System", *Bulletin of Japanese Society of Mechanical Engineering,* Vol 151, No. 21, pp. 64-71.

Irwin, A. (1983), "Perception, Comfort, and Performance Criteria for Human Beings Exposed to Whole Body Yaw Vibration and Vibration Containing Yaw and Translational Components", *Journal of Sound and Vibration*, Vol. 76, No.4.

Isaacson, M. and Premasiri, S. (2001). "Hydrodynamic Damping Due to Baffles in a Rectangular Tank", *Canadian Journal of Civil Engineering*, Vol. 28, pp.608-616.

Isyumov, N., (1993). "Criteria for Acceptable Wind-Induced Motions of Tall Buildings", *International Conference on Tall Buildings,* CTBUH, 1993, Rio De Janerio.

Kaneko, S. and Ishikawa, M. (1999). "Modeling of Tuned Liquid Damper with Submerged Nets", *Journal of Pressure Vessel Technology,* Transactions of ASME, Vol. 121, pp. 334-343.

Kareem, A. (1983). "Mitigation of Wind Induced Motion of Tall Buildings", *Journal of Wind Engineering and Industrial Aerodynamics*, No. 11, pp. 273-284.

Kareem, A., Kijewski, T., and Tamura, Y. (1999). "Mitigation of Motions of Tall Buildings with Specific Examples of Recent Applications", *Wind and Strucutres,* Vol.2 No.3, pp. 201-251.

Keulegan, G.H. and Carpenter, L.H. (1958). "Forces on Cylinders and Plates in an Oscillating Fluid", *Journal of Research of the National Bureau of Standards,* Vol. 60, No. 5, pp. 423-440.

Lepelletier, T.G. and Raichlen, F. (1988). "Nonlinear Oscillations in Rectangular Tanks", *Journal of Engineering Mechanics*, Vol. 114, No.1, pp 1-23.

Lamb, H. (1932). *"Hydrodynamics",* The University Press, Cambridge, England.

Luft, R.W. (1979). "Optimal Tuned Mass Dampers for Buildings", *Journal of the Structural Divison, ASCE,* Vol. 103, pp. 2766-2772.

McNamara, R.J. (1977). "Tuned Mass Dampers for Buildings", *Journal Struct. Div. ASCE*, Vol. 103, pp. 1785-1798.

McNamara, R.J., Kareem, A. and Kijewski, T. (2002). "Ask the Experts...Perception of Motion Criteria for Tall Buildings Subjected to Wind," *Proceedings of Structures Congress 2002,* ASCE, Denver, April 4-6.

Miles, J.W. (1967). "Surface Wave Damping in Closed Basins", *Proceedings of the Royal Society of London,* Vol. 297, pp. 459-475.

Modi, V.J. and Welt, F. (1985). "On the Control of Instabilities of Fluid-Structure Interaction Problems", *Proceedings of the 2nd International Symposium on Structural Control*, pp.473-486.

Modi, V.J. and Seto, M.L. (1995). "On the Energy Dissipation Through Liquid Sloshing and Suppression of Wind Induced Instabilities", *Proceedings of the 9th International Conference on Wind Engineering*, No. 4, pp. 1619-1630.

Modi, V.J. and Munshi, S.R. (1998). "An Efficient Liquid Sloshing Damper for Vibration Control", *Journal of Fluids and Structures*, Vol. 12, pp. 1055-1071.

Modi, V.J., Akinturk, A., and Tse, W. (2003). "A Family of Efficient Sloshing Liquid Dampers for Suppression of Wind-Induced Instabilities", *Journal of Vibration and Control,* Vol. 9, pp. 361-386

Morrison, J.R., O'Brien, M.P., Johnson, J.W., and Schaaf, S.A. (1950). "The Force Exerted by Surface Waves on Piles", *Society of Petroleum Engineers of the American Institute of Mining, Metallurgical and Petroleum Engineers Transactions,* Vol. 189, pp.149-154.

Motioneering (2004).
<www.motioneering.ca/User/Doc/pp_wall_centre.pdf> (online) Project Brochure. Accessed: 20 July, 2007.

Randall, S.E., Halsted, D.M., and Taylor, D.L. (1981). "Optimum Vibration Absorbers for Linear Damped Systems", *Journal of Mechanical Design, ASME,* Vol. 103, pp.908-913.

Reed, D., Yu, J., Yeh, H. and Gardarsson, S. (1998). "Investigation of Tuned Liquid Dampers under Large Amplitude Excitation", *Journal of Engineering Mechanics,* ASCE, Vol. 124, No.4, pp.405-413.

Sarpkaya, T. (1975). "Forces on Cylinders and Spheres in a Sinusoidally Oscillating Fluid", *Transactions of the ASME Journal of Applied Mechanics.* Vol. 42, pp. 32-37.

Shimiz, T. and Hayama, S. (1987). "Nonlinear Responses of Sloshing Based on Shallow Water Wave Theory", *JSME International Journal*, Vol. 30, No. 263.

Skyscrapers (2007).
<www.skyscrapers.com> (Online) Last Accessed 17 July 2007.

Soong, T.T. and Dargush, G.F. (1997). *"Passive Energy Dissipation Systems in Structural Engineering"*, 1st Edition, John Wiley and Sons: New York, NY.

Sun, L.M. and Fujino, Y. (1994). "A Semi-Analytical Model for Tuned Liquid Damper (TLD) with Wave Breaking", *Journal of Fluids and Structures*, Vol. 8, pp.471-488.

Sun, L.M., Fujino, Y., Chaiseri, P., and Pacheco, B. M. (1995). "The Properties of Tuned Liquid Dampers Using TMD Analogy", *Earthquake Engineering and Structural Dynamics*, Vol. 24, pp. 967-976.

Taipei-101 Webpage (2007). www.taipei-101.com
(online) Accessed: 6th July 2007.

Tait, M. (2007). "Modelling and Preliminary Design of a Structure-TLD System", Submitted to *Engineering Structures.*

Tait, M. (2004). *"The Performance of 1-D and 2-D Tuned Liquid Dampers"*, Ph. D Thesis, University of Western Ontario, London, Canada.

Tait, M., El Damatty, A.A., Isyumov, N., Siddisue, M.R. (2005). "Numerical Flow Models to Simulate Tuned Liquid Dampers (TLD) with Slat Screens", *Journal of Fluids and Structures*, Vol. 20, No.8, pp.1007-1023

Tamura, Y., Fujii, K., Obtsuki, T., Wakahara, T., and Kohsaka, R. (1995). "Effectiveness of Tuned Liquid Dampers Under Wind Excitation", *Engineering Structures,* Vol. 17, No. 9, pp. 609-621.

Vickery, B.J. and Davenport, A.G. (1970). "An Investigation of the Behaviour in Wind of the Proposed Centre Point Tower, in Sydney, Australia', *Research Report BLWT-1-70,* The Boundary Layer Wind Tunnel Laboratory, The University of Western Ontario, London, Canada.

Warburton, G.B. (1982). "Optimum Absorber Parameters for Various Combinations of Response and Excitation Parameters", *Earthquake Engineering and Structural Dynamics*, Vol. 10, pp. 381-401.

Warnitchai, P. and Pinkaew, T. (1999). "Modelling of Liquid Sloshing in Rectangular Tanks with Flow-Dampening Devices", *Engineering Structures,* Vol. 20, No. 7, pp.593-600.

Weisbach, J. (1855). *Die Experimental Hydraulik*, Freiburg: Engelhardt-Verlag.

Welt, F. and Modi, V.J. (1992). "Vibration Damping Through Liquid Sloshing: Part I and Part II", *ASME Journal of Vibration and Acoustics,* No. 114, pp. 10-23.

Wiesner, K.B. (1979). "TMD to Reduce Building Wind Motion", *ASCE Spring Convention,* Boston MA.

Yeh, H.H. and Shrestha, M. (1989). "Free-Surface Flow Through Screen", *Journal of Hydraulic Engineering,* Vol. 115, No. 10, pp. 1371-1385.